JAEA-Review
2008-054

JAEA-Review

JAEA-Tokai Tandem Annual Report 2007

April 1, 2007 - March 31, 2008

Department of Research Reactor and Tandem Accelerator

Nuclear Science Research Institute
Tokai Research and Development Center

November 2008

Japan Atomic Energy Agency

日本原子力研究開発機構

独立行政法人日本原子力研究開発機構　研究技術情報部　研究技術情報課
〒319-1195　茨城県那珂郡東海村白方白根 2 番地 4
電話 029-282-6387, Fax 029-282-5920, E-mail:ird-support@jaea.go.jp

JAEA-Review 2008-054

JAEA-Tokai Tandem Annual Report 2007
April 1, 2007 - March 31, 2008

Department of Research Reactor and Tandem Accelerator

Nuclear Science Research Institute
Tokai Research and Development Center
Japan Atomic Energy Agency
Tokai-mura, Naka-gun, Ibaraki-ken

(Received September 11, 2008)

The JAEA-Tokai tandem accelerator facility has been used in various research fields of heavy-ion nuclear science and material science not only by JAEA personnel but also by researchers from universities, institutes and companies. This annual report describes a summary of research activities carried out in the period between April 1, 2007 and March 31, 2008. The forty-nine summary reports from users were categorized into seven research/development fields:

(1) accelerator operation and development
(2) nuclear structure
(3) nuclear reaction
(4) nuclear chemistry
(5) nuclear theory
(6) atomic physics and solid state physics
(7) radiation effects in materials

Also contained are lists of publications, meetings, technical staff, researchers in JAEA and cooperative researchers with universities.

Keywords : JAEA-Tokai Tandem Accelerator, Operation Results, Nuclear Structure, Nuclear Reaction, Nuclear Chemistry, Nuclear Theory, Atomic Physics, Solid State Physics, Radiation Effects in Materials, Progress Report.

Editors : Yuichiro NAGAME, Satoshi CHIBA, Norito ISHIKAWA, Shin-ichi MITSUOKA,
Yosuke TOH, Makoto MATSUDA and Tetsuro ISHII

JAEA-Review 2008-054

原子力機構東海タンデム加速器 2007 年度年次報告

日本原子力研究開発機構
東海研究開発センター原子力科学研究所
研究炉加速器管理部

(2008 年 9 月 11 日受理)

原子力機構東海タンデム加速器施設は、重イオンを用いた原子核科学や物質科学などの様々な分野において、原子力機構の職員を初め、大学や研究機関、民間企業の研究者に利用されている。本年次報告書は、2007 年４月１日から 2008 年３月 31 日までの期間に実施された研究活動の要約をまとめたものである。総数 49 件の要約を下記の７部門に分類した。

（１）加速器の運転状況と開発
（２）原子核構造
（３）原子核反応
（４）核化学
（５）原子核理論
（６）原子物理及び固体物理
（７）材料の照射効果

さらに、発表論文と会議での口頭発表、タンデム加速器に関係する技術者および原子力機構の研究者ならびに大学等の共同研究者の一覧を掲載した。

原子力科学研究所：〒319-1195　茨城県那珂郡東海村白方白根 2-4
編集者：永目　諭一郎、千葉　敏、石川　法人、光岡　真一、藤　暢輔、松田　誠、
石井　哲朗

Foreword

This report covers research and development activities with the tandem accelerator, its superconducting booster and the TRIAC (Tokai Radioactive Ion Accelerator Complex) at JAEA Tokai, for the period of FY 2007 (April 1, 2007 to March 31, 2008). During this period, the tandem accelerator was operated over a total of 105 days and delivered 23 different ions to the experiments in the fields of nuclear physics, nuclear chemistry, atomic physics, solid state physics and radiation effects in materials. Fifty-six research programs were carried out in collaboration with a total of about 240 researchers from universities and research institutes. The TRIAC was operated for 9 days. The following are some of the highlights in FY 2007.

In the development of the tandem accelerator and the booster, we took a long maintenance period for replacing the aged coil inside the 180 degree bending magnet in the terminal. In this period, the 10 GHz in-terminal ECR ion source, NANOGAN, was replaced with the 14.5 GHz ECR ion source, SUPERNANOGAN. The beam-line components at the terminal were also realigned. This alignment greatly improved the transmission of ion beams through the terminal. As a result, we have achieved the acceleration of a 3 μA proton beam and a 1.3 particle μA fluorine beam.

In research of nuclear reactions, fusion barrier distributions were extracted in the ^{86}Kr + ^{208}Pb reaction, relating to cold fusion for the production of super-heavy elements Z = 118. Fission fragment mass distribution in ^{36}S + ^{238}U was measured to study nuclear orientation effects of well-deformed actinides.

In research of nuclear structure, in-beam γ-ray spectroscopy experiments for ^{36,38}Cl, ^{36}S, ^{168}Ta and ^{188}Pt, and a Coulomb excitation experiment for ^{100}Ru have been made by utilizing the γ-ray detector array, GEMINI-II; Shape coexistence in ^{188}Pt and band structures of ^{168}Ta have been clarified. By in-beam γ-ray spectroscopy using heavy-ion transfer reactions, eight Nilsson orbitals in ^{249}Cm, including an L=8 orbital, were identified. The deformed shell gap at N = 152 was found to be reduced for ^{246}Pu. Energy levels in ^{255}Fm were established by the α-γ spectroscopy of ^{259}No.

In research of nuclear chemistry, the anion-exchange experiment of Db has been conducted in HF/HNO_3 solution with AIDA. The preliminary result on the adsorption of Db on the resin is reported. To obtain more accurate data of Db with high statistics, an improved AIDA system, AIDA-II, based on continuous sample collection and evaporation of effluents, and successive α-particle measurement, has been developed. The successful oxidation of element 102, No, on an atom-at-a-time scale using the newly developed flow electrolyte column chromatography is presented.

In the field of nuclear theory, exotic shell structure in the neutron-rich region around N = 28 was explored by the shell model. The effective interaction was constructed based on general interactions, and the cross-shell interaction was also generated. It was found that the observed spectroscopic factors are reproduced satisfactorily and there is a strong dependence of them on the tensor force. Hyperon suppression in hadron-quark mixed phase, stability of the superheavy nuclei and other topics were also investigated.

In research of atomic physics and solid state physics, high resolution measurements were performed for Coster-Kronig electron spectra from high Rydberg states of Be-like four-electron N and O ions. Non-destructive on-line Li diffusion measurements are conducted for Li ionic conductors using short-lived α-emitting radiotracer ^{8}Li produced as a pulsed ion beam from TRIAC. Li-content dependence of diffusion coefficients observed for β-LiGa suggests that excess Li vacancies induce formation of a defect complex which may suppress Li motion.

In research of radiation effects in materials, radiation damage process of UO_2 and CeO_2 ceramics was investigated in order to elucidate the radiation damage process of high burnup nuclear fuels. Surface morphology change is observed for both ion-irradiated UO_2 and CeO_2, suggesting that same damage formation mechanism may be underlying for both materials.

Masao Sataka
Deputy Director
Department of Research Reactor
and Tandem Accelerator

Contents

目　　次

This is a blank page.

CHAPTER 1

Accelerator Operation and Development

This is a blank page.

1.1 Operation and usage of tandem accelerator and booster

M. Sataka[1], Y. Tsukihashi[1], S. Hanashima[1], S. Abe[1], N. Ishizaki[1], A. Osa[1], M. Matsuda[1], T. Nakanoya[1], H. Kabumoto[1], N. Nakamura[1], K. Kutsukake[1], Y. Otokawa[1], and T. Asozu[1]

The tandem accelerator and booster were operated for experiments from May 21, 2007 to July 10, 2007, and from January 28, 2008 to May 15, 2008. The total operation time of the tandem accelerator for FY2007 (from April 1, 2007 to March 31, 2008) was 105 days and 23 different beams were delivered for experiments. The experimental proposals and the usage of the beam times for FY2007 are summarized in table 1 and table 2, respectively.

In FY2007, we had a maintenance period of 6 months for replacing the aged coil inside the 180 degree bending magnet in the terminal. In this period, the 10 GHz in-terminal ECR ion source, NANOGAN, was replaced with the 14.5 GHz ECR ion source, SUPERNANOGAN. The beam-line components at the terminal were also realigned. This alignment greatly improved the transmission of ion beams through the terminal. As a result, we have achieved the acceleration of a 3μA proton beam and a 1.3 particle μA fluorine beam.

Table 1. Experimental Proposals.

Research proposals accepted by the program advisory committee:	
In-house staff proposals	6
Collaboration proposals	33
Number of experiment proposed	56
Total number of scientists participating in research	
from out side	239
in-house	269
Number of institutions presented	36

Table 2. Usage of beam-times in different research fields.

Research field	Beam time	
	(days)	(%)
Nuclear physics	42	40.0
Nuclear chemistry	11	10.5
Atomic and solid state physics	10	9.5
Radiation effects in materials	26	24.8
Accelerator development	16	15.2
total	105	

[1] Japan Atomic Energy Agency (JAEA)

Distributions of the terminal voltage and ion species for experiments are shown in fig. 1 and fig. 2, respectively. Most of the beams were extracted from three negative ion sources, SNICS-2. The hydrogen beam and multiply charged ion beams of nitrogen, oxygen and rare gases were accelerated from the in-terminal ECR ion sources. The ECR ion sources were used as much as 38 % of all the beam time.

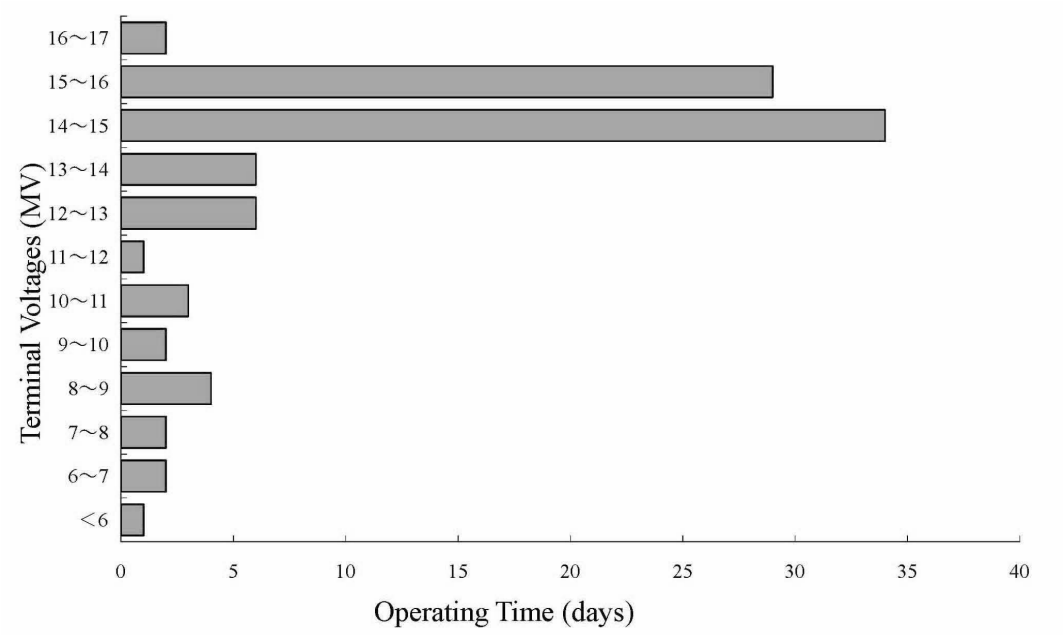

Fig. 1 Distribution of terminal voltages.

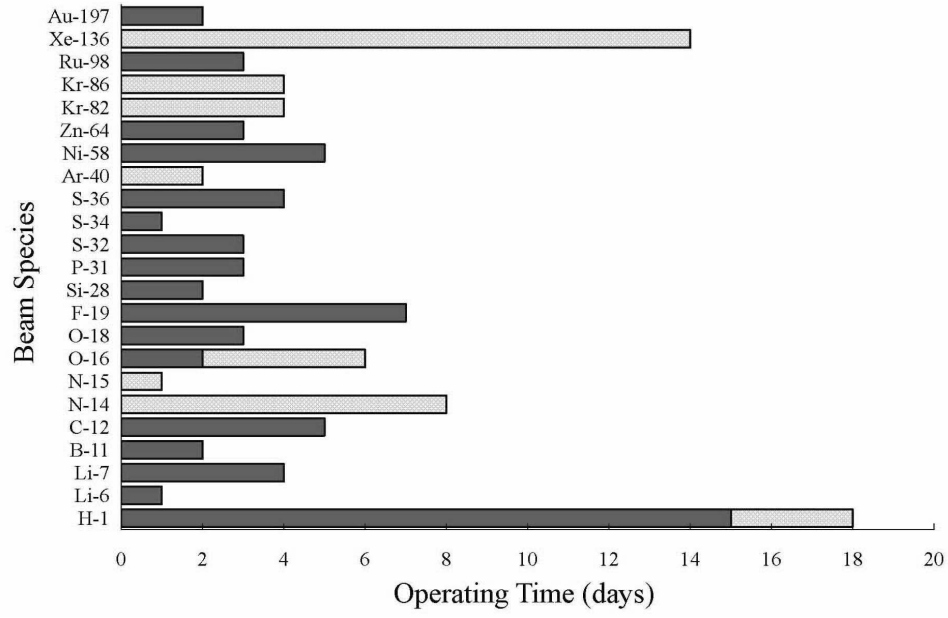

Fig. 2 Distribution of beam species accelerated for experiments.
Dark and light color bars represent ion beams supplied by negative ion sources and in-terminal ECR ion source, respectively.

The super-conducting booster was operated for a total of 19 days to boost the energies of 7 different beams from the tandem accelerator, as is summarized in table 3. These beams were used for experiments of nuclear physics. Eight resonators out of 40 resonators had been treated by a high-pressure water jet spray rinse (HPWR). Although the accelerating field gradients of these resonators were well recovered by HPWR, there have been some decreases in those gradients one year after HPWR.

The ^{7}Li and proton beams were supplied to the TRIAC (Tokai Radioactive Ion Accelerator Complex) experiments for 9 days. The radioactivities of ^{8}Li, ^{123}In, and ^{143}Ba were ionized and separated by ISOL and injected into the TRIAC.

Table 3. Boosted ion beams for experiments.

Beam species	Boosted energies (MeV)	Beam times (days)
^{18}O	180	3
^{36}S	345	1
^{58}Ni	205-245 (15 energy points)	3
^{64}Zn	344	3
^{82}Kr	380	3
^{86}Kr	395-437 (25 energy points)	3
^{98}Ru	430	3

1.2 KEK-JAEA Joint RNB Project

TRIAC Collaboration[1]

The Tokai Radioactive Ion Accelerator Complex (TRIAC) is operating for nuclear physics and materials science experiments at the JAEA-Tokai tandem accelerator facility under the collaboration between KEK and JAEA (TRIAC collaboration). In FY2007, we developed medium-mass radioactive ion (RI) beams. Radioisotopes of ^{123}In and ^{143}Ba, especially required in experimental proposals, were successfully accelerated up to 178 keV/*A*. Their intensities at the secondary target were ~10^4 particles/sec. Produced by the proton-induced fission reactions of $^{nat}UC_x$, they were extracted and mass-separated as singly charged ions by the isotope separator on-line (ISOL) of JAEA. They were charge-bred to higher charge states with a charge-to-mass ratios of about 1/7 by the charge-breeding electron cyclotron resonance ion source (CB-ECRIS) called as KEKCB. And then the charge-bred radioactive ions were accelerated by using a series of heavy ion linacs, the split-coaxial radiofrequency quadrupole (SCRFQ) and the inter-digital H (IH) linacs. The acceleration of the radioactive ion beams charge-bred by CB-ECRIS was the first time over the world.

The developments for acceleration of medium-mass radioactive ion beams were focused on improving the CB efficiency (ε_{CB}) and the vacuum at the low-energy beam line for better transport efficiency. The ε_{CB} for metallic elements increased from 0.1% to about 2% by tuning the injection of singly charged ions from ISOL to the KEKCB with double collimators. In the case of noble-gas element of Kr, we achieved that ε_{CB} was larger than 8%. For the highly charged ions in flight along the low-energy beam line, high vacuum is necessary to reduce their electron capture rates through the collisions with residual gases. To obtain high vacuum, we installed five cryopumps along the beam line. In a case of $^{129}Xe^{19+}$, the escape fraction to lower charge states reduced from 40% to 20%. The total transmission from ISOL to the secondary target including ε_{CB} was about 2%, especially for gaseous RI.

Under a typical charge breeding condition of the KEKCB , we have observed background of several nAs in the region of A/q of around 8 and between 6 and 7, presently and in future interested at TRIAC, respectively (refer to fig. 1). It is a challenging problem in the development of the ECR charge breeder for radioactive ion beam facilities how to reduce the background components (dotted line in fig. 1) in the ion spectrum, which would be an intolerable problem in experiments using the RI beams. We have tried to reduce such contaminations by careful selection of the inner-wall materials of the ECR plasma chamber. As such an effort, we first identified the background ions by acceleration. Measuring their total energy, we can identify their masses since their acceleration ends up with the same energy per nucleon. The background ions of a specific value of A/q were selected by the analyzing dipole magnet and the slits at the focal point of the magnet. The mass resolving power of the magnet is about 100 with the horizontal slits of ±1 mm. For the impurities at A/q = 7.68 which corresponds to $^{123}In^{16+}$ requested for the β-NMR experiments at TRIAC,

[1] Corresponding author, S.C. Jeong : High Energy Accelerator Research Organization (KEK)

we observed various heavy elements (light transition metals and Mo) with the intensity of $10^{7\sim8}$ particles/s, possibly originating from the inner-surface of the plasma chamber heavily contaminated in the fabrication. Afterwards we changed the materials facing ECR plasma to aluminum (A1050 and A6030 in Japanese Industrial Standards). Before installing, we made clean their surface by a sand-blasting and high-pressure distilled-water jet rinsing. As a result, the metallic elements almost disappeared and the intensity was dramatically reduced to ~600 particles/s. The remaining impurities turned out to be Kr, which is naturally abundant in residual gases inside KEKCB. When the A/q is defined more rigorously by horizontal slits, say ±5 mm to ±1 mm, the reduction by more than a factor of 5 (almost one order of magnitude) is expected at the expense of the reduction of what we want by a factor of 2. We also examined the region of A/q between 6 and 7, where background ions was about 1nA as shown in fig. 1. As an example, we looked at A/q of 6.45, which was very close to 6.4 ($^{32}S^{5+}$) and 6.5 ($^{13}C^{2+}$) with the horizontal slits of ±1 mm. The background intensity after acceleration was found to be several tens per second. It should be noted that the intensity of background components measured at the focal plane of the analyzing magnet of the KEKCB was about 1 nA, regardless of the surface-cleaning: Most of them were removed not only by additional beam optics fine-tuned to A/q of 6.45 in the beam transport line of TRIAC but also during acceleration.

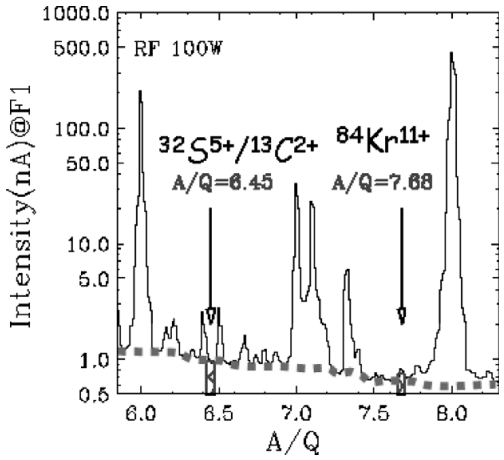

Fig. 1 A/q distribution of ions at the focal plane of the analyzing magnet of KEKCB. The A/q selections introduced for further transport and acceleration are indicated by arrows. Residual ion species very close to the selections are also presented. The dotted line representing continuous background ions is introduced just for eye-guide.

The following experiments were carried out in FY2007 using the RI beams of ^{8}Li, ^{123}In, and ^{143}Ba from TRIAC: (1) Measurement of Li diffusion coefficients in Li ionic conductors (RNB07-J02). (2) Development of the spin-polarized beam with tilted foils for spectroscopic studies on nuclear structure (RNB07-K02, K03). (3) Search for the time reversal symmetry break by using spin polarized RI beams (RNB07-K04).

Some details of the experiments can be found elsewhere in this report.

1.3 Impedance measurement of the bending magnet in the Tokai-Tandem high voltage terminal

S. Hanashima[1]

In the annual report of fiscal year 2006, we have reported about the impedance measurement [1]. In this fiscal year, we started the design work of the power supply. On the other hand, the coil of the bending magnet have been replaced to new one, as a part of overhaul processes of the magnet in its old age. The new coil has somewhat different specifications against old one. So, we measured the impedance for the new coil. The new measurement was made using an FFT (Fast Fourier Transform) analyzer.

The previous measurement for the old coil was made using a sine wave generator, a power amplifier and a digital storage oscilloscope. Measurements for several frequency points were treated one by one, so the process was very time consuming and it was difficult for us to view whole profile of the circuit in the data collecting stage. After the measurements, we got a new tool, FFT analyzer. In a method using FFT analyzer, the signal source was a pseudo random noise generator. The noise was fed to the coil through a power amplifier. The coil current was converted to a voltage signal by a current probe. The FFT analyzer sensed the voltage fed on the coil through channel number 1 and the current signal form the current probe through channel number 2, simultaneously. The admittance of the coil was analyzed as a transfer function from the coil voltage to the coil current. A wide frequency range of the admittance data could be acquired in a run in this method. In our measurements, range from 0.01Hz to 100kHz was covered by 3 frequency bands. The acquired data were processed to suppress large noises and to reduce number of data points for lightening the burden of later processing. Figure 1 shows the processed data, which have been used to design the power supply. There is a clear resonance near 22kHz. We found an anomaly around that region in the previous measurement, but the resonance was not realized at that time, because data points were sparse. The amplitude of the admittance in the figure represents conversion factor from a voltage ripple to a current ripple at a specified frequency. For example we are interested in harmonics of 400Hz, especially 1.2kHz, because our power supply works on AC 400Hz 3-phase primary power. The graph shows that the admittance at the 1.2kHz is about $7x10^{-3}$ ohm^{-1}. It means that if ripple voltage at 1.2kHz is 1 volts, associated ripple current is about $7x10^{-3}$ amperes (1V x $7x10^{-3}$ ohm^{-1}).

In the design process of the power supply, the measured data are used. Figure 2 (a) shows a design example for a power module of the supply. In the design, 4 identical power modules work parallel to establish desired output power. Figure 2 (b) shows a simplified model of the power stage. The model of magnet coil is connected to the output of the fig. 2 (b) to construct a simulation model from the duty cycle control of pulse width modulation(PWM) to the magnet current. Figure 3 shows the results. In the calculation, the magnet model is given by a table, and a model of the power modules is set by mathematical formulas on a spreadsheet. It must be noted that the result is not applicable directly to the frequency region above about

[1] Japan Atomic Energy Agency (JAEA)

one 10th of PWM switching frequency. There is a sharp change of phase near 1.2kHz, caused by a second order low pass filter for the PWM output. It is desired to shift the frequency to reduce ripple, because the frequency is very close as the third harmonics of the primary AC supply.

We must add a current sensor and an error amplifier working as a loop filter to the model to close a feedback loop. The loop filter must fulfill both terms for stability of feedback loop and terms for suppressing disturbances in a level desired as the power supply for the bending magnet. The information about the impedance of the magnet eases the design process.

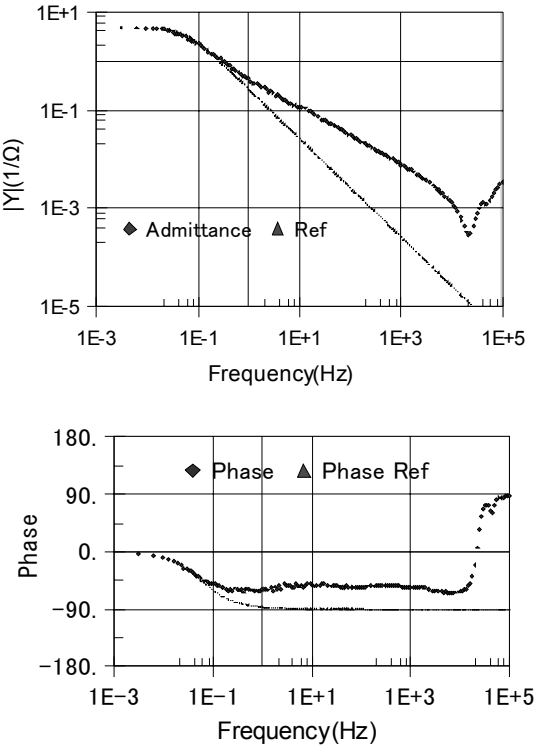

Fig. 1 Admittance of BM TL-1. Arranged to use power supply design from raw data obtained by the FFT analyzer. Characteristic of a series circuit of 0.2Ω resister and 0.6H inductance is also shown for comparison.

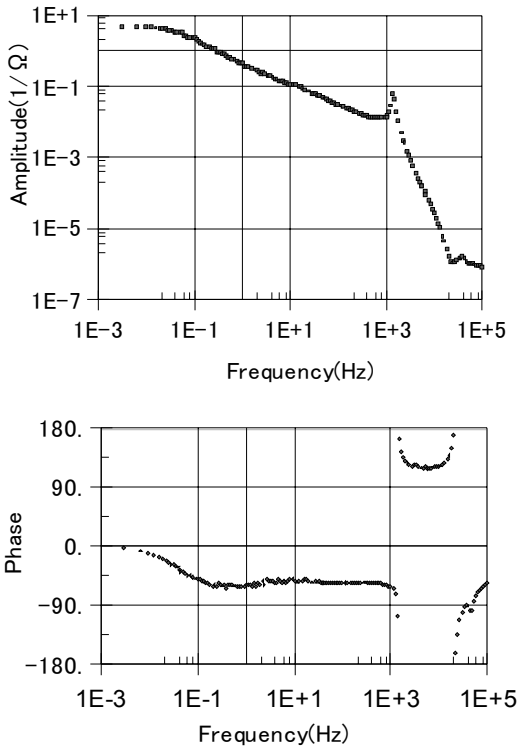

Fig. 3 Simulated transfer function from PWM control to current output.
Note that 180º is associated to -180º.

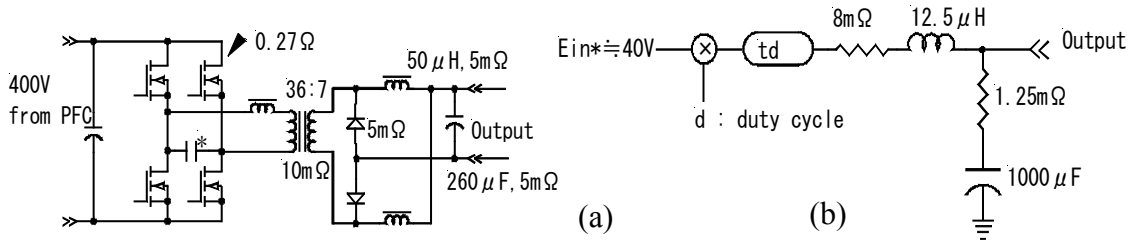

Fig. 2 Example circuit of power module for the power supply and simplified simulation model.

Reference

[1] S. Hanashima, JAEA-Tokai TANDEM Ann. Rep. 2006, JAEA-Review 2007-046 (2008) 6.

1. 4 Beam acceleration results of the new 14.5 GHz in-terminal ECR ion source

M. Matsuda[1], T. Asozu[1], T. Nakanoya[1], Y. Otokawa[1], K. Kutsukake[1], and S. Hanashima[1]

In-terminal ECR ion source [1] was upgraded by employing a high performance all-permanent-magnet type 14.5GHz ECR ion source SUPERNANOGAN in place of a compact 10GHz ECR ion source during a long maintenance period in FY2007. The arrangement of the new ion source is shown in fig. 1. For this upgrade, an extractor electrode and an einzel lens were replaced to the optimized ones.

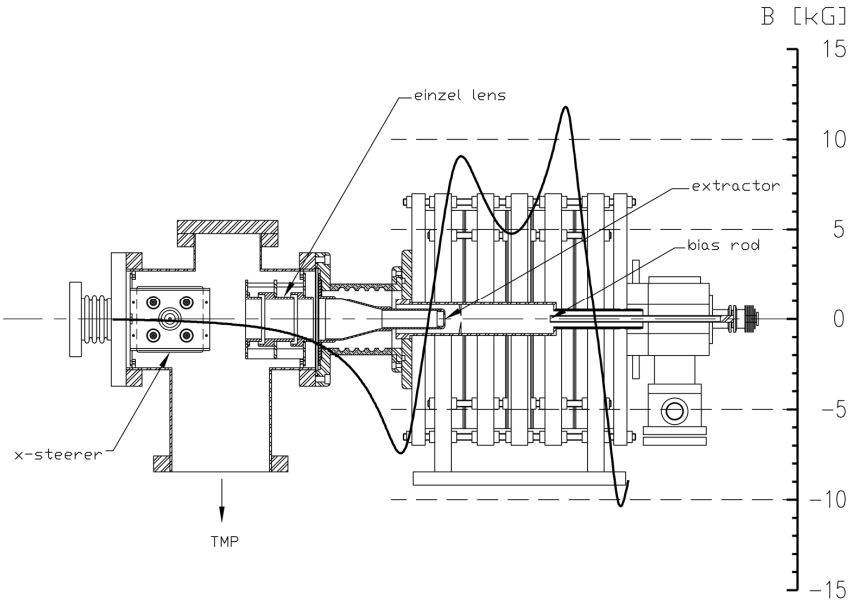

Fig. 1 Cross section of the new 14.5GHz in-terminal ECR ion source with electrode. The solid curve corresponds to the axial magnetic field distribution.

The RF system of the ion source was replaced because of the frequency change to 14.5 GHz. A traveling wave tube (TWT) module with 200W output is used as the main amplifier and its power consumption is only 800W. To protect it from compressed insulation gas and electric surges from a high voltage discharge, TWT, DC power supply, oscillator, and attenuator for the output control were put into the pressure-resistant container which kept the inside at 1 atm. regrettably, RF output power was limited to 16 W due to a trouble of the circulator at the amplifier output.

For an ECR ion source composed of powerful permanent magnets, the influence of leakage magnetic fields on an ion beam can not be ignored. We measured magnetic field on a vertical beam line in the terminal and found a maximum field of 2mT. This much leakage makes beam acceleration difficult because it bends a beam far beyond a tolerance of about 2mm. Especially, in the beam acceleration from the negative ion source, this is an important problem because it is not possible for our concerned beam handling system to correct such a steered beam orbit. In a simple calculation for the case of accelerating a hydrogen beam from

[1] Japan Atomic Energy Agency (JAEA)

the negative ion source at the terminal voltage of 15MV, the beam orbit is steered by about 25mm at the entrance of 180 degree bending magnet. Therefore, we made a new shield panel which covered up the ion source and its extraction and focus chamber with 3.2mm thick iron plates. With the iron shield, the leakage magnetic field was suppressed to about 1/50 and there was no beam steering problem in actual acceleration of negative ion beams after the upgrade.

Highly charged krypton and xenon ions were accelerated from the tandem accelerator. The intensities of these ions are shown in fig. 2. The beam handling from the new ion source was easily done in the same way as the old 10GHz in-terminal ECR ion source. The extracted ion beam was stable and the beam transmission efficiency was nearly 100% for acceleration from the terminal to the tandem exit. The intensities were increased 3-5 times as much as those before. Xenon ion energy reached 375MeV which is the highest energy this tandem ever had.

The highly charged ion intensities which were generated by an RF output of 16W agreed with the result of our bench test. We, therefore, expect that beam intensities will be increased ten times by fixing RF amplifier system.

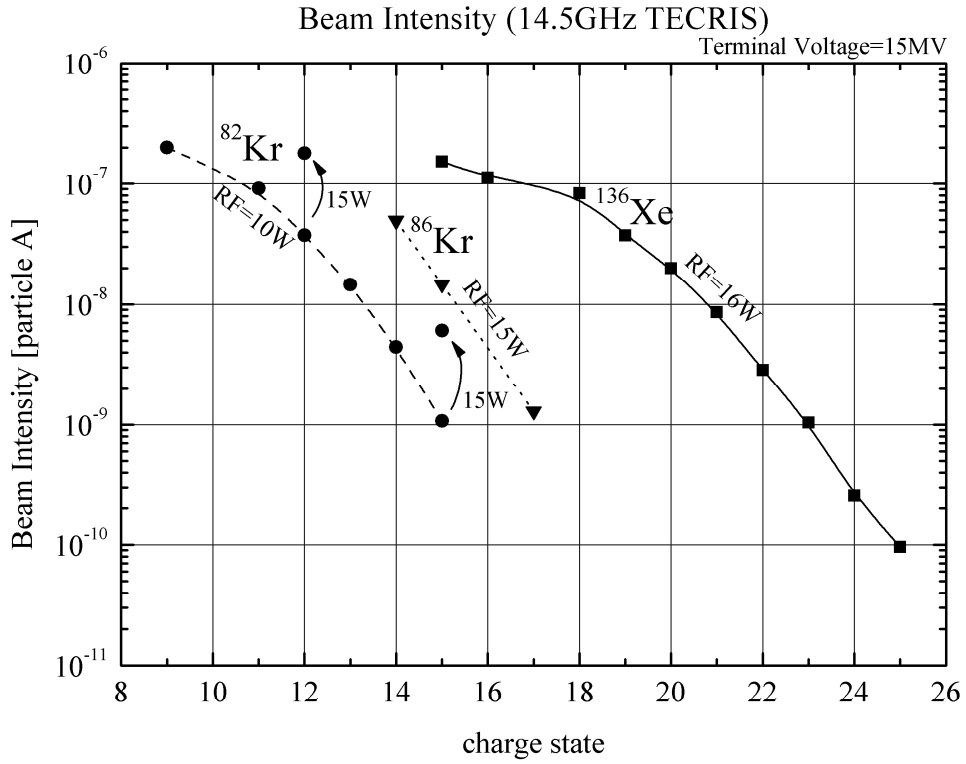

Fig 2. Charge state distributions of Kr and Xe ions from 14.5GHz in-terminal ECR ion source. Beam intensities were measured at exit of accelerator.

References

[1] M. Matsuda *et al.*, JAEA-Tokai TANDEM Ann. Rep. 2005, JAEA-Review 2006-029 (2006) 14-15.

1. 5 Study for installing a beam profile monitor in the high-voltage terminal

T. Asozu[1] and M. Matsuda[1]

Many control devices are installed in the high voltage terminal of the JAEA-Tokai tandem accelerator. In the terminal, ion beams are bent 180°by a bending magnet (BM) and focused at the entrance of the high energy acceleration tube by three electrostatic quadrupole triplet lenses (EQ) as shown in fig. 1. The beam optics has a high degree of freedom so that it needs precise control in the terminal. Then we planned to install a beam profile monitor (BPM) to monitor the beam profile at the last waist point in the terminal. The BPM has a wire which turns and crosses a beam in two (x and y) directions during a turn so that secondary electrons from the wire can be collected to produce a signal in a series of x and y beam profiles (see fig. 4). And we can see spreading widths and center positions of a beam on a display. Figure 1 also shows the location where the BPM will be installed.

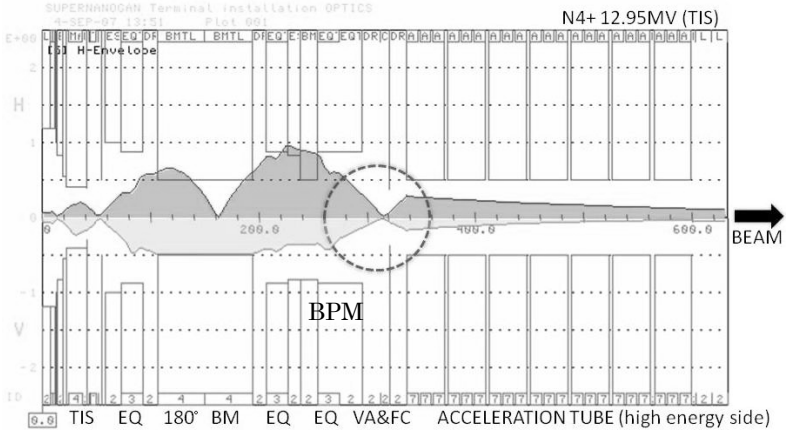

Fig. 1 Calculated beam envelope and the location of the terminal BPM.

The BPM must be insulated electrically from outside of the high voltage terminal. Then we designed a terminal BPM system using fiber-optic modules as shown in fig. 2. We receive BPM signal through fiber-optic modules and control the gain of the signal by the BPM controller and CAMAC system. For accelerator operation, the BPM signal should be sent and received quickly in real time. Then we use fiber-optic modules for transmitting BPM instead of using an existing CAMAC system. We use a plastic optical fiber of which insulation quality has been established well in transmitting signals from CCD camera looking at an electron-stripping carbon foil in the terminal.

The fiber-optic modules were checked, and the linearity and frequency response were observed (see fig. 3). Though the linearity was limited by an output voltage of 5V, we could control the gain of BPM signals with the BPM controller.
The frequency components of BPM signal spread over a range of about 30~10k Hz and the frequency response covered the range as is seen from the curve in fig. 3. These modules were also tested with signals from BPM I1-1 which was actually monitoring an ion beam, and we found out the beam profiles shown in

[1] Japan Atomic Energy Agency (JAEA)

fig. 4. Comparing two profiles of a raw signal from the BPM and a signal transmitted through the fiber-optic modules, the latter one shows distorted profiles. The distortion was caused by AC coupling between the two fiber-optic modules. The distortion is not so serious for our purpose to manipulate the beam, because we concentrate our attention to the beam spreading width and center position. As a result, it was found that the fiber-optic modules were useful to send and receive BPM signals.

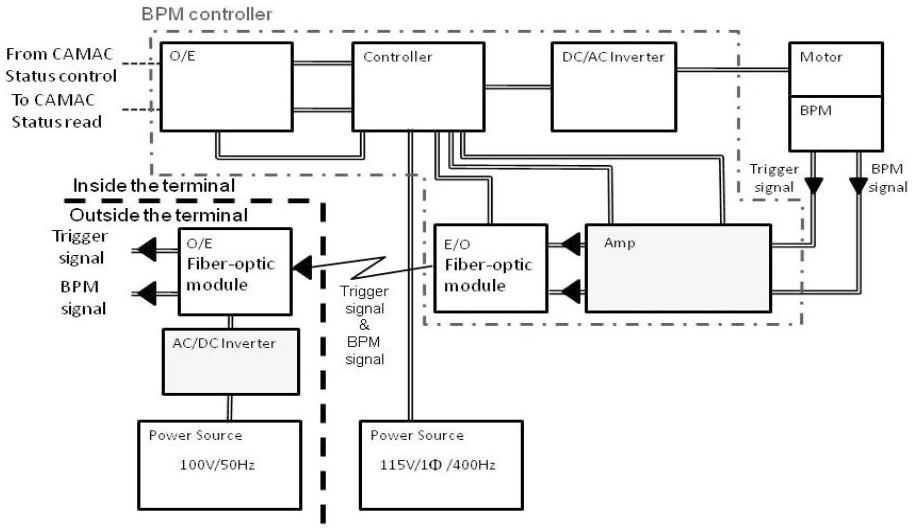

Fig. 2 Control block diagram for the terminal BPM system.

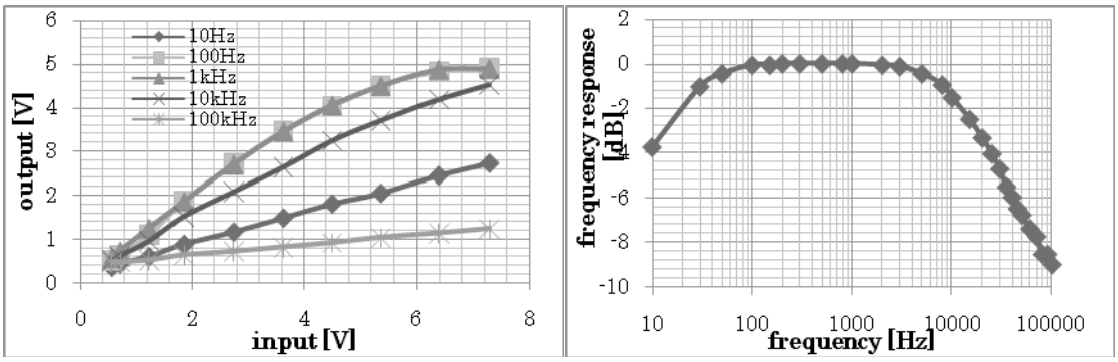

Fig. 3 Linearity (left) and frequency response (right) of the fiber-optic modules.

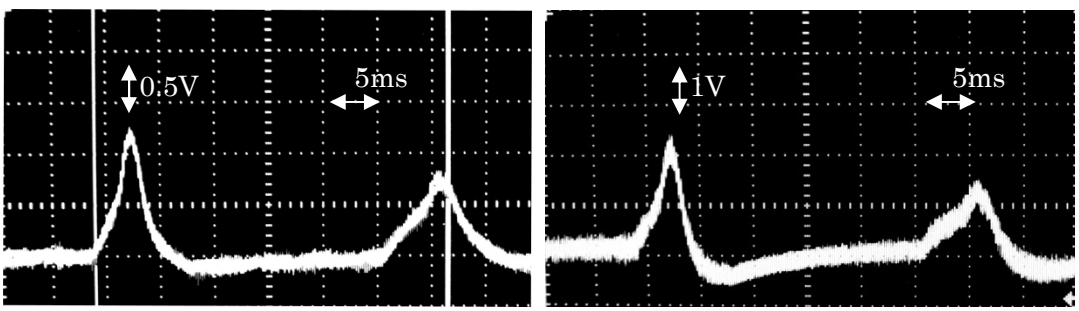

Fig. 4 BPM signals. Raw (left) and using fiber-optic modules (right).

1. 6 Performance test of low beta superconducting twin quarter wave resonator

H. Kabumoto[1], S. Takeuchi[1], N. Ishizaki[1], M. Matsuda[1], and Y. Otokawa[1]

We started development of superconducting twin quarter wave resonator (Twin-QWR) for the purpose of acceleration of low velocity heavy ions (β_{opt}=0.06) in FY2004, and fabricated a prototype Twin-QWR in FY2005. We carried out off-line performance test in FY2006, and confirmed the performance of that the quality factor (Q_0) was 2×10^8 at 4.2 K at low electric field, the acceleration electric field (E_{acc}) was 2.9 MV/m at RF power input of 4.0 W.

Figure 1 shows a cutaway drawing of Twin-QWR. We disassembled Twin-QWR because it was thought that the connection between top end plate and outer conductor was insufficient. Figure 2 shows the main parts of Twin-QWR. It consists of inner conductors made of pure-Nb and outer conductor made of Nb-Cu composite plate. The inner conductor part and outer conductor are connected by a superconducting Nb-gasket. We found that the Nb-gasket was dislocated by 0.4mm and not completely connected to outer conductor. We made the holder of Nb-gasket for the purpose of preventing dislocation, and assembled Twin-QWR again. Figure 3 shows the resonator Q_0-values at 4.2 K before and after changing the Nb-gasket. The performance of Twin-QWR was improved to Q_0= 9×10^8 at low electric field, and E_{acc}=5.8 MV/m at RF power input of 4.0 W. The Q_0-values degraded slightly around E_{acc}=6.0 MV/m, and the thermal breakdown was observed at E_{acc}=6.5 MV/m.

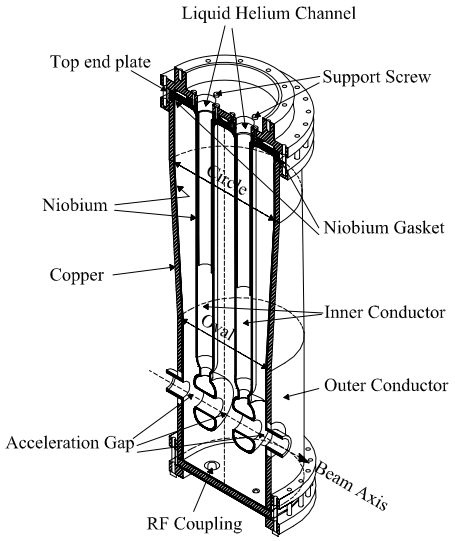

(Size：0.67m×0.24m×0.26m)

Fig. 1 Cutaway drawing of Twin-QWR.

Figure 4 shows the frequency shift as a function of helium pressure. This frequency instability happens because of the deformation of the top end plate by the helium pressure. This effect of Twin-QWR is bigger than that of QWR, because Twin-QWR has two inner conductors that affect the change of electric capacitance by deformation of the top end plate sensitively. The frequency shift of Twin-QWR was about 0.71 kHz/(kgf/cm^2), and it was about 2.6 times as large as QWR's 0.27 kHz/(kgf/cm^2).

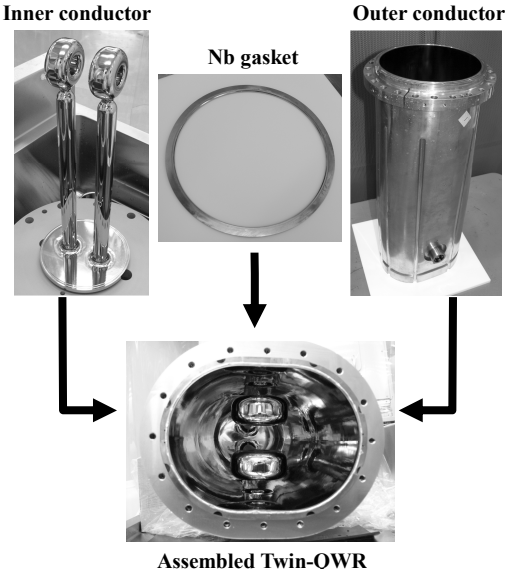

Fig. 2 Main parts and assembled Twin-QWR.

[1] Japan Atomic Energy Agency (JAEA)

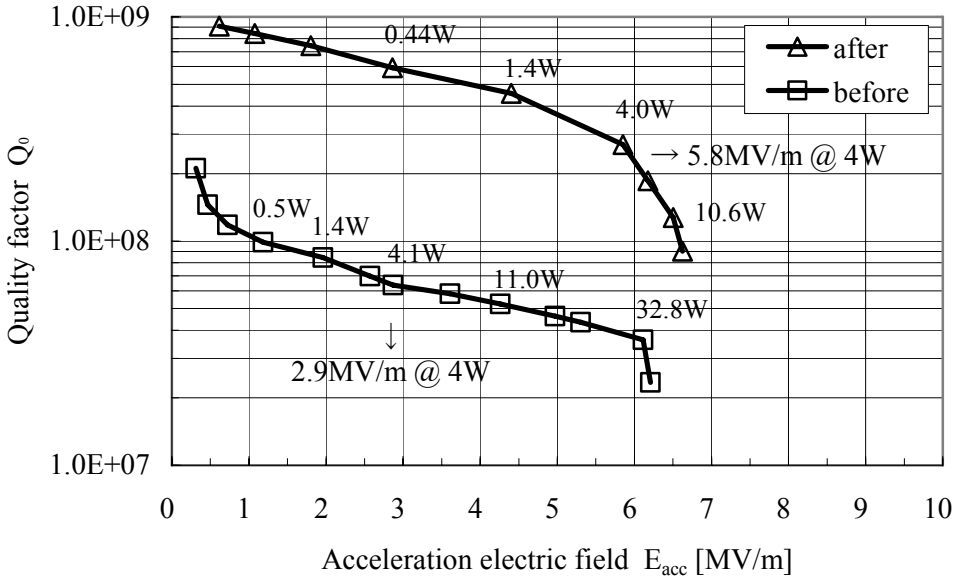

Fig. 3 Resonator Q_0-values at 4.2K before and after changing Nb-gasket.

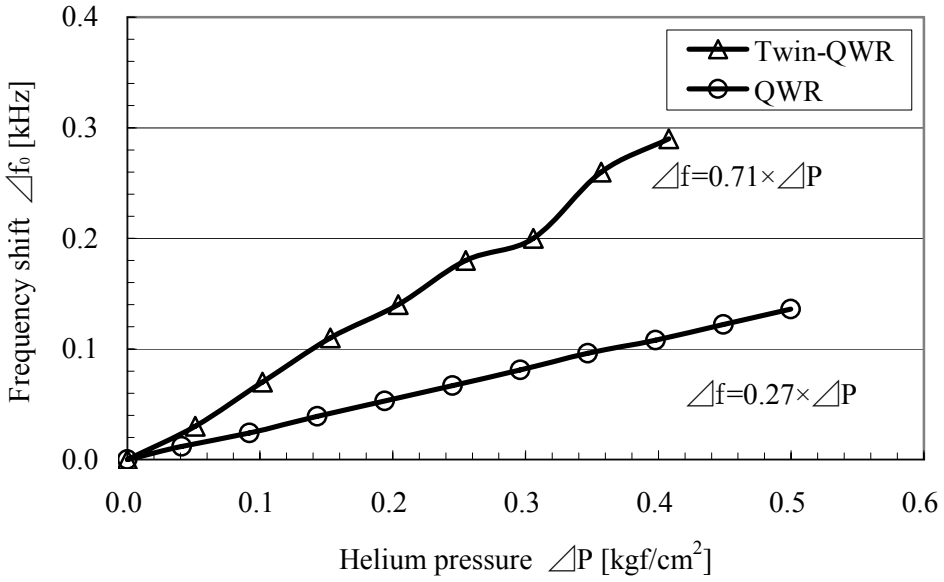

Fig. 4 Frequency shift of Twin-QWR and QWR as a function of helium pressure.

References

[1] H. Kabumoto *et al*., JAEA-Tokai TANDEM Ann. Rep. 2006, JAEA-Review 2007-046 (2008) 13-14.

[2] H. Kabumoto *et al*., JAEA-Tokai TANDEM Ann. Rep. 2005, JAEA-Review 2006-029 (2006) 12-13.

[3] H. Kabumoto *et al*., JAERI TANDEM Ann. Rep. 2003, JAERI-Review 2004-027 (2004) 13-14.

1. 7 Improvement of acceleration electric fields of superconducting booster resonators using high pressure water jet rinse

H. Kabumoto[1], S. Takeuchi[1], N. Ishizaki[1], T. Yoshida[2], T. Ishiguro[2], and K. Yamaguchi[2]

We curried out a high-pressure water jet rinse (HPWR) to on-line superconducting resonators (L37-L40) in FY2006, and it was confirmed that HPWR was effective for improvement of acceleration electric field. We carried out HPWR to other 8 resonators in FY2007 (L25-28 and L33-36). Our HPWR procedure is as follows. First, we rinse the resonators using methanol for the purpose of washing contaminations, like indium particles, oil and other chemical pollutions. Then, we do HPWR for two hours using water pressurized to 6-8MPa. We use the CO_2-melted water for the purpose of preventing anodizing the niobium surface. After HPWR, we rinse the resonators using methanol again for the purpose of early drying. Finally, we carry out mild baking at 120℃ for 2days at a pressure of ultra high vacuum.

Figure 1 shows the change of acceleration electric fields (E_{acc}) at RF power input of 4.0 W before and after HPWR. The E_{acc} of 8 resonators (L25-28 and L33-36) were improved after HPWR, and the average of E_{acc} at RF power of 4.0 W of 8 resonators was improved from 4.96 MV/m to 6.53 MV/m. We have measured the acceleration electric fields of L37-L40 resonators after one year from HPWR. The average of E_{acc} at RF power of 4.0 W was reduced from 5.91 MV/m to 4.94 MV/m.

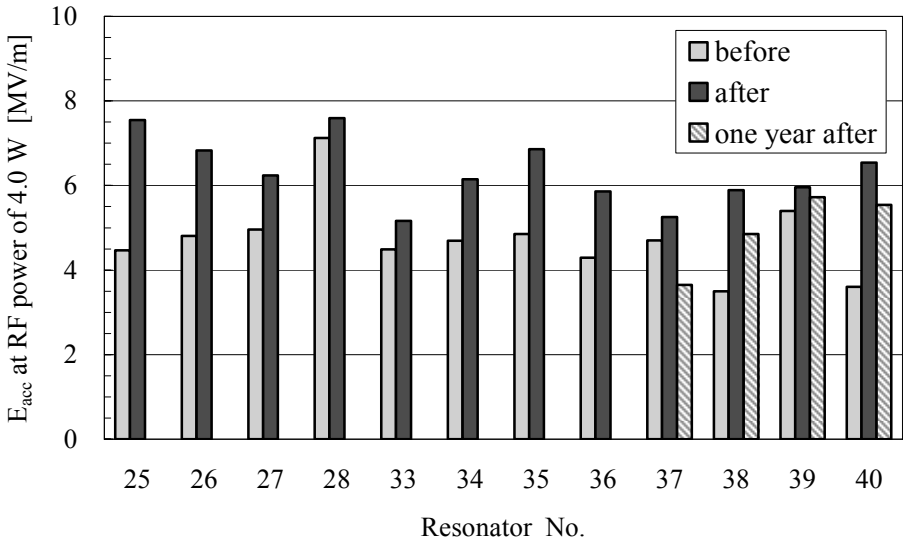

Fig. 1 E_{acc} at RF power input of 4.0 W before and after the HPWR.

References

[1] H. Kabumoto *et al*., JAEA-Tokai TANDEM ANN. Rep. 2006, JAEA-Review 2007-046 (2008) 15-16.

[1] Japan Atomic Energy Agency (JAEA)
[2] Atox Co., Ltd.

1. 8 Status of the JAEA-ISOL

Y. Otokawa[1], A. Osa[1], T.K. Sato[1], Y. Fuchi[2], and S. Ichikawa[1]

In the FY2007, the isotope separator connected on line to the JAEA-Tokai tandem accelerator (JAEA-ISOL) was operated 18 days to deliver radioactive nuclear beams (RNB) for experimental research programs. It was also operated 19 days for an ion-source development and to optimize the use of apparatus connected to the JAEA-ISOL.

We served RNB for experiments using two kinds of ion sources: a surface ionization-type ion source (SIS) and a forced electron beam induced arc discharge (FEBIAD) type one. A uranium-carbide target which used to produce neutron-rich nuclei in the proton-induced fission of ^{238}U, and thin metal-foil target for production of neutron-deficit nuclei in the nuclear fusion and nucleon transfer reactions, respectively, are available in both ion sources. Alkali, alkaline-earth and rare earth elements are effectively ionized by SIS and many volatile elements are ionized by FEBIAD type ion source. Provided RNB to the experiments are summarized in table 1.

As shown in table 1, we were successful in providing neutron-rich nuclei produced in proton-induced fission of ^{238}U, ^{123}In and ^{143}Ba, for acceleration with Tokai Radioactive Ion Accelerator Complex (TRIAC). Beam intensities including the ^{8}Li provided to TRIAC are shown in table 2. These intense beams were achieved by increase in the primary beam from the tandem accelerator which was progressed with precise realignment of beam optical devices. We confirmed that the neutron-rich RNB intensity was proportional to the primary beam one and both integrated-target-ion sources were steadily worked under experimental condition.

The acceleration of two neutron-rich RNB, ^{123}In and ^{143}Ba, with TRIAC were successfully performed for the first time. However, concerning experimental research program with TRIAC, tenfold and/or hundredfold intense RNB are required. For enhancement of the beam intensity, we have been developed FEBIAD-E type ion source which works at high temperature up to 2300K, and study of the configuration of the base material of the uranium-target to make short release time of fission products is under progress [1].

On the other hand, experiments scheduled at the irradiation room, where the JAEA-ISOL is installed in, becomes so tight and the residual radiation dose level has been so high. We have to think a safer procedure to exchange irradiated ion source at every experiments.

[1] Japan Atomic Energy Agency (JAEA)
[2] High Energy Accelerator Research Organization (KEK)

Table 1. Radioactive nuclear beams delivered to experiments using the JAEA-ISOL.

Date	RNB	Reaction	Ion source[1)]	Primary beam	Research program
28-29,May, 2007	^{94}Y etc.	^{238}U(p,f)	U-SIS	$^{1}H^{+}$/30 MeV	Decay spectroscopy
5-6,May, 2007	^{94}Y etc.	^{238}U(p,f)	U-SIS	$^{1}H^{+}$/30 MeV	Decay spectroscopy
11-14,Jun,2007	^{8}Li	^{13}C(^{7}Li,^{8}Li)	F-SIS	$^{7}Li^{3+}$/60 MeV	Development of TRIAC, Experiment use in TRIAC
13, Feb., 2008	^{21}Na	^{12}C(^{12}C,p2n)	F-SIS	$^{12}C^{5+}$/90 MeV	Development of RF linear-trap
18-20, Feb., 2008	^{94}Y etc.	^{238}U(p,f)	U-SIS	$^{1}H^{+}$/30 MeV	Decay spectroscopy
10-12,Mar., 2008	^{123}In	^{238}U(p,f)	U-FEBIAD	$^{1}H^{+}$/30 MeV	Experiment use in TRIAC
25, Mar., 2008	^{92}Rb, ^{142}Cs	^{238}U(p,f)	U-SIS	$^{1}H^{+}$/30 MeV	Development of RF linear-trap
26-27,Mar., 2008	^{143}Ba	^{238}U(p,f)	U-SIS	$^{1}H^{+}$/30 MeV	Experiment use in TRIAC

[1)] uranium-carbide target attached to the ion source indicated by U-SIS, U-FEBIAD and thin metal foil target attached to the ion source indicated by F-SIS, F-FEBIAD, respectively.

Table 2. Beam intensity of ^{8}Li, ^{123}In and ^{143}Ba providing to TRIAC.

RNB	Intensity	Ion source	Primary beam from Tandem accelerator
^{8}Li	1.0x10^{5} pps	F-SIS	$^{7}Li^{3+}$/60 MeV/83 pnA
^{123}In	1.0x10^{6} pps	U-FEBIAD	$^{1}H^{+}$/30 MeV/680 nA
^{143}Ba	1.4x10^{6} pps	U-SIS	$^{1}H^{+}$/30 MeV/1000 nA

References

[1] A.Osa *et al*., JAEA-Tokai TANDEM Ann. Rep. 2006, JAEA-Review 2007-046 (2007) 18.

1. 9 Development of ion source for the JAEA-ISOL

A. Osa[1], Y. Otokawa[1], T.K. Sato[1], and S. Ichikawa[1]

For the purpose of perturbed angular correlation measurements in solid state physics, we developed a metal foil target for the JAEA-ISOL to produce a radioactivity of ^{111}In ($T_{1/2}$=2.8047d). We are required to implant ^{111}In into sample in the dose of 10^{11}~10^{12} particles/sample. It corresponds to the intensity of several 10^5 pps and the irradiation time of 1 day. With this beam intensity and the long half-life of ^{111}In, the increase of ^{111}In radioactivity is only a few Bq/s, so that the method of radiation measurements is not useful for the beam handling. Therefore, we planed to produce short-lived isobars in heavy ion reactions, ^{111}Sb ($T_{1/2}$=1.25m) and ^{111}Sn ($T_{1/2}$=35.3m), in addition to the ^{111}In and separate them at the same time for the convenience of the beam handling.

The FEBIAD ion source is used for the ionization of indium, tin and antimony. A high-melting metal target, such as $_{41}$Nb, $_{42}$Mo and $_{45}$Rh, has to be used because the FEBIAD ion source for the heavy ion reactions is operated at a high temperature (about 1550 ^{o}C). A schematic view of the FEBIAD ion source is shown in fig. 1. A ^{nat}Mo target with a thickness of 3 μm was previously irradiated by ^{19}F ion beam to produce A=111 isobar. In this reaction, the intensity of ^{111}In beam was several 10^4 pps with the primary beam intensity of 100 p-nA. It is estimated that ^{96}Mo+^{19}F→^{115}Sb* is a major reaction to produce ^{111}Sb and ^{111}Sn. From the fact that natural abundance of ^{96}Mo isotope is 16.68%, it is expected that the sixfold intensity of ^{111}In beam when we use isotopically-enriched ^{96}Mo target.

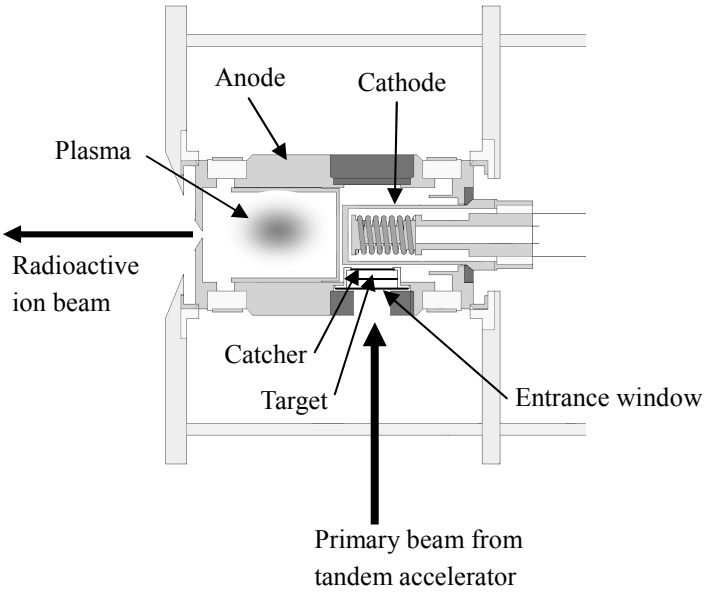

Fig. 1 Schematic view of the FEBIAD ion source.

[1] Japan Atomic Energy Agency (JAEA)

The enriched ^{96}Mo target is costly to prepare so that we made a comparison experiment of bombarding ^{12}C to the naturally mono-isotopic ^{103}Rh target; this reaction produces the same compound nucleus ^{115}Sb*. The intensity of ^{111}In beam was 1.1×10^5 pps with the primary beam intensity of 100 p-nA. However, the beam intensity was obviously decreasing as time went on. We found that Rh made a binary metallic alloy [1] with Ta, which was a structural material of the ion source, and melted in a few hours at the ion-source operational temperature.

We estimate to provide A=111 isobars beam with the intensities of several 10^5 pps. To satisfy the demands of users, we will proceed to investigate the intensities of A=111 isobars by improving endurance of the enriched ^{96}Mo target foil and the Ta foil for the primary beam entrance window, as well as another comparison experiment with a naturally mono-isotopic ^{93}Nb target and a ^{22}Ne beam.

Reference

[1] H. Baker, Editor, ASM Handbook. Vol. 3: Alloy Phase Diagrams, ASM International, New York (1992).

1.10 Electrostatic collection method for identification of natural radon (^{222}Rn)

M. Nakamura[1], M. Matsuda[1], T. Ishii[1], N. Ishizaki[1], A. Osa[1], T. Nakanoya[1], H. Kabumoto[1], K. Kutsukake[1], Y. Otokawa[1], T. Asozu[1], M. Asai[1], and T. Ohkura[1]

On an occasion of surveying contamination all over floors, alpha rays (0.06Bq/cm^2) were detected on the first basement passage of the Tandem Accelerator Facility. We attempted to identify the alpha-emitting nuclide in parallel with conducting more surveys in this area. In the survey, we found a crack of concrete at the spot where alpha rays were detected. We identified all nuclides emitting gamma rays at the crack as Naturally Occurring Radioactive Materials, (NORM: ^{40}K, ^{214}Bi, ^{228}Ac and so on) by in-situ gamma-ray measurement. Therefore, we inferred that radon seeped out of the crack.

Radon is not easy to be collected and detected because of its nature of noble gas. There have been several methods to measure natural radon in the atmosphere. One of them is the double filtering [1]: after separation of all radioactive gases except for radon at the first filter, radon is collected at the second filter. This method needs a long time (from hours to days) and large amount of sampling gas to measure. Another one is the electrode collection [2]: positively charged alpha-decay products of radon, for example ^{218}Po are collected at a negatively charged electrode. The concentration of radon is estimated by measuring its radioactivity. This measurement can be completed in several minutes because a half-life of ^{218}Po (3.05min) is fairly shorter than that of radon (3.8days). We needed to confirm promptly that radon seeped out of the crack, but not to measure the concentration (nor its time variation). And we were unprepared to carry out either of those methods which required a large apparatus connected to a power source. Therefore, we applied a new method which was speedier and handier than those methods.

We have developed an electrostatic collection method: after collection of ^{218}Po using a negatively charged Teflon sheet in place of the electrode collection, we measured alpha rays and gamma rays from this sheet. We identified decay products of radon (^{218}Po, ^{214}Pb and ^{214}Bi) with this collection method. Figure 1 shows the decay-curve of alpha rays which were measured by putting alpha-ray survey meter and the sheet face to face. The analyzed half-life was 3.45±0.45min; it indicated that purely ^{218}Po was collected on the sheet. Figure 2 shows that of gamma rays which were measured by putting the sheet in front of Ge detector several minutes after collected ^{218}Po have decayed. They were insulated by the lead shield to decrease background radiations. The analyzed half-life (25.6±4.7min) was coincident with that of ^{214}Pb. From these results, we have identified radon seeping out of the crack.

Our developed collection method has several advantages over the previous methods. First of all, this method is more convenient. All you need are alpha-ray survey meter and one sheet which gets easily negatively charged electrostatically, for example Teflon or polyvinyl chloride. Secondly, advanced

[1] Japan Atomic Energy Agency (JAEA)

measurements can be carried out, for example a half-life measurement because concentrated ^{218}Po on the sheet dose not diffuse quickly. After collection, you can identify ^{222}Rn immediately. Third, with portability of the collection sheet (we used a Teflon sheet: 5cm wide, 15cm long and 3mm thick), the sheet can be carried in low background environment to measure gamma rays more sensitively.

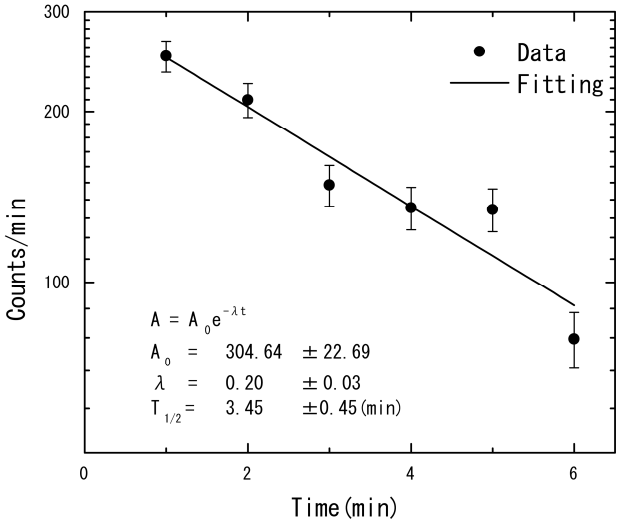

Fig. 1 Alpha-ray counts as a function of time with electrostatic collection method. The solid line is a fit with a single decay curve.

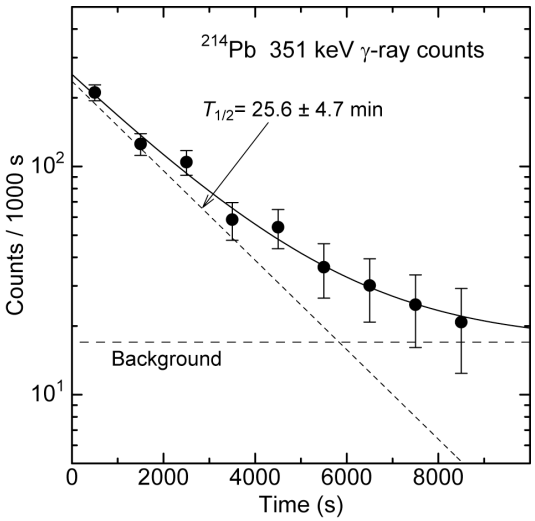

Fig. 2 Gamma-ray counts of ^{214}Pb 351keV as a function of time measured after collection of ^{218}Po on Teflon sheet. The solid curve is a fit with a single decay curve, inclusive of background.

References

[1] Thomas J.W. and LeClare P.C., Health Physics, 18 (1970) 113-122.

[2] G. Dalu and G.A. Dalu, Aerosol Science, Vol.2 (1971) 247-255.

CHAPTER 2

Nuclear Structure

This is a blank page.

2. 1 Study of high-spin states in ^{36}S and ^{36}Cl

E. Ideguchi[1], T. Morikawa[2], M.L. Liu[1], Y. Toh[3], M. Koizumi[3], A. Kimura[3], H. Kusakari[4], M. Oshima[3], B. Cederwall[5], K. Furutaka[3], Y. Hatsukawa[3], S. Mitarai[2], M. Sugawara[6], and Y. Zheng[1]

High-spin level structures of A ≈ 30 nuclei have been receiving increased attention in recent years [1,2]. In this region several interesting phenomena can be investigated such as violation of mirror symmetry, cluster structure, shape coexistence, and the interplay between single-particle and collective motion [1,2]. Among them ^{36}S is known as a puzzling nucleus, where several microscopic models such as configuration mixing and the shell model are unable to reproduce the B(E2;$2_1^+ \rightarrow 0_1^+$) value and inelastic proton scattering angular distribution [3,4]. The study of the high-spin level structures in ^{36}S and its neighboring nuclei will give a testing ground to the models and will help for solving the problem. In this report, experimental studies on high-spin states in ^{36}S and its neighboring nucleus ^{36}Cl were presented.

An in-beam γ-ray spectroscopy was employed to study high-spin states of ^{36}S and ^{36}Cl via a ^{18}O + ^{24}Mg fusion-evaporation reaction. The ^{18}O beam of 70 MeV was provided by the tandem accelerator of the Japan Atomic Energy Agency. A target of an isotopically enriched ^{24}Mg foil of 1 mg/cm^2 thickness with 8 mg/cm^2 ^{nat}Pb backing was used. Fourteen HPGe detectors with BGO anti-Compton shields from the GEMINI-II array [5] were used to detect γ rays in coincidence with a charged particle filter, Si-Ball [6]. The HPGe detectors were placed at 6 different angles, namely 47º (4 Ge's), 72º (2 Ge's), 90º (2 Ge's), 105º (4 Ge's), 144º (1 Ge) and 147º (1 Ge) with respect to the beam direction, which enables to perform angular distribution and DCO analyses. The Si-Ball consists of 20 ΔE Si detectors [6] surrounding the target. Events were collected when at least two HPGe detectors and one Si detector were fired in coincidence.

Based on the γ-γ coincidence relations, γ-ray energy sum, and intensity balances of the transitions, previously reported level scheme for ^{36}S [7] was confirmed up to the 6.69 MeV level. In the present study, new γ-ray peaks at 1182, 1315 and 2218 keV were identified in coincidence with a 3291 keV transition as shown in fig. 1. The results of the DCO analysis suggest stretched quadrupole character for the 1182 and 2218 keV transitions and dipole character for the 1315keV transition. In ^{36}Cl, high-spin levels up to $(7)^+$ state at 5.313 MeV were previously assigned. On top of the $(7)^+$ state a 466 keV transition was tentatively placed and it was reported to be in coincidence with 1019 and 2795 keV transitions from $(7)^+$ to (6^+) and from $(7)^+$ to 5^- levels, respectively [8]. Figure 2 shows the γ-ray energy spectrum by gating on a 466 keV transition and it was found that 1019 and 2795 keV peaks did not appear in the spectrum. Consequently, the 466 keV transition was assigned as de-exciting from the $(7)^+$ state in parallel with 1019 and 2795 keV transitions. After the γ-γ coincidence analysis of ^{36}Cl data, 16 γ-ray peaks were newly identified. Data analysis is in progress.

[1] CNS, University of Tokyo
[2] Kyushu University
[3] Japan Atomic Energy Agency (JAEA)
[4] Chiba University
[5] Royal Institute of Technology
[6] Chiba Institute of Technology

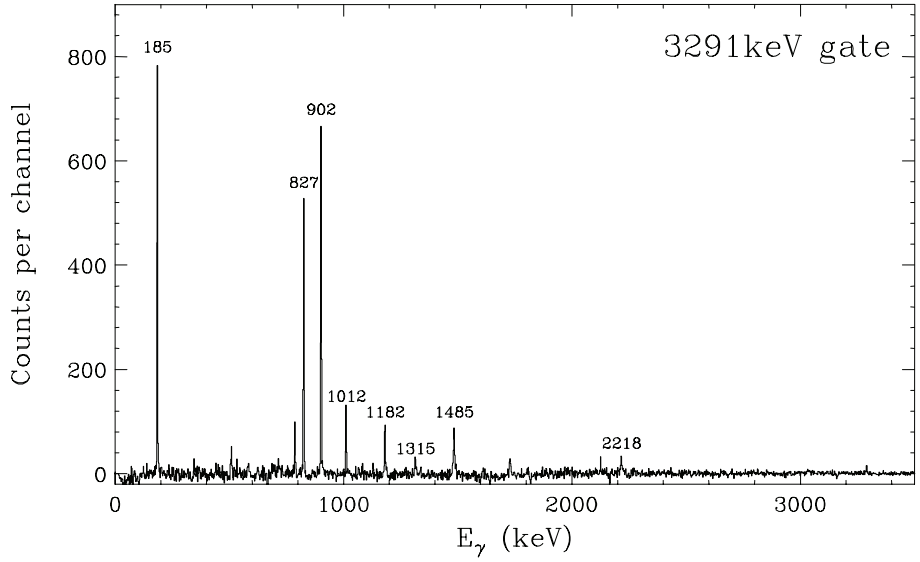

Fig. 1 γ-ray spectrum by gating on 3291 keV transition between 2_1^+ and 0_1^+ level in ^{36}S.

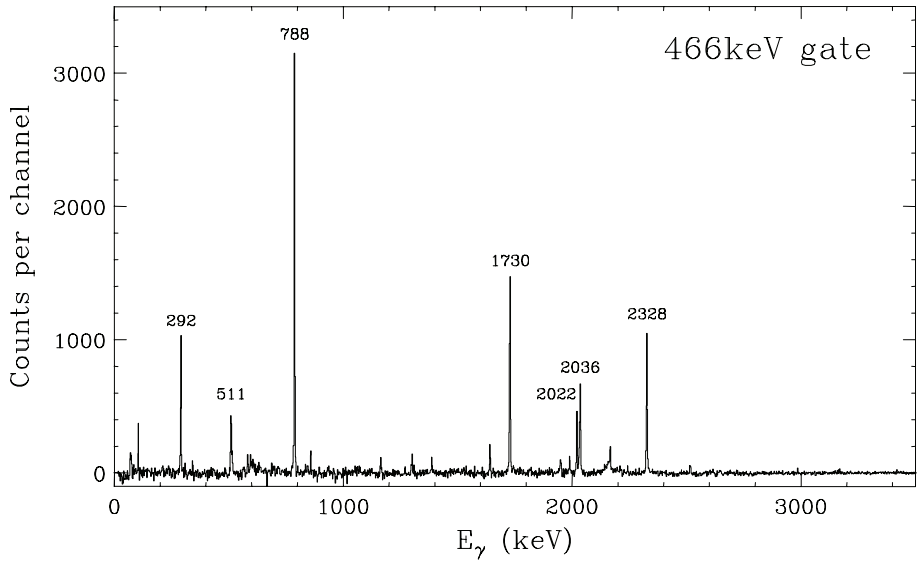

Fig. 2 γ-ray spectrum by gating on 466 keV transition in ^{36}Cl.

References

[1] P. Mason *et al*., Phys. Rev., C71 (2005) 014316/1-8.

[2] F. Della Vedova *et al*., Phys. Rev., C75 (2007) 034317/1-7, and references there in.

[3] F. Maréchal *et al*., Phys. Rev., C60 (1999) 034615/1-12.

[4] E. Khan *et al*., Nucl. Phys., A694 (2001) 103-131.

[5] M. Oshima *et al*., J. Radioanal. Nucl. Chem., (2008) to be published.

[6] T. Kuroyanagi *et al*., Nucl. Instrum. Methods Phys. Res., A316 (1992) 289-296.

[7] X. Liang *et al*., Phys. Rev., C66 (2002) 014302/1-4.

[8] E.K. Warburton *et al*., Phys. Rev., C14 (1976) 996-1009.

2. 2 Spectroscopy of ^{38}Cl

T. Morikawa[1], E. Ideguchi[2], M.L. Liu[2], Y. Zheng[2], M. Oshima[3], M. Koizumi[3], Y. Toh[3],
A. Kimura[3], A. Osa[3], H. Harada[3], K. Furutaka[3], S. Nakamura[3], F. Kitatani[3],
Y. Hatsukawa[3], M. Sugawara[4], H. Kusakari[5], and S. Mitarai[1]

Motivated by the recent discovery of an island of inversion [1], a systematic investigation of high-spin states in nuclei in neutron-rich A = 30 ~ 40 region has been underway as a cooperative study at the JAEA tandem accelerator facility. Since the evolution of shell structure is a function of nuclear deformation and rotation as well as isospin, systematic understanding of high-spin levels in nuclei in the neutron-rich region is of great interest. Identification and study of the levels involving the {sd} to {fp} cross-shell excitation would be a key to clarify the evolution of N = 20 neutron shell gap.

The excited levels in ^{38}Cl have been investigated by using an ^{18}O + ^{26}Mg reaction at 3.72 and 5.00 MeV/u. The ^{18}O beams delivered from the JAEA tandem accelerator were incident on the 4 mg/cm^2 thick ^{26}Mg target. γ-rays were detected with the GEMINI-II Ge detector array [2]. The VME-CAMAC based data acquisition system was triggered by the γγ two-fold events within a 1 μsec coincidence window. Data were stored on the HDD storage of a UNIX PC and were off-line sorted into γγ correlation matrices for the detailed analysis. A γ-ray spectrum gated by transitions in ^{38}Cl is presented in fig. 1. Based on the γγ coincidence relations, γ-ray energy sum and intensity balance, the level scheme of ^{38}Cl has been extended up to the $J^{\pi} = (8^+)$ state at 4836 keV. As the result, ^{38}Cl has turned to be the heaviest chlorine isotope of which the high-spin states are identified. Spin assignments of the new levels were tentatively made by using the coincidence relation and the observed γ-ray anisotropy with respect to the beam direction. Based on the consideration that the heavy-ion induced fusion reaction predominantly populates the yrast levels while the maximal spin for the $\pi\{0d_{3/2}\}^1 \otimes \nu\{0f_{7/2}\}^1$ configuration is J = 5, the assignment of the negative parity for the states of J > 5 may be unlikely.

For the comparison with the nuclear theory, shell model calculations were performed in the $\{1s_{1/2}, 0d_{3/2}, 0f_{7/2}, 1p_{3/2}\}$ model space by using the jj-coupled shell model code jjSMQ [3] with the surface delta interaction (SDI) as presented in fig. 2. The two-body matrix elements were calculated with the strength parameters A_0 = 0.90 and A_1 = 0.56, which are known to give a very good reproduction of the level structure of ^{43}Sc by using the $0d_{3/2}$-$0f_{7/2}$ shell gap of 4.9 MeV [4]. In the present case for the ^{38}Cl nucleus, however, the positive parity levels, i.e. $J^{\pi} = (6^+)$ at 3645 keV, $J^{\pi} = (7^+)$ at 3816 keV, and $J^{\pi} = (8^+)$ at 4836 keV, were found to be better reproduced with a smaller gap of 3.9 MeV. Since the similar trend is also seen in a ^{33}P nucleus [5], it might suggest a possible onset of the shell gap reduction in this region. The analysis is still in progress.

[1] Kyushu University
[2] CNS, University of Tokyo
[3] Japan Atomic Energy Agency (JAEA)
[4] Chiba Institute of Technology
[5] Chiba University

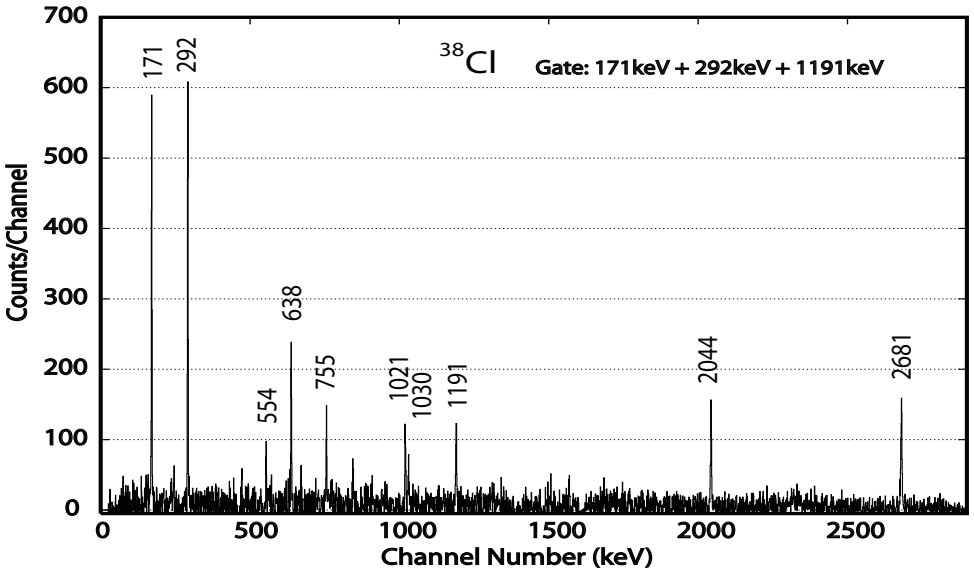

Fig. 1 γ-ray spectrum gated by the transitions in ^{38}Cl.

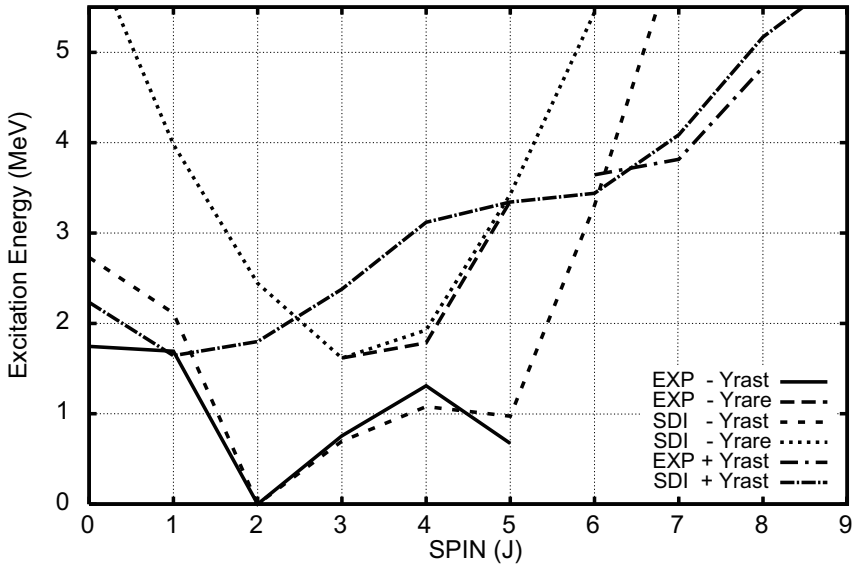

Fig. 2 A plot of ^{38}Cl levels in comparison with the shell model calculations using SDI. In the calculations, the gap energy between $0d_{3/2}$ and $0f_{7/2}$ single particle levels was chosen to be 3.9 MeV for better reproduction of positive parity yrast levels.

References

[1] T. Motobayashi *et al.*, Phys. Lett., B346 (1995) 9-14, and references therein.

[2] K. Furuno *et al*., Nucl. Instrum. Methods Phys. Res., A421 (1999) 211-226.

[3] K. Takada *et al*., code available at ftp.kutl.kyushu-u.ac.jp:/pub/takada/jjSMQ/ (accessed 2008-05-30).

[4] T. Morikawa *et al*., Phys. Rev., C70 (2004) 054323/1-7.

[5] T. Morikawa *et al*., Kyushu University Tandem Accelerator Laboratory Report Vol.10 (2007) 56-58.

2. 3 Study of low-lying collective modes in ^{100}Ru by multiple Coulomb excitation

Y. Toh[1], M. Koizumi[1], M. Oshima[1], A. Kimura[1], H. Harada[1], K. Furutaka[1], F. Kitatani[1], S. Nakamura[1], Y. Hatsukawa[1], A. Osa[1], M. Sugawara[2], and T. Morikawa[3]

Shape transitions of ground states can occur with the variation of neutron numbers in Ru isotopes. In fact the spherical shape for ^{98}Ru and deformed for ^{108}Ru are reported in theoretical studies[1,2]. Recently, Iachello has introduced an analytic treatment of critical shape transition point solutions with development of the new class of symmetries which are based on the solutions to different equation[3,4]. A dynamical symmetry called E(5) applies to nuclei undergoing transitions from spherical to γ-unstable shapes. Ruthenium isotopes are proposed to lie at this phase-transition point. Multiple Coulomb excitation is a useful method to deduce electromagnetic properties, which reflect shapes of nuclei, without taking into account the effects of nuclear interactions [5,6]. Therefore the low-lying excited states in ^{100}Ru were studied by Coulomb excitation experiment.

A 440 MeV ^{100}Ru beam was excited on a ^{208}Pb target with approximately 2 mg/cm^2 thickness. A γ-ray detector array, GEMINI-II (upgraded version of GEMINI [7]), consisting of 16 Ge detectors with BGO Compton suppression shields, was used to detect deexcitation γ rays. The Ge detectors were placed at θ = 47˚, 72˚, 90˚, 105˚, 147˚, and 144˚ relative to the incident beam. The scattered particles are detected with a position-sensitive particle detector system [8] with four plastic scintillators each of which is coupled to a position-sensitive photomultiplier tube. It covered approximately 30% of the total solid angle, ranging from

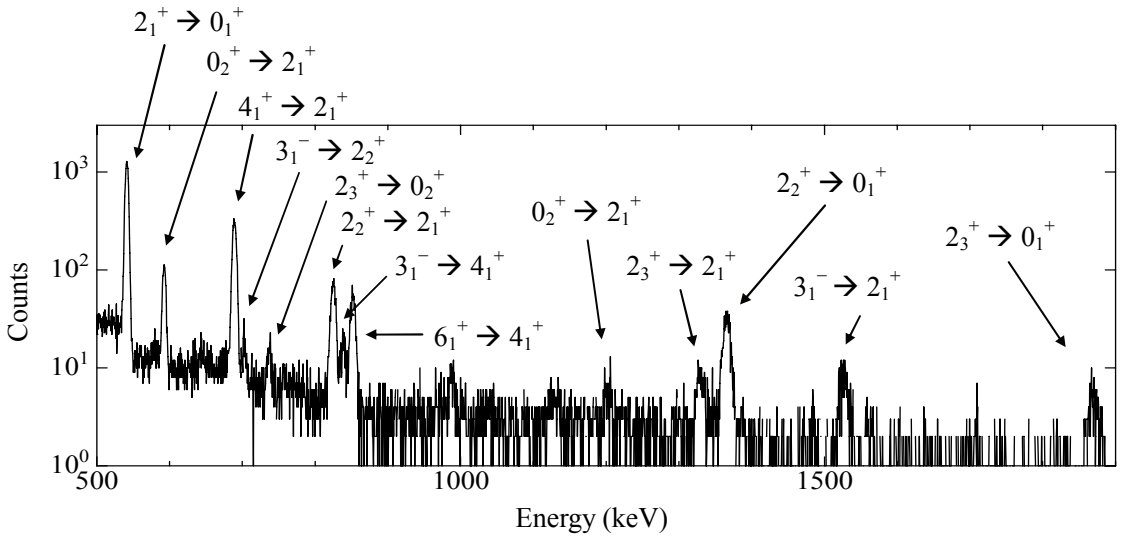

Fig. 1 An example of Doppler-shift corrected spectra. Thirteen peaks were identified as the γ rays of ^{100}Ru.

[1] Japan Atomic Energy Agency (JAEA)
[2] Chiba Institute of Technology
[3] Kyushu University

20° to 67° and from 113° to 160° to the incident beam direction. The angular resolution was 3.1° in FWHM near the edge of the detector and 1.9° at the center. The information on a particle position was used for Doppler-shift corrections of the γ rays from ^{100}Ru, simultaneously providing the impact-parameter dependence of the γ-transition intensity. The experimental data were recorded event by event on a hard disk when one Ge detector and one particle detector gave coincident signals. Figure 1 gives an example of Doppler-corrected spectra of γ rays in coincidence with scattered particles. The typical energy resolution of Doppler-corrected γ-ray peaks was approximately 1.0%.

Thirteen γ-ray peaks were identified as the γ rays of ^{100}Ru. By connecting the observed transitions, we can construct the level scheme of the ground band and low-lying band structure. The detailed data analysis of this experiment is in progress with the least-squares search code GOSIA [9,10], which will reveal the B(E2) and B(E3) transition probabilities and some of the quadrupole moments. This will help us to understand the low-lying collective mode of ^{100}Ru.

References

[1] D. Troltenier *et al*., Z. Phys., A338 (1991) 261-270.
[2] A. Flank, Phys. Rev., C 39 (1989) 652.
[3] F. Iachello, Phys. Rev. Lett., 85 (2000) 3580-3583.
[4] F. Iachello, Phys. Rev. Lett., 87 (2001) 052502[1]-[4].
[5] K. Alder and A. Winther, Coulomb Excitation, Academic, NewYork, (1966).
[6] K. Alder and A. Winther, Electromagnetic Excitation, North Holland, Amsterdam, (1975).
[7] K. Furuno *et al*., Nucl. Instrum. Methods Phys. Res., A421 (1999) 211-226.
[8] Y. Toh *et al*., Rev. Sci. Instrum., 73 (2002) 47-50.
[9] T. Czosnyka *et al*., Nucl. Phys., A 458 (1986) 123-136.
[10] T. Czosnyka, C.Y. Wu and D. Cline, Bull. Am. Phys. Soc., 28 (1983) 745-746.

2. 4 In-beam gamma spectroscopy of ^{168}Ta

Y.H. Qiang[1,2], Y.H. Zhang[1], X.H. Zhou[1], M. Oshima[3], M. Koizumi[3], Y. Toh[3], A. Kimura[3], H. Harada[3], K. Furutaka[3], F. Kitatani[3], S. Nakamura[3], Y. Hatsukawa[3], M. Ohta[3], K. Hara[3], T. Kin[3], and J. Meng[4]

As a part of research work to investigate band structures of odd-odd nuclei in the A=170 mass region, the high-spin states in odd-odd ^{168}Ta have been investigated via the ^{145}Nd(^{27}Al, 4nγ) reaction at a beam energy of 140 MeV. The ^{27}Al beam was provided by the tandem accelerator in the Japan Atomic Energy Agency. The target was a 2.5 mg/cm^2 ^{145}Nd neodymium powder evaporated onto an 8 mg/cm^2 Au backing. The in-beam γ rays were detected using the gamma detector array of GEMINI-II [1] which consists of 19 HPGe's with BGO anti-Compton shields. A total of 3×10^8 γ-γ coincidence events were accumulated. The experimental data were analyzed in a same way as described in ref. [2].

The level scheme of ^{168}Ta, which is composed of two strongly coupled bands, was established and presented in fig. 1 as band 1 and 2. Compared with the previous result of Theine et al. [3], the present level scheme was extended both to higher- and lower-spin states. In particular, the 121-keV γ-ray in band 1 has been assigned as an out-of-band transition rather than the in-band transition as proposed in ref. [3]. This is supported by the observation of a 266.7-keV cross-over transition and coincidence relationships between the 121- and 198-keV γ-rays and others. The 225-keV cross-over transition reported in ref. [3] has not been observed in this work. Although a number of doublet or triplet γ rays appear in band 2, this band has been extended up to (27^+) due to high statistics of the data.

Band 1 and 2 have been assigned to be built on the $\pi h_{11/2}\otimes\nu i_{13/2}$ and $\pi d_{5/2}\otimes\nu i_{13/2}$ 2-qp configurations, respectively. This configuration assignment is supported by the measured in-band B(M1)/B(E2) ratios as shown in fig. 2. One can see in this figure that the experimental B(M1)/B(E2) ratios can be well reproduced theoretically under the assumption of the proposed configurations. On the other hand, since the one-qp bands built on the $\pi h_{11/2}$, $\pi d_{5/2}$, and $\nu i_{13/2}$ intrinsic states in neighboring odd-A nuclei were strongly populated in heavy-ion-induced fusion-evaporation reactions, it is naturally expected that the $\pi h_{11/2}\otimes\nu i_{13/2}$ and $\pi d_{5/2}\otimes\nu i_{13/2}$ bands in odd-odd nuclei may lie close to the yrast line and be observed intensely. Indeed such bands have been identified in the neighboring ^{170}Ta [4], providing a supplementary evidence for our configuration assignments. No connection to the ground state of ^{168}Ta could be established for these bands, the spin assignments are based on level spacing systematics and additivity rule of quasiparticle alignments in the crancked shell model.
Further analysis is still in progress and the final result will be published in a coming article.

[1] Institute of Modern Physics, Chinese Academy of Sciences
[2] Graduate School of Chinese Academy of Science
[3] Japan Atomic Energy Agency (JAEA)
[4] Peking University

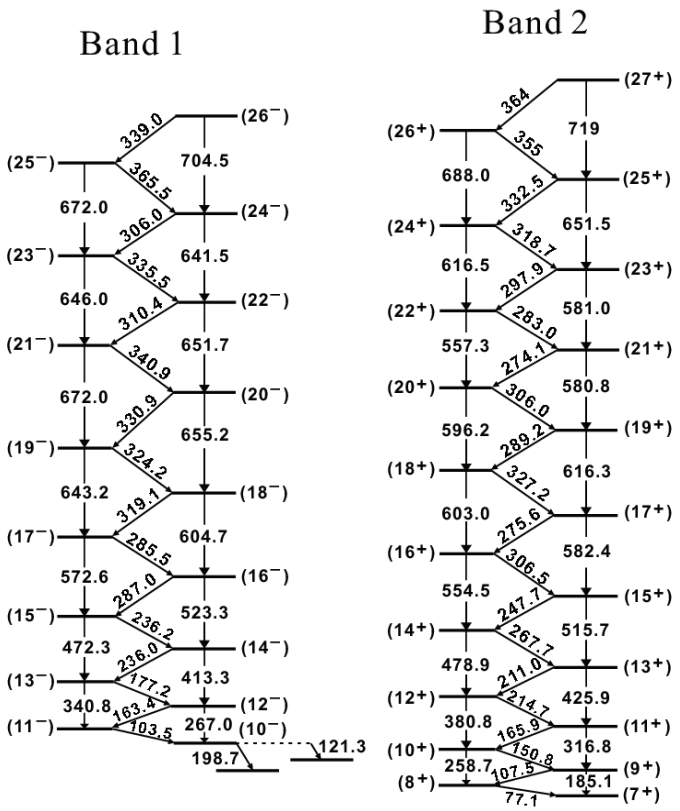

Fig. 1 Partial level scheme of ^{168}Ta established in the present work.

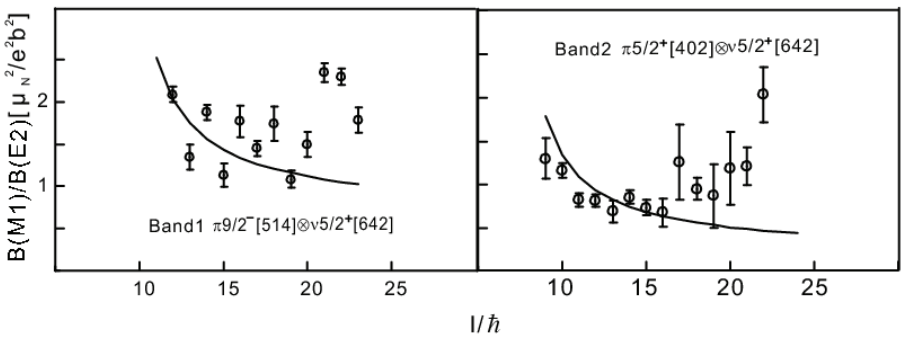

Fig. 2 In-band B(M1)/B(E2) ratios extracted from the present experiment. The solid lines are theoretical calculations using the proposed configurations indicated in the figure.

References

[1] M. Oshima *et al*., J. Radioanal. Nucl. Chem., (2008) to be published.

[2] Y. H. Zhang *et al*., Phys. Rev., C68 (2003) 054313.

[3] K. Theine *et al*., Nucl. Phys., A536 (1992) 418.

[4] Y. H. Zhang *et al*., Phys. Rev., C60 (1999) 044311.

2. 5 Isomers in neutron-rich tantalum isotopes

T. Shizuma[1], T. Ishii[1], H. Makii[1], T. Hayakawa[1], M. Matsuda[1], E. Ideguchi[2], and T. Morikawa[3]

In A～180 nuclei, low-lying isomers due to the K quantum number conservation (where K is defined as the angular momentum projection on the nuclear symmetry axis) are systematically observed. The majority of K isomers in this region are found in nuclei on the neutron-deficient side of the valley of β stability, because of the inaccessibility to the neutron-rich nuclei using fusion-evaporation reactions with stable beam and target combination. However, the recent progress in γ-ray spectroscopic techniques using ^{18}O-induced transfer reactions has enabled us to investigate the near-yrast structures of neutron-rich nuclei [1,2].

Excited states in neutron-rich Ta nuclei have been populated in ^{18}O-induced transfer reactions on ^{186}W and ^{181}Ta targets. The 180-MeV ^{18}O beams were provided by the tandem accelerator at Japan Atomic Energy Agency, Tokai. The target thickness was thick enough to stop residual nuclei inside the target materials. Outgoing projectile-like ions were detected by four sets of surface barrier Si ΔE-E detectors placed at a position close to the grazing angle of the reactions used. In-beam γ rays were measured by eight HP-Ge detectors in coincidence with the scattered ions. Four of these detectors with relative efficiency of 60% were arranged symmetrically in a plane perpendicular to the beam axis at a distance of 6 cm from the targets.

From the analysis of the delayed coincidence data, a $K^{\pi}=1/2^{+}$, $T_{1/2}$=900 ns isomer at 406 keV was found in ^{185}Ta produced by the one-proton pickup reaction of ^{186}W(^{18}O,^{19}F) [3]. Several γ-ray peaks were observed above this isomer as shown in fig. 1. The data obtained in the ^{181}Ta+^{18}O reaction also reveal the existence of an isomer in ^{183}Ta produced by the two-neutron transfer. Further analysis of this data is in progress.

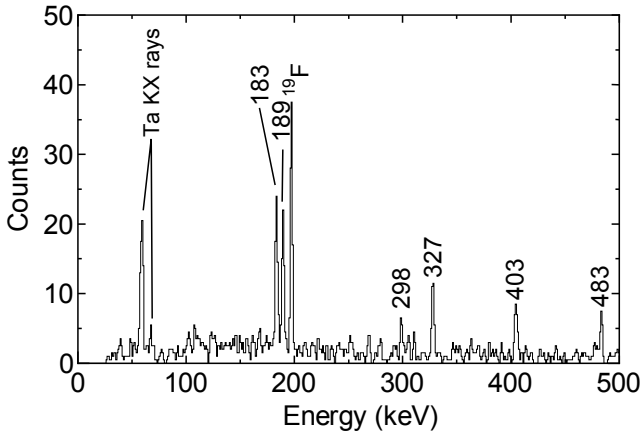

Fig. 1 A γ-ray coincidence spectrum gated on the delayed 406 keV transition in ^{185}Ta produced in the ^{18}O-induced reaction on ^{186}W.

References

[1] T. Ishii *et al*., Phys. Rev., C72 (2005) 021301(R).

[2] T. Shizuma *et al*., Eur. Phys. J., A30 (2006) 391-396.

[3] T. Shizuma *et al*., Eur. Phys. J., A34 (2007) 1-4.

[1] Japan Atomic Energy Agency (JAEA)
[2] Tokyo University
[3] Kyushu University

2. 6 Prolate and oblate shape co-existence in ^{188}Pt

X.H. Zhou[1], M. Oshima[2], Y. Toh[2], M. Koizumi[2], A. Osa[2], Y. Hatsukawa[2],
Y.H. Zhang[1], and M. Sugawara[3]

Shape coexistence is a major theme in nuclear structure study. The neutron-deficient Pt-Hg nuclei with neutron number N~110 are well known to exhibit interesting shape co-existence phenomena [1]. The isotope shift measurements have shown a sharp change of the nuclear charge radius around ^{188}Pt [2], suggesting an oblate ground-state shape for the Pt nuclei with A>188 and a near prolate shape for A<188. Therefore, the spectroscopic information of ^{188}Pt is of particular interest as it would show competing collectivity of prolate and oblate shapes. Prior to the present work, the high-spin level scheme of ^{188}Pt was reported in the literature [3].

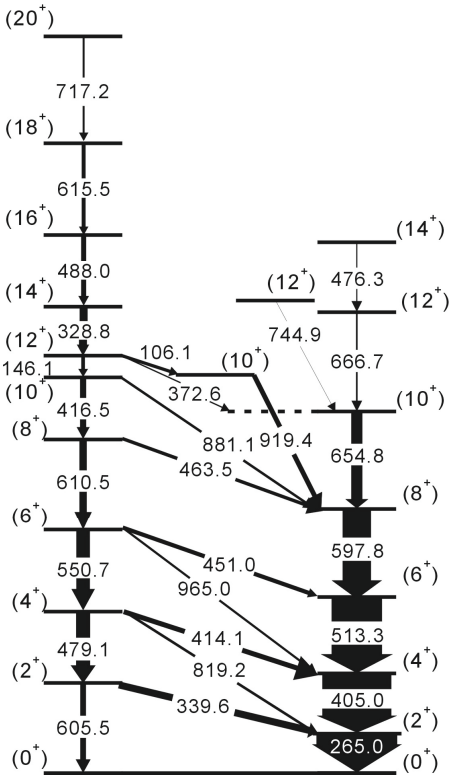

Fig. 1 A partial level scheme of ^{188}Pt.

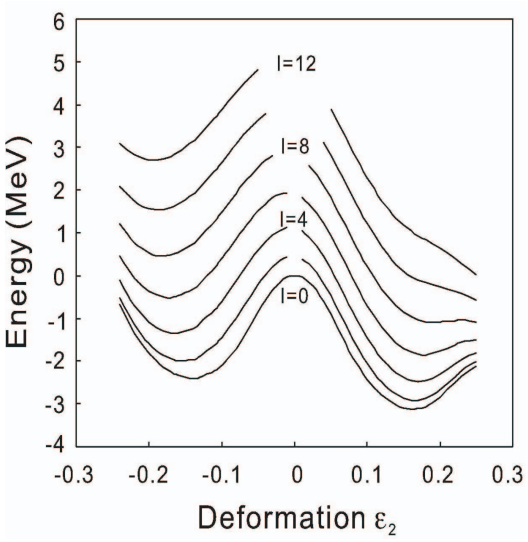

Fig. 2 Energy surface calculation for ^{188}Pt obtained with projection on quasi-particle vacuum states only.

The excited states in ^{188}Pt were populated via the ^{176}Yb(^{18}O, 6n) reaction. The $^{18}O^{7+}$ beam was provided by the tandem accelerator at the Japan Atomic Energy Agency (JAEA). The target was an isotopically enriched ^{176}Yb metallic foil of 2.0 mg/cm^2 thickness with a 7.0 mg/cm^2 Pb backing. The γ-ray detector array, GEMINI-II, at JAEA was used [4].γ-γ-t coincidence measurements were performed at beam energies of 88 and 95 MeV, at which energies the yields of ^{188}Pt were large. A total of 240×10^6 coincidence events were accumulated. After accurate gain matching, these coincidence events were sorted into symmetric and DCO matrices for off-line analysis. Assignments of the observed new γ-rays to ^{188}Pt were based on the

[1] Institute of Modern Physics, Chinese Academy of Sciences
[2] Japan Atomic Energy Agency (JAEA)
[3] Chiba Institute of Technology

coincidences with the known γ-rays [3]. Gated spectrum was produced for each of the γ-rays assigned to ^{188}Pt. On the basis of the analysis of γ-γ coincidence relationships, a partial level scheme for ^{188}Pt has been proposed and presented in fig. 1. The transition character was deduced from the measured DCO results.

Variant kinds of nuclear models have been applied to study nuclear shape co-existence. The Projected Shell Model (PSM) [5] is a shell model that uses deformed bases and the projection technique. The PSM's two-body residual interactions are of the quadrupole plus pairing type, with the quadrupole-pairing term included [5]. The calculated energy surface for ^{188}Pt is shown in fig. 2. These curves show the energies for states with different angular momenta while varying deformation ε from negative values to positive values. There are two pronounced minima, sitting respectively at the prolate and oblate side. Therefore, the calculation predicts a competing between prolate and oblate shapes with two sets of corresponding collective states. The minimum $\varepsilon \approx 0.16$, corresponding to a prolate shape, is lower in energy. The calculations suggest that the ground state of ^{188}Pt has a prolate shape. Comparing the calculated results with the experimental observation, we can assign the level sequence, shown in the right hand of fig. 1, as a prolate band built on the ground state, and the rotational band based on the 605.5-keV state as an oblate band. Therefore, the transitional nucleus ^{188}Pt presents an excellent example of prolate and oblate shape co-existence.

Very recently, a new kind of shape phase transition, occurring along an yrast line between states of prolate and oblate shape in an isolated nucleus ^{190}W, has been predicted by Sun et al [5]. However, the experimental data on the exited states of ^{190}W is sparse due to its neutron richness, and the predicted shape phase transition has not yet been proven experimentally. As shown in fig. 1, the yrast states up to the spin value of $10\hbar$ are the members of the ground state band. However, the yrast states change to the states based on the 12^+ level depopulated by the 328.8-keV transition. If the shape is oblate, occupation of low-K $i_{13/2}$ neutron intruder orbits favors rotation alignment. The $\nu i_{13/2}^2$ configuration was proposed to the 12^+ state. The level scheme of ^{188}Pt clearly shows that the path for the lowest state at each I starts from the prolate ground state, goes up till I=10, and then jumps to the oblate side. The wave functions for the prolate and oblate shapes should be very different, with a very small overlap between them. It is expected that the oblate state at the phase transition point might be a shape isomer. Indeed, the yrast 12^+ state was identified to be an isomer [3], and theγtransition between the oblate and prolate states was strongly hindered. Therefore, a prolate to oblate shape phase transition might occur along the yrast line in ^{188}Pt. In the present case, the order parameter is the total spin I.

References

[1] D. T. Joss *et al*., Phys. Rev., C74 (2006) 014302-10.
[2] H. T. Duong *et al*., Phys. Lett., B217 (1989) 401-405.
[3] M. Piiparinen *et al*., Phys. Rev. Lett., 34 (1975) 1110-1113.
[4] M. Oshima *et al*., J. Radioanal. Nucl. Chem. (2008) to be published.
[5] Y. Sun *et al*., Phys. Lett., B659 (2008) 165-169.

2. 7 Gamma-rays in ground-state band of ^{246}Pu

H. Makii[1], T. Ishii[2], M. Asai[2], K. Tsukada[2], A. Toyoshima[2], M. Matsuda[2], A. Makishima[3]
J. Kaneko[4], H. Toume[2,5], S. Ichikawa[2], S. Shigematsu[2,6], T. Kohno[6], and M. Ogawa[4]

We have measured deexcitation γ-rays in neutron-rich transuranium nuclei of ^{246}Pu for the first time. The ^{246}Pu was produced by the (^{18}O, ^{16}O) two-neutron transfer reaction. A ^{244}Pu target (98.0 % enrichment in ^{244}Pu), 0.7 mg/cm^2 in thickness and 3 mm in diameter, electrodeposited on a 3.4 μm aluminum foil was bombarded by a 162 MeV ^{18}O beam of 0.3 particle nA. Outgoing projectile-like particles were detected by four sets of Si $\Delta E - E$ detectors. γ rays emitted from the residual nuclei were measured by six Ge detectors, in coincidence with outgoing particles. A detailed description of the measurement system is given in ref. [1].

Deexcitation γ rays in ^{246}Pu were identified by setting a gate on ^{16}O particles with kinetic energies corresponding to the excitation energies of ^{246}Pu between 0 and 6 MeV. γ rays in the ground-state band of ^{246}Pu were clearly observed as shown in fig. 1. These γ rays were coincidence with each other. Furthermore, the in-plane to out-of-plane intensity ratios of these γ-rays confirm that these transitions are stretched *E2* types. On the basis of these results, we have established the ground-state band of ^{246}Pu up to 12^+ as shown in fig. 2. In fig. 1, the $2^+ \rightarrow 0^+$ γ ray of about 47 keV was not observed owing to its large internal conversion coefficient ($\alpha_T \approx 600$ [2]). γ-rays in ^{245}Pu produced by one-neutron evaporation from ^{246}Pu following the (^{18}O, ^{16}O) reaction are also seen in fig. 1.

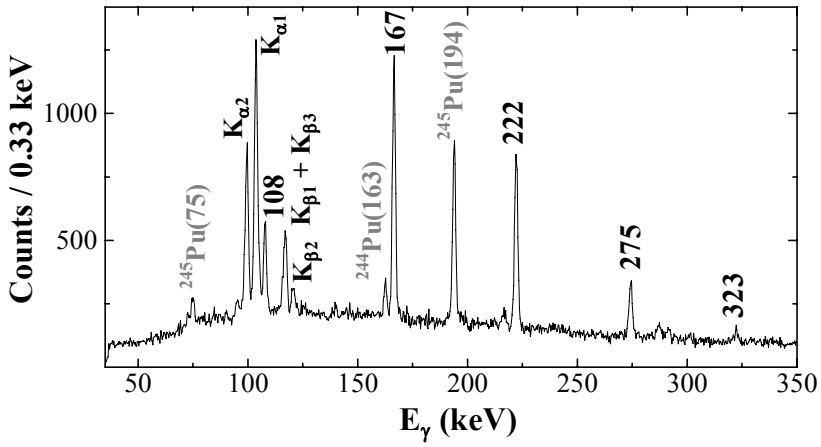

Fig. 1 A γ-ray spectrum in coincidence with ^{16}O particles with kinetic energies corresponding to the excitation energies of ^{246}Pu between 0 and 6 MeV. γ peaks of ^{246}Pu are labeled by energies in units of keV.

[1] High Energy Accelerator Research Organization (KEK)
[2] Japan Atomic Energy Agency (JAEA)
[3] National Defense Medical College
[4] Komazawa University
[5] Ibaraki University
[6] Tokyo Institute of Technology

Figure 3(a) shows systematics of the 2^+ energies $E(2^+)$ for the ground-state bands of even-even actinide nuclei whose excitation energies were measured precisely. The $E(2^+)$ values were derived from the moment of inertia deduced from the higher levels. Sobiczewski et al. [3] calculated the $E(2^+)$ energies on the basis of a macroscopic-microscopic approach taking account of higher order deformations and a cranking approximation. The calculated values are shown in fig. 3(b). This calculation predicted and reproduced the systematics of the $E(2^+)$values around N = 152 very well. They pointed out that the pairing gap becomes smaller at a deformed shell gap, which leads to large values of the moment of inertia and, as a result, to small values of the $E(2^+)$ at N = 152. In fig. 3, the $E(2^+)$ values for isotopes from $_{96}$Cm to $_{102}$No are pulled down to lower energies at N = 152. In contrast, the $E(2^+)$ values for $_{94}$Pu isotopes increase gradually with neutron number. This systematics of the $E(2^+)$ values suggests that the deformed shell-gap size at N = 152 is reduced in $_{94}$Pu isotopes. The reduction of the shell-gap size of N = 152 was confirmed from one-quasi levels in ^{245}Pu as described in ref. [4].

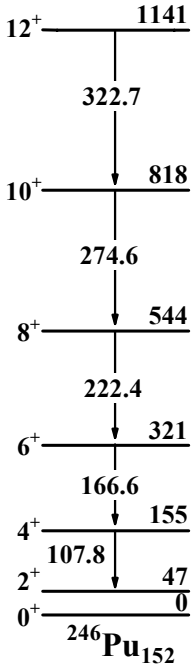

Fig. 2. Level scheme of the ground state band of ^{246}Pu. The energy of the 2^+ level was derived from the moment of inertia deduced from the higher levels.

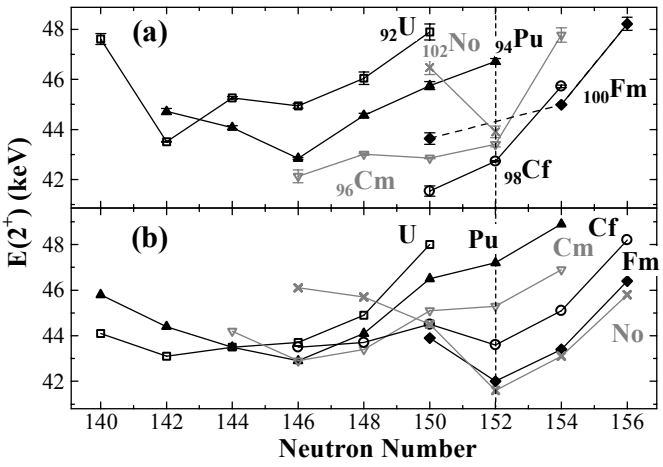

Fig. 3. (a) Systematics of the 2^+ energies $E(2^+)$ for the ground-state bands of even-even actinide nuclei. Because there are no accurate measurements for $^{252}Fm_{152}$, the data for ^{250}Fm and ^{254}Fm are connected by a dashed line. (b) Calculated $E(2^+)$ energies by a macroscopic-microscopic approach [3].

References

[1] T. Ishii *et al*., J. Phys. Soc. Jpn., 75 (2006) 043201.

[2] I. M Band *et al*., At. Data Nucl. Data Tables, 81 (2002) 1-334.

[3] A. Sobiczewski, I Muntian and Z. Patyk, Phys. Rev., C 63 (2001) 034306.

[4] H. Makii *et al*., Phys. Rev., C 76 (2007) 061301(R).

2. 8 Quasi-particle states in ^{249}Cm measured by in-beam γ-ray spectroscopy

T. Ishii[1], H. Makii[1], M. Asai[1], K. Tsukada[1], A. Toyoshima[1], M. Matsuda[1], A. Makishima[2], S. Shigematsu[3], J. Kaneko[4], T. Shizuma[1], H. Toume[1], I. Hossain[5], T. Kohno[3], and M. Ogawa[4]

We have measured deexcitation γ-rays in ^{249}Cm populated by one-neutron stripping reactions with a ^{248}Cm target and a 162 MeV ^{16}O, a 162 MeV ^{18}O, and a 120 MeV ^{13}C beams. γ rays in ^{249}Cm were identified by selecting outgoing particles and measuring their kinetic energies using Si Δ E-E detectors [1-4]. We have observed eight quasi-particle states above the deformed shell gap of N=152. The level scheme is shown in fig. 1. The 1/2[620], 1/2[750], and 7/2[613] bands were extended up to $19/2^+$, $19/2^-$, and $13/2^+$ states, respectively. We have established the $9/2^+$ 9/2[615] state at 526.3 keV, the $9/2^+$ 9/2[604] state with a short life ($T_{1/2}$<< 2ps) at 1029.8 keV, and the $11/2^-$ 11/2[725] state with a half life of 19(1) ns at 375.1 keV. Furthermore, the $17/2^+$ member of the 1/2[880] state originated from the $k_{17/2}$(L=8) spherical single-particle state was assigned to a level at 1504.8 keV. The γ-ray spectra for the 637 keV transition depopulating this state are shown in fig. 2. The 1505 keV level is close in energy to one of the candidates for the$17/2^+$ 1/2[880] state observed by the (^{4}He, ^{3}He) reaction using a magnet spectrometer [5]. We have also demonstrated that higher-spin states were populated in the (^{16}O, ^{15}O) reaction with Q_{gg}= -11.0 MeV than those in the (^{13}C,^{12}C) reaction with Q_{gg}= -0.2 MeV as shown in fig. 3. This is caused by the matching condition of angular momentum.

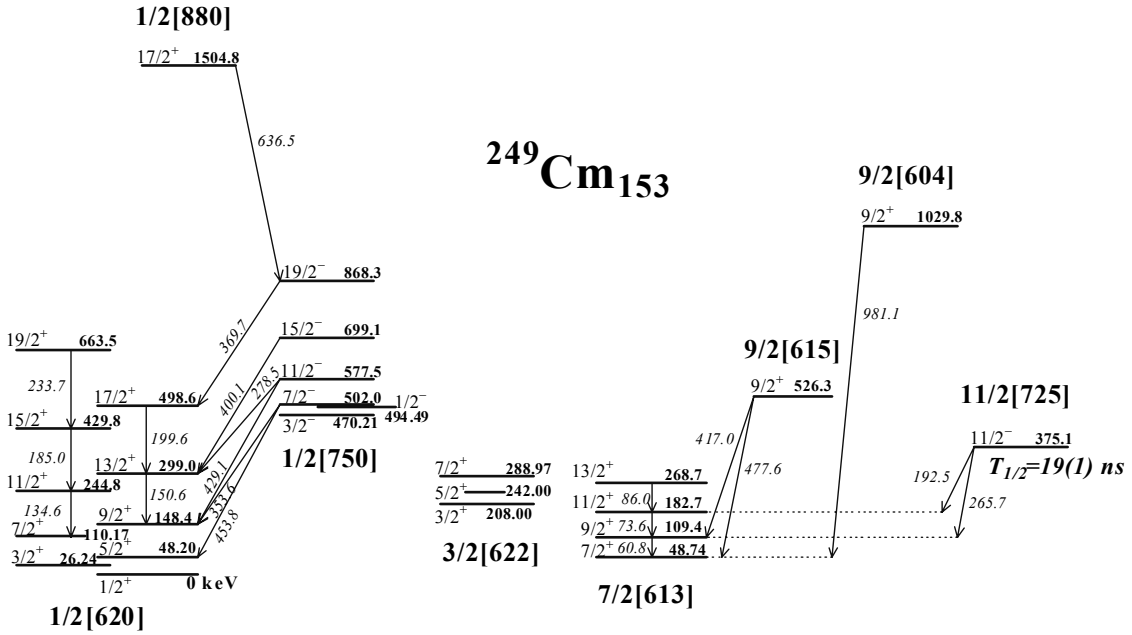

Fig. 1 Level scheme of ^{249}Cm. γ-rays observed in the (^{16}O,^{15}O) reaction are depicted.

[1] Japan Atomic Energy Agency (JAEA)
[2] National Defense Medical College
[3] Tokyo Institute of Technology
[4] Komazawa University
[5] Osaka University

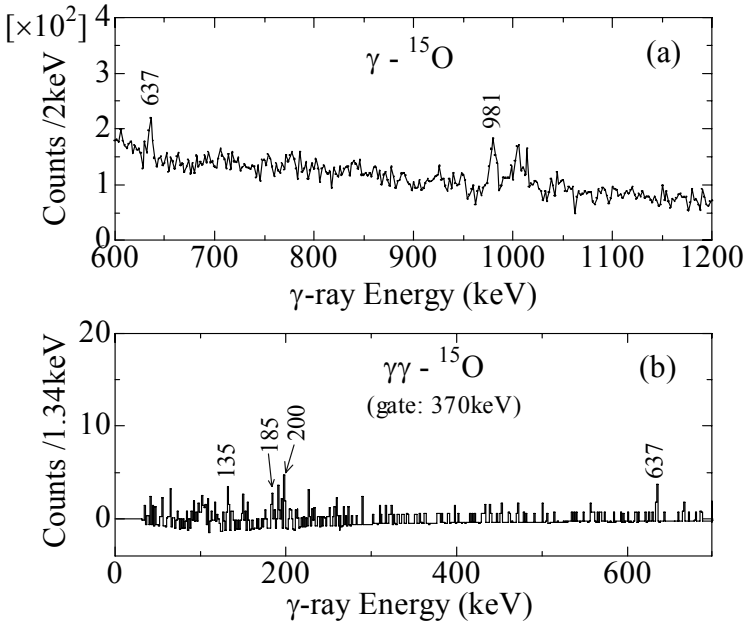

Fig. 2 γ-ray spectra for the 637 keV transition depopulating the 1/2[880] band.
(a) γ-ray spectrum in coincidence with ^{15}O. (b) γγ coincidence spectrum by setting the gate on the 370 keV transition. Both spectra were obtained by the (^{16}O, ^{15}O) measurement.

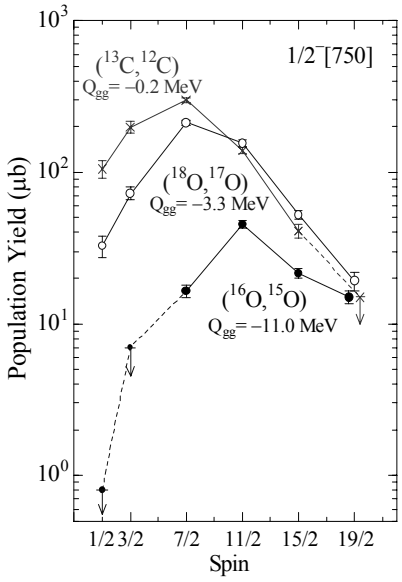

Fig. 3 Population yields for members of the 1/2[750] band in ^{249}Cm. These yields were obtained from the intensities of γ rays depopulating these states.

References

[1] T. Ishii *et al*., Phys. Rev., C72 (2005) 021301(R)(1-5).

[2] T. Ishii *et al*., J. Phys. Soc. Japan, 75 (2006) 043201(1-4).

[3] T. Ishii *et al*., Phys. Rev., C76 (2007) 011303(R)(1-5).

[4] H. Makii *et al*., Phys. Rev., C76 (2007) 061301(R)(1-5).

[5] I. Ahmad, Nucl. Phys., A646 (1999) 175-186.

2. 9 Alpha-gamma coincidence spectroscopy of ^{259}No

M. Asai[1], K. Tsukada[1], M. Sakama[2], Y. Ishii[1], A. Toyoshima[1], T. Ishii[1], I. Nishinaka[1], Y. Nagame[1], Y. Kasamatsu[1], M. Shibata[3], H. Hayashi[3], H. Haba[4], and Y. Kojima[5]

The stability of superheavy nuclei essentially depends on nuclear shell structure. Many theoretical studies have predicted the stability and shell structure of superheavy nuclei, while experimental information is very scarce. In this work, α-γ coincidence spectroscopy of ^{259}No has been performed to establish excited states in the daughter nucleus as well as to assign spin-parities and single-particle configurations of the ground state of ^{259}No. Having the neutron number N = 157, ^{259}No is one of the most neutron-rich nuclei that experimental spin-parity assignments have ever been performed for. These experimental data allow us to extract energy spacings and order of single-particle orbitals, which are direct measure to see the shell structure of superheavy nuclei.

^{259}No was produced by the ^{248}Cm(^{18}O,α3n) reaction whose maximum cross section is about 13 nb. The beam energy was 94 MeV on target. Reaction products recoiling out of the target were continuously transported through a 20-m long capillary with a He/KCl aerosol jet into a rotating wheel α-γ detection system, and were deposited on a thin foil forty of which were set on the wheel [1]. The wheel periodically rotated to move the deposited sources to two consecutive detector stations each of which were equipped with two Si detectors and two Ge detectors. Since the half-life of ^{259}No is 58 min, we rotated the wheel at 2400-s intervals. However, the collection of KCl aerosol for such a long time results in a deposition of KCl material too thick to measure α-energy spectra. To prepare much thinner sources, a tip of the capillary was moved to draw an 8-mm diameter circle on the foil, which reduces the thickness of the deposited KCl by about an order of magnitude. Alpha-singles and α-γ coincidence events were recorded event by event together with time information.

Figure 1(a) shows a γ-ray spectrum in coincidence with α particles of ^{259}No. About 900 α-singles events were accumulated for a total of 9-day experiment. Three weak γ rays were observed at 61.7, 169.9, and 231.4 keV in addition to intense Fm K and L X rays. The decay scheme of ^{259}No was established as shown in fig. 1(b). From K X- to γ-ray intensity ratios, the 169.9 and 231.4 keV γ rays were found to be $M1/E2$ transitions.

The spin-parity and neutron configuration of the ground state of ^{255}Fm is known to be $7/2^+[613]$ [2]. The first excited 61.7 keV level is considered to be the $9/2^+$ state in the $7/2^+[613]$ rotational band by analogy with neighboring nuclei. The 231.4 keV level is populated by the favored α transition, indicating that this

[1] Japan Atomic Energy Agency (JAEA)
[2] The University of Tokushima
[3] Nagoya University
[4] The Institute of Physical and Chemical Research (RIKEN)
[5] Hiroshima University

level should be a one-quasiparticle state with the same configuration as that of the ground state of ^{259}No. The 231.4 keV level is depopulated by the $M1/E2$ transitions to the $7/2^+$ and $9/2^+$ states, which restricts the spin-parity of the 231.4 keV level to $7/2^+$ and $9/2^+$. Around ^{259}No, only the $9/2^+[615]$ orbital exists near the Fermi surface with $\Omega = 7/2^+$ or $9/2^+$, except the $7/2^+[613]$ orbital which is already assigned to the ground state of ^{255}Fm. Thus, we have assigned the $9/2^+[615]$ configuration to the 231.4 keV level in ^{255}Fm as well as to the ground state of ^{259}No. Note that the 169.5 and 231.1 keV γ rays were also observed in the EC decay of ^{255}Md [3]. This experiment also suggested the $9/2^+[615]$ configuration for the 231.1 keV level, consistent with the present result.

It is found that the α decay scheme of ^{259}No is very similar to that of the $N = 157$ isotone ^{257}Fm; the ground-state configuration of both the nuclei is $9/2^+[615]$, and the $9/2^+[615]$ state in the daughter nuclei is located at 241 keV in ^{253}Cf and 231 keV in ^{255}Fm. On the other hand, theoretical calculations predicted the $9/2^+[615]$ states at 300–400 keV in $N = 155$ isotones [4,5], and could not reproduce the $9/2^+[615]$ ground states for $N = 157$ isotones; the $9/2^+[615]$ states were calculated at 200–300 keV above the ground state [4,5]. This indicates that the location of the $9/2^+[615]$ orbital is too high in the calculations, probably due to inadequate deformation parameters used in the calculations.

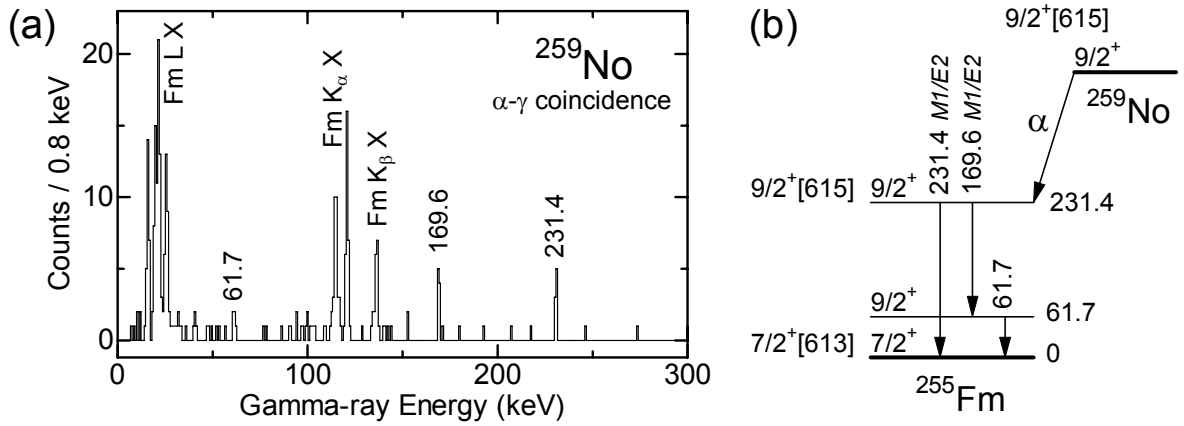

Fig. 1 (a) Gamma-ray spectrum observed in coincidence with α particles of ^{259}No. (b) Proposed decay scheme of ^{259}No.

References

[1] Y. Nagame *et al*., J. Nucl. Radiochem. Sci., 3 (2002) 85-88.

[2] F. Asaro, S. Bjørnholm and I. Perlman, Phys. Rev., 133 (1964) B291-B300.

[3] I. Ahmad, R.R. Chasman and P.R. Fields, Phys. Rev., C61 (2000) 044301.

[4] S. Ćwiok, S. Hofmann and W. Nazarewicz, Nucl. Phys., A573 (1994) 356-394.

[5] A. Parkhomenko and A. Sobiczewski, Acta Phys. Pol. B, 36 (2005) 3115-3137.

2.10 Decay study on fission products with on-line isotope separator

M. Shibata[1], M. Asai[2], A. Osa[2], M. Oshima[2], A. Kimura[2], M. Koizumi[2], and T. K. Sato[2]

Atomic masses are the most fundamental physical quantities and play an important role for study on structure of unstable nuclei, nuclear stability or nucleosynthesis in astrophysics. Beta-decay energy (Q_β) measurement is one of the precise methods to determine atomic masses and it is also important for evaluation of the decay heat of the nuclear power plants in nuclear engineering. We had already developed two type total absorption detector to measure Q_βs of low yielded nuclei such as new isotopes [1,2]. At first, using a BGO total absorption detector, we succeeded in Q_βs determination of some new fission products produced with ^{238}U(n,*f*) reaction with the accuracy of 60 keV [1]. Next, a total absorption detector, which are composed of a large volume Ge detector having a through hole in the center itself and a surrounding annular BGO Compton suppression detector, was developed. It was also applied to Q_β energy measurements and succeeded in determination them within 20 keV [3]. However, the efficiency of the Ge detector and the solid angle of the BGO Compton suppression are still small, then, the efficiency as the total absorption detector is less effective for the nuclei having Q_β higher than 5 MeV. So the 3rd total absorption detector with high-efficiency and high-resolution have been developed. This detector is composed of large volume clover detector (80 mm$^{\phi}$ × 90 mm^{t} × 4) having a through hole (15 mm$^{\phi}$) in the center, and five BGO Compton suppression detectors (2 × top, 2 × side, 1 × bottom, each is 30 mm thick.) which surround the clover detector with almost 100% solid angle. Scattered photons by clover detector are detected with BGO detectors with high efficiency, then Q_βs for the fission products are expected to be measured up to 10 MeV with the accuracy of 20 keV. The determinations of the Q_βs for rare isotopes including new isotopes are useful for mass prediction in neutron-rich nuclei and also decay heat evaluation. In this experiment, the performance of the detector was tested by measuring the Q_βs for the nuclei with mass number A ~ 90 or 140.

Uranium carbide (UC_2) target containing 670 mg/cm^2 ^{238}U was bombarded with 30 MeV proton beams with the intensity of about 10nA generated by the TANDEM accelerator at JAEA. The ^{88,89}Rb, $^{92\text{-}95}$Y, ^{138,139}Cs, ^{139}Ba and ^{142,143}La isotopes were separated from the fission products by an on-line isotope separator (Tokai-ISOL). The Q_βs and half-lives for the nuclei are between 2 and 5.4 MeV, and between 9.3 min and 3.5 h, respectively. The radioactive ion beams were implanted into thin Mylar tapes and were put into the center position of the clover detector. Singles spectra with the clover detector and coincidence spectra between the clover and the BGO detectors were also measured. These procedures were iterated many times to get good statistics for every nucleus. The measurement period for each nucleus was between 4 and 10 hours. The counting rate of each activity was kept around 2 kcps to reduce pulse pile-ups.

The total absorption events were extracted by subtracting the coincidence spectra by multiplied a factor of 1.25 from the singles one. This factor was determined from the experimental analysis for the monoenergetic γ-rays and also from the Monte Carlo simulation (GEANT4). Typical total absorption spectrum of ^{88}Rb is shown in fig.1 together with singles and coincidence ones. The end-point energies were deduced by processing the folding spectra to total

[1] Nagoya University
[2] Japan Atomic Energy Agency (JAEA)

absorption spectra as shown in fig.2 using the simulated response functions for monoenergetic electrons by GEANT4 parameterized as shown in fig.3.

By measuring the eleven nuclei which Q_βs are well determined [4], then the performance of the detector concerning the determination of Q_β was evaluated. It is found that the experimental Q_βs are a certain value, which corresponds to the energy loss owing to the well of the detector, smaller than the values in ref. 4 (fig. 4) and it was evaluated to be 190 ± 20 keV for the $Q_\beta$values between 2.3 and 5.4 MeV. As the results, this total absorption detector are expected to determine the Q_βs of rare isotopes precisely including new isotopes.

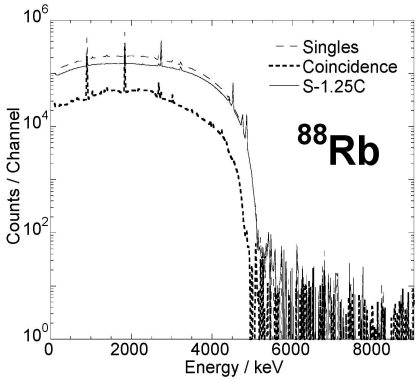

Fig. 1 Typical total absorption spectrum of ^{88}Rb. The solid line indicates the total absorption events.

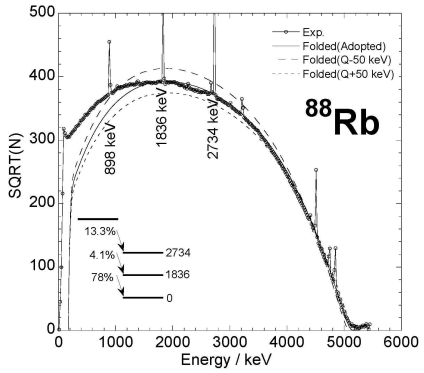

Fig. 2 End-point analysis of ^{88}Rb by folding procedure.

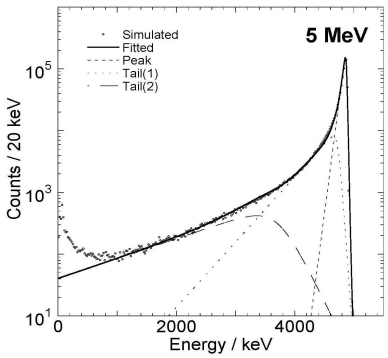

Fig. 3 Typical response function for monoenergetic electrons of 5 MeV.

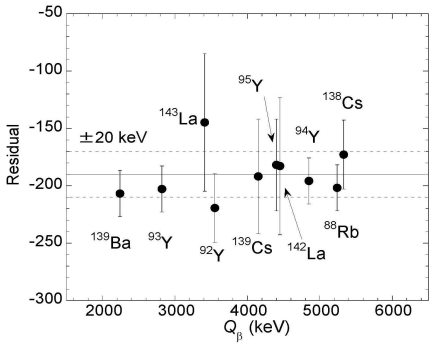

Fig. 4 The evaluation of the energy loss for the detector.

Present study includes the result of "Study on nuclear data by using a high intensity pulsed neutron source for advanced nuclear system" entrusted to Hokkaido University by the Ministry of Education, Culture, Sports, Science and Technology of Japan (MEXT).

References

[1] M. Shibata *et al*., J. Phys. Soc. Jpn., 71 (2002) 1401-1402.

[2] H. Hayashi *et al*., Euro. Phys. J., A 34 (2007) 363-370.

[3] H. Hayashi *et al*., Int. Conf. on Nucl. Data for Sci. and Tech., Nice, France, April 22-27, 2007.

[4] G. Audi *et al*., Nucl. Phys., A 729 (2003) 337-676.

2.11 A gas cell for on-line laser spectroscopy of radioactive isotopes of refractory elements

H. Iimura[1], M. Miyabe[1], M. Oba[1], and M. Koizumi[1]

High resolution laser spectroscopy of radioactive isotopes can provide important information on nuclear structure such as the electromagnetic moments and the changes of nuclear charge radii. However, those information are scarce for the radioactive isotopes of refractory elements such as in the rhenium region, since usual collinear laser spectroscopy using an ion source can not be applied to these isotopes. We plan to do laser spectroscopy for these isotopes by stopping the recoiled reaction-products in gas. They are irradiated with the laser beam while diffusing through the gas. The gas cell for this experiment has recently been set up in a beam line of the JAEA tandem accelerator in Tokai. In this report we describe an overview of the gas cell. Similar gas cell has already been constructed at the Stony Brook tandem accelerator facility and successfully used for the isotope-shift measurements of radioactive ytterbium isotopes [1].

The basic geometry of the gas cell is shown in fig. 1. The nickel foil window isolates the gas cell from the accelerator beam line. By filling the cell with about 10 Torr of argon gas, the reaction products being recoiled from the target stop at the center of the inner cell where they are illuminated by the laser beam.

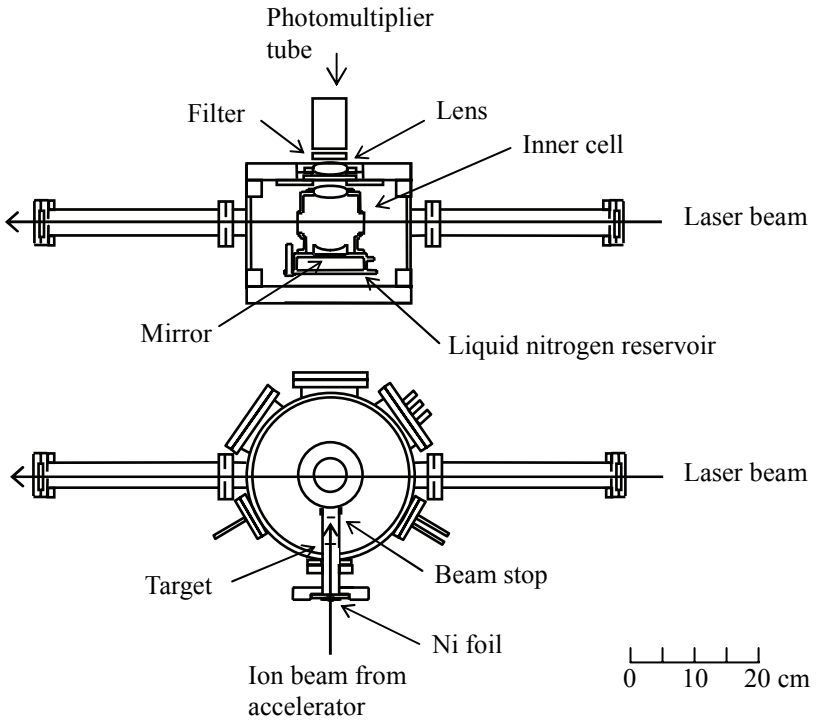

Fig. 1 Schematic layout of the gas cell. The upper and lower sections of the figure are side and top views of the cell, respectively.

[1] Japan Atomic Energy Agency (JAEA)

The inner cell is connected on the liquid nitrogen reservoir. By cooling the inner cell, the gas is cooled and thus the Doppler width of the resonance peak becomes narrower. At the gas temperature of 150 K, the Doppler width is expected to be about 300 MHz. This cooling also helps to increase the fluorescence yield since the time for the reaction products to diffuse out from the laser beam becomes longer. The laser-induced fluorescence is collected on a photomultiplier tube by using a mirror and lenses. The resonance peaks are observed by scanning the frequency of a tunable laser. Since the production rate of radioactive isotopes by heavy-ion fusion reaction is expected to be less than 10^5 atoms/sec, it is important to reduce the background to observe the laser-induced fluorescence signal. The largest part of the background is the light coming from the collisions between the argon atoms and the ions from the accelerator. To reduce this background a beam-stop consisting of a disk 7.5 mm in diameter is placed between the target and the inner cell. While it blocks most part of the ion beam from the accelerator, some of the reaction products can get into the inner cell because low-energy recoils undergo small-angle scattering when they pass through the target and gas. Additionally, the ion beam is chopped by using a deflector, and the counter of the photomultiplier is gated so that it record only when the ion beam is off.

Prior to studies of radioactive isotopes in the rhenium region, we are now working to optimize the sensitivity of the apparatus. Particularly, the transition for laser excitation is crucial to achieve high sensitivity. In order to find the most efficient transition, we will use the ion beams of stable isotopes of these elements. These ions are injected from the accelerator into the gas cell without the beam stop. By exciting some transitions with laser, we can determine the transition which has the strongest laser-induced fluorescence.

References

[1] A. Berger *et al*., Nucl. Instrum. Methods Phys. Res., A311 (1992) 224-239.

2.12 On-line test of RI ion trap system

H. Makii[1], T. Ishii[2], D. Nagae[2], T.K. Sato[2], A. Osa[2], and S. Ichikawa[2]

The low-energy and low-emittance pulsed radioactive nuclear beam (RNB) is useful for the measurements of fundamental properties of nucleus such as binding energy, charge radius, and magnetization distribution with high accuracy. Construction of a new beam line and an RF linear ion trap for deceleration, bunching, and emittance improvement of RNB is now in progress at a central beam line of an isotope separator on-line (ISOL). The overview of the beam line and trap system is given in ref. [1]. By adjusting the ion optical elements, the continuous ion beam from an ISOL is transported to the trap. The transported ions are electrostatically decelerated and injected into the trap, which is filled with a buffer gas. The trap system consists of four segmented rods which provide transverse and longitudinal confinement by an oscillating electric quadrupole field and DC electric field along the axis of the system, respectively. Ions entering the trap system lose their energy due to the collision with the buffer gas, and then the cooled ions are extracted as bunches [2].

On-line test of the trap system was carried out using unstable $^{21}Na^{+}$ ($t_{1/2}$ = 22.49 s), $^{92}Rb^{+}$ ($t_{1/2}$ = 4.492 s), and $^{142}Cs^{+}$ ($t_{1/2}$ = 1.70 s) beams provided by the ISOL. The ^{21}Na was produced by $^{12}C + ^{12}C$ fusion reaction, and the ^{92}Rb and ^{142}Cs nuclei were produced by proton-induced fission of uranium. The beam energies from the ISOL were 21 keV. The extracted ions were stopped on a Micro-channel plate (MCP) detector placed on the exit of the trap system and we measured time distributions of the ions with the MCP detector. Figure 1 shows the time-of-flight spectrum of $^{21}Na^{+}$ ions ejected out of the trap system. We also measured the γ-rays emitted by daughter nuclei with a Ge detector placed near the MCP detector. The γ-rays emitted by ^{21}Na, ^{92}Rb and ^{142}Cs were clearly observed in figs. 2(a), 2(b) and 2(c), respectively. From the result of this on-line test, it is proved that our new trap system has capability to decelerate and bunch the unstable ions up to $A \sim 140$. Systematic investigations of trap system to improve efficiency for heavier ions ($A >$ 200) are now in progress.

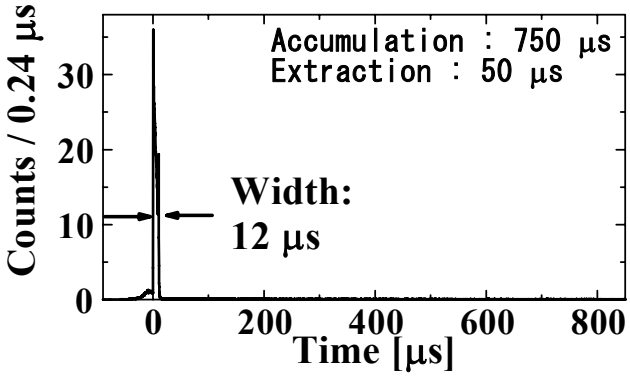

Fig. 1 Time-of-flight spectrum of $^{21}Na^{+}$ ions ejected out of the trap system.

[1] High Energy Accelerator Research Organization (KEK)
[2] Japan Atomic Energy Agency (JAEA)

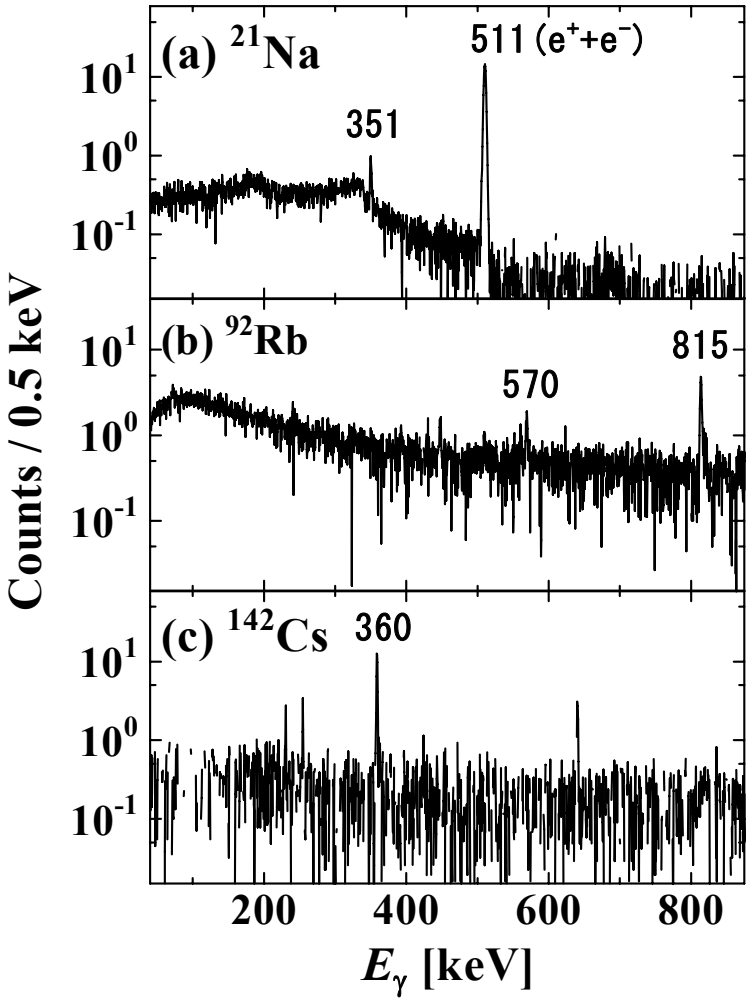

Fig. 2 γ-ray spectra taken by Ge detector. γ-ray peaks of decaying ^{21}Na (a), ^{92}Rb (b) and ^{142}Cs (c) are labeled by energies in units of keV.

References

[1] H. Makii *et al*., JAEA-Tokai TANDEM Ann. Rep. 2005, JAEA-Revew 2006-029 (2006) 37-38.

[2] F. Herfuth *et al*., Nucl. Instrum. Methods Phys. Res., A469 (2001) 254-275.

2.13 Development of spin-polarized radioactive nuclei around ^{132}Sn for nuclear spectroscopy

Y. Hirayama[1], K. Matsuta[2], M. Mihara[2], S.C. Jeong[1], H. Miyatake[1], T. Hashimoto[3], Y.X. Watanabe[1], N. Imai[1], H. Ishiyama[1], S. Ichikawa[3], T. Ishii[3], T. Izumikawa[4], D. Kameda[5], I. Katayama[1], H. Kawakami[1], H. Kawamura[6], H. Makii[3], S. Mitsuoka[3], S. Momota[7], D. Nagae[3], D. Nishimura[2], K. Nishio[3], T. Otsubo[4], A. Osa[3], T.K. Sato[3], and T. Shimoda[2]

Spin-polarized radioactive nuclear beam (RNB) is a useful tool to study nuclear structures and electromagnetic property of materials. For nuclear spectroscopy around the doubly magic nucleus ^{132}Sn at TRIAC, we have been developing a tilted-foil (TF) technique for production of spin-polarized RNBs. As the first step in the development of TF technique, we could produce the 5.9±0.5% polarized ^{8}Li ($T_{1/2}$=838ms) beam [1] at the experiment in Jan. 2007. To establish the TF technique in the region of heavy nuclei as the next step, we have tried to produce the polarized ^{123}In ($T_{1/2}$=6.0 sec, $I^{\pi} = 9/2^{+}$, g =1.220) and ^{143}Ba ($T_{1/2}$=14.3 sec, $I^{\pi}=5/2^{-}$, g=0.1772) in the experiments RNB06K02 (spokesperson: Y. Hirayama) and RNB06K03 (K. Matsuta), respectively, in Mar. 2008.

^{123}In and ^{143}Ba nuclei were produced by proton-induced fissions of uranium at JAEA-ISOL, and were accelerated up to 178 keV/A by TRIAC. Typical beam intensities of ^{123}In and ^{143}Ba RNBs at the entrance of the tilted foils were about 4x10^{3} pps and 2x10^{3} pps, respectively. ^{123}In (^{143}Ba) nuclei passing through the twenty 3μg/cm^{2} thick polystyrene foils at the tilt angle 70^{o} were implanted in an InP (BaF_2) crystal at a temperature of about 10K (300K), where the magnetic field B_0 ~ 0. 5 T was applied to preserve the nuclear polarization. The nuclear polarization was measured with β-NMR technique.

The finite polarizations of ^{123}In and ^{143}Ba have not been confirmed in these experiments. It is necessary to further check the TF system and the stopper material independently. The present TF system could be examined by applying to TDPAD measurements of short-lived isomers, whose quadrupole moments are known. It is also possible to search the stopper materials by utilizing the polarized RNBs of In (Ba) isotopes near the stability line, since these polarized RNBs will be produced by projectile-like fragmentation reactions. After these examinations, we will perform the production of polarized In and Ba isotopes with TF technique.

References

[1] Y. Hirayama *et al*., JAEA-Tokai TANDEM Ann. Rep. 2006, JAEA-Review 2007-046 (2007) 28-29.

[1] High Energy Accelerator Research Organization (KEK)
[2] Osaka University
[3] Japan Atomic Energy Agency (JAEA)
[4] Niigata University
[5] The Institute of Physical and Chemical Research (RIKEN)
[6] Rikkyo University
[7] Kochi University of Technology

CHAPTER 3

Nuclear Reaction

This is a blank page.

3. 1 Measurement of quasi-elastic backscattering in ^{58}Ni+^{124}Sn

Y.X. Watanabe[1], S. Mitsuoka[2], K. Nishio[2], S.C. Jeong[1], T. Hashimoto[2],
Y. Hirayama[1], N. Imai[1], H. Ishiyama[1], H. Miyatake[1], and H. Ikezoe[2]

The fusion excitation functions for the five systems of ^{40}Ca+^{90,94,96}Zr and ^{48}Ca+^{90,96}Zr at near- and sub-barrier energies were measured at the Laboratori Nazionali di Legnaro, and it was reported that the two systems possessing multi-neutron transfer channels with positive *Q*-values (^{40}Ca+^{94,96}Zr) have a large enhancement of cross sections at lower energies with respect to the other systems [1]. This suggests that the positive *Q*-value multi-neutron transfer channels enhance the sub-barrier fusion cross sections. In the two systems of ^{58}Ni+^{124}Sn and ^{64}Ni+^{118}Sn which forms the same compound nucleus ^{182}Pt, the former system has the positive *Q*-value multi-neutron transfer channels, but the both systems show similar fusion cross sections below the barriers [2]. In the entrance channel of the fusion process, the projectile nucleus gets over a barrier generated by the Coulomb potential and the nuclear potential, and then it is captured by the target nucleus. They undergo the non-equilibrium process, forming a compound nucleus or getting apart again from each other as deep-inelastic scattering or quasi-fission. The entrance barrier may be modified by a tunnel effect, collective excitations and nucleon transfer channels. The positive *Q*-value multi-neutron transfer channels are likely to promote the capture cross section which directly enhances the compound nucleus formation for the systems of ^{40}Ca+^{94,96}Zr. Although the system of ^{58}Ni+^{124}Sn shows no enhancement of the compound nucleus formation, it is possible that the capture cross section is promoted by the positive *Q*-value multi-neutron transfer channels, leading to deep-inelastic scattering or quasi-fission, not to the compound nucleus. In order to investigate a possible effect of the positive *Q*-value multi-neutron transfer channels on the capture cross sections, we intended to measure quasi-elastic backscattering in the two systems of ^{58}Ni+^{124}Sn and ^{64}Ni+^{118}Sn.

In FY2007, we performed the measurement for the system of ^{58}Ni+^{124}Sn with the same experimental setup which we used for the system of ^{64}Ni+^{118}Sn in FY2006. The ^{58}Ni beam was accelerated by the JAEA tandem accelerator and the superconducting booster linac, and impinged on the ^{124}Sn target, which was made on the carbon film (~30 μg/cm^2) by a sputtering method with the thickness of ~110 μg/cm^2. The quasi-elastic backscattered particles were detected by four silicon semiconductor detectors located at angles of 162° and 172° to the beam direction. The Rutherford scattering was also detected by two silicon semiconductor detectors located at the forward angle of 45°. Tuning the superconducting booster linac, beam energies were altered between 195 and 245 MeV by 2 MeV step. Correcting the centrifugal potential for each energy and each angle, the excitation function of the quasi-elastic backscattering at the 42 incident energies was obtained.

[1] High Energy Accelerator Research Organization (KEK)
[2] Japan Atomic Energy Agency (JAEA)

The upper panel of fig. 1 shows the measured differential quasi-elastic cross sections relative to the Rutherford ones. The lower panel shows the fusion cross sections from ref. [2]. The abscissa indicates the energy in the center-of-mass system. The data for the system of ^{64}Ni+^{118}Sn are shifted to higher energy by the barrier difference (1.09 MeV) between the two systems for comparison, which was calculated using the Bass potential [3]. Several curves in the lower panel indicate the results of coupled-channel calculations with the CCFULL code [4]. The quasi-elastic excitation functions (curves in the upper panel) are deduced by differentiating the products of the calculated fusion cross sections and the energies. The broken and solid lines indicate the results of the calculations with collective excitations. They contain one-phonon excitation of the quadrupole state for Ni and one- and two-phonon excitations of the quadrupole and octupole states for Sn. The dot-dashed line indicates the result of the calculation for the system of ^{58}Ni+^{124}Sn containing a pair-neutron transfer channel as well as the collective excitations. Although the measured quasi-elastic excitation function of ^{58}Ni+^{124}Sn shows larger values than one for the system of ^{64}Ni+^{118}Sn around the energy of 160 MeV, the result of the calculation with a pair-neutron transfer channel reproduces the ^{58}Ni+^{124}Sn data qualitatively. The fusion excitation functions show the similar situation. This suggests that the multi-neutron transfer channels have no significant effect on the capture cross sections for the system of ^{58}Ni+^{124}Sn, which is qualitatively explained by the one transfer channel of a pair of neutrons.

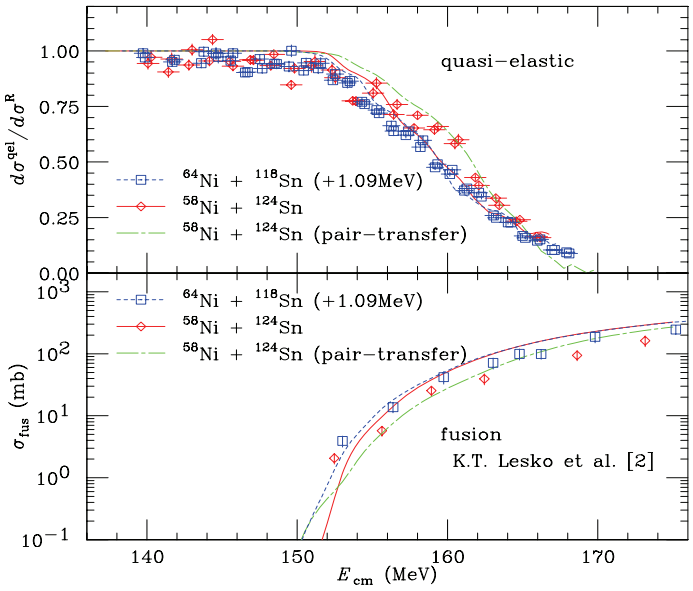

Fig. 1 The upper panel shows the ratio of the differential quasi-elastic scattering cross sections relative to the Ruthrford ones ($d\sigma^{qel}/d\sigma^{R}$) and the lower panel shows the fusion cross sections (σ_{fus}) from ref. [2]. Details are discussed in the text.

References

[1] A.M. Stafanini *et al.*, Phys. Rev., C76 (2007) 014610.

[2] K.T. Lesko *et al.*, Phys. Rev., C34 (1986) 2155-2164.

[3] R. Bass, Phys. Rev. Lett., 39 (1977) 265-268.

[4] K. Hagino, N. Rowley and A.T. Kruppa, Comp. Phys. Comm., 123 (1999) 143-152.

3. 2 Barrier distribution of quasi-elastic backscattering in ^{86}Kr+^{208}Pb

S. Mitsuoka[1], H. Ikezoe[1], K. Nishio[1], T. Hashimoto[1], Y.X. Watanabe[2],
S.C. Jeong[2], Y. Hirayama[2], N. Imai[2], H. Ishiyama[2], and H. Miyatake[2]

We have systematically measured the barrier distributions in ^{48}Ti, ^{54}Cr, ^{56}Fe, ^{64}Ni and ^{70}Zn+^{208}Pb relating to the Pb-based cold fusion reactions for the production of super-heavy elements Z=104, 106, 108, 110 and 112, respectively [1]. The barrier distributions were derived from the first derivative of the quasi-elastic (QE) backscattering cross sections relative to the Rutherford scattering cross section. The shape of the barrier distributions was well reproduced by the results of a coupled-channel calculation taking account of the coupling effects of two phonon excitations of the quadrupole vibration for the projectiles and of the octupole vibration for the ^{208}Pb target [1,2]. The centroid of the barrier distributions showed a good agreement with that from the Christensen-Winther (C-W) potential, but showed a deviation from the Bass and several predicted barrier heights by about 3-10 MeV toward the low energy side [1]. Recently, a similar work on the QE barrier distribution has been measured in the ^{86}Kr+^{208}Pb reaction relating to the cold fusion for Z=118 [3]. They reported that such deviation was very small except for the C-W potential. Their data were taken at various detector angles down to 125° in the steps of 5° at five beam energies by using the cyclotron accelerator. Here we measured the QE distribution in the same ^{86}Kr+^{208}Pb reaction by using the JAEA tandem-booster accelerator.

A ^{86}Kr^{15+} beam was supplied from an ECR ion source in the high voltage terminal of the tandem accelerator. A ^{208}Pb target (100 μg/cm^2 in thickness, 3 mm in diameter, 99% enriched) with carbon backing (30 μg/cm^2) was bombarded by the ^{86}Kr beam with changing the energy about 30 times in the steps of 1.5 MeV. As shown in fig. 1, the backward QE scattering was detected by 16 solid state detectors (SSDs) arranged annularly with respect to the beam axis at the laboratory angles of 172° and 164°. Other SSDs at ±45° monitored the beam intensity. The barrier distributions were obtained by taking the first derivative of the QE excitation function $\sigma_{QE}(E)$ relative to the Rutherford scattering $\sigma_R(E)$ as a function of center-of-mass energy E, that is $-d\{\sigma_{QE}(E)/\sigma_R(E)\}/dE$. Detailed analysis is in progress for QE cross sections where deep-inelastic scattering should be carefully excluded by considering the reaction Q-values of inelastic and transfer reaction channels.

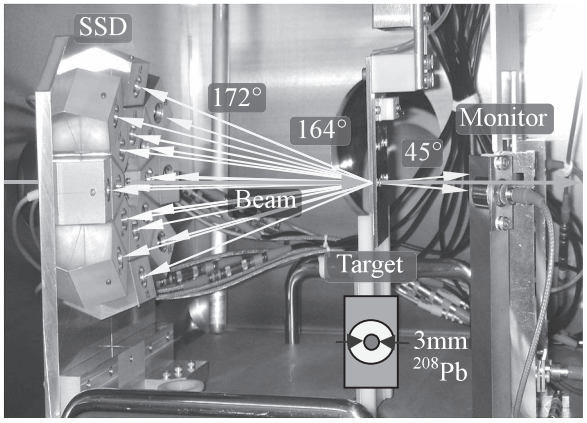

Fig. 1 Experimental set up.

References

[1] S. Mitsuoka *el al*., Phys. Rev. Lett., 99 (2007) 182701.
[2] Z. Muhammad *el al*., Phys. Rev., C77 (2008) 034604.
[3] S.S. Ntshangase *et al*., Phys. Lett., B651 (2007) 27-32.

[1] Japan Atomic Energy Agency (JAEA)
[2] High Energy Accelerator Research Organization (KEK)

3. 3 Effects of nuclear orientation on fission fragment mass distributions in the reaction of $^{36}S + ^{238}U$

K. Nishio[1], H. Ikezoe[1], S. Mitsuoka[1], I. Nishinaka[1], Y.X Watanabe[2],
Y. Nagame[1], T. Ohtsuki[3], and K. Hirose[3]

In the production of super-heavy elements based on the ^{48}Ca projectiles and actinide target reactions, the measured evaporation residue (ER) cross-sections for $^{48}Ca + ^{238}U$ and $^{48}Ca + ^{242,244}Pu$ [1,2] have maxima at bombarding energies close to the barrier for equatorial collisions, suggesting a higher fusion probability at this orientation. In the case for light projectile ^{16}O, the measured ER cross-sections suggest that fusion occurs for every colliding angles and is independent of the nuclear orientation [3]. In the reaction using heavier projectiles $^{30}Si + ^{238}U$ [4], competition between fusion and quasifission was suggested at the sub-barrier energy region, whereas no significant fusion hindrance was found at equatorial collisions. Based on the argument in [5], we expect a symmetric mass distributions for compound nucleus fission, and an asymmetric distribution for quasifission. In a reaction where fusion is influenced by orientation effects, we expect an increase of asymmetric fission at sub-barrier energies due to an increase of quasifission at polar collisions. In the present work we have measured the fragment-mass distributions for $^{36}S + ^{238}U$ in order to study a transition from quasifission to compound-nucleus fission as function of the bombarding energy.

The experiment was carried out by using sulfur beams supplied by the JAEA tandem accelerator. Two fission fragments were detected in coincidence with position-sensitive multi-wire proportional counters. Fission events after the transfer of full momentum of the projectiles to the system were separated from those following nucleon transfer reactions by measuring the emission angles and out-of-plane angles.

Figure 1 shows the dependence of the mass distributions for $^{36}S + ^{238}U$ on the center-of-mass energy ($E_{c.m.}$). At the two highest energies of 180.0 and 176.0 MeV, the mass distributions are symmetric. With decreasing bombarding

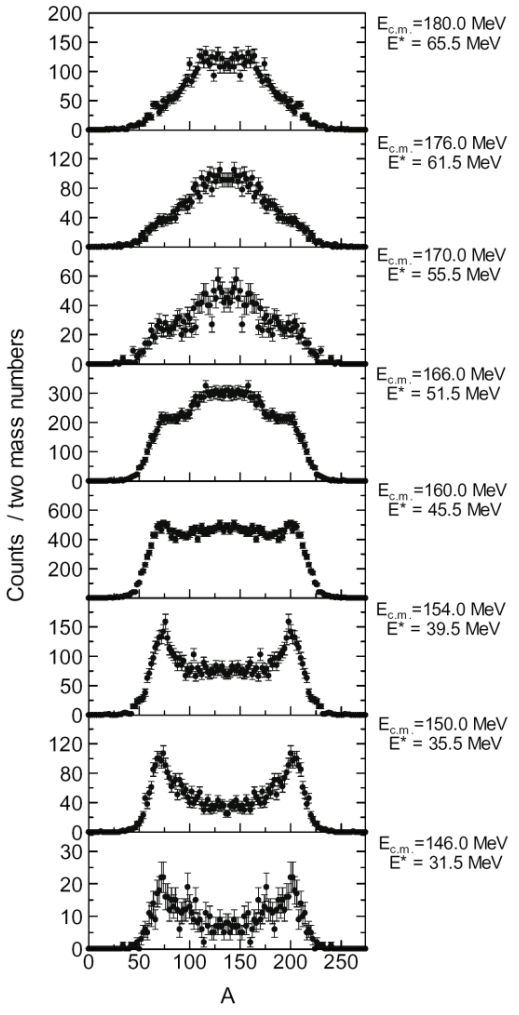

Fig. 1 Fission fragment mass distribution for $^{36}S + ^{238}U$. Center-of-mass energies ($E_{c.m.}$) and excitation energies (E^*) are indicated.

[1] Japan Atomic Energy Agency (JAEA)
[2] High Energy Accelerator Research Organization (KEK)
[3] Tohoku University

energy an additional asymmetric mass distribution becomes evident. A remarkable change occurs at sub-barrier energies of $E_{c.m.}$<160.0 MeV, where the distribution becomes dominantly asymmetric with peaks at A_H = 200 and A_L = 74.

The variation of the mass distribution with bombarding energy results from the orientation effects of the deformed target nucleus ^{238}U on the reaction. The potential energy surface for ^{274}Hs in fig. 2, calculated by a modified two center shell-model, shows that the nucleus ^{274}Hs has a fission valley leading to mass asymmetry around A_H / A_L ~ 192 / 82 in addition to the one leading to symmetric fission. In this figure, (α, z_0) values for the polar and equatorial collisions are shown. The z_0 value for the polar collisions is larger than the one for the asymmetric saddle point **A**, whereas the z_0 value for equatorial collisions has smaller z_0 values. At deep sub-barrier energy, where only polar collisions lead to nuclear contact, most of the reactions with projectile and target captured inside the Coulomb barrier disintegrate as quasifission by the repulsive Coulomb force through the asymmetric fission valley. The measured mass asymmetry A_H / A_L ~ 200 / 74 at sub-barrier region is reasonably reproduced by the calculation. At the higher bombarding energy, where equatorial collisions dominate, the system has larger probability to form the compound nucleus **C** and fissions through over the symmetric saddle point **S**. The contributions of the two components to the total cross-section vary gradually with the beam energy.

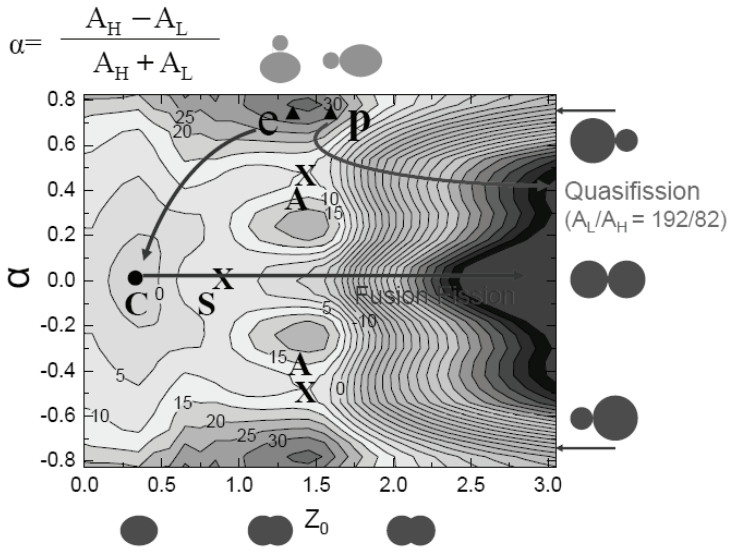

Fig. 2 Potential energy surface for ^{274}Hs plotted on the charge distance z_0 and mass asymmetry parameter α. The contact points for polar and equatorial collisions are indicated by **p** and **e**. Symmetric and asymmetric fission paths are found, stating respectively from the saddle points **S** and **A**.

References

[1] Yu.Ts. Oganessian, J. Phys., G34 (2007) R165-R242.

[2] Yu.Ts. Oganessian *et al*., Phys., Rev. C, 70 (2004) 64609.

[3] K. Nishio *et al*., Phys. Rev. Lett., 93 (2004) 162701.

[4] K. Nishio *et al*., Eur. Phys., J. A29 (2006) 281-287.

[5] M.G. Itkis *et al*., Nucl. Phys., A787 (2007) 150c-159c.

3. 4 Fusion reaction ^{82}Kr + ^{140}Ce using JAEA recoil mass separator

K. Nishio[1], H. Ikezoe[1], S. Mitsuoka[1], M. Matsuda[1], I. Nishinaka[1],
T.K. Sato[1], T. Hashimoto[1], and Y.X. Watanabe[2]

Neutron shell at N = 126 plays an important role in the properties of nuclei investigated so far. In the region of neutron deficient actinide nuclei, the liquid drop model predicts that ^{222}Cm (N=126) has low fission barrier of only 1.4 MeV, so that the nucleus is unstable against spontaneous fission and the half-life is calculated to be about 10^{-12} s. However, in the calculation which takes into account the microscopic properties of the nucleus, the shell-energy correction at N = 126 forms a deep minimum at the ground state and creates a fission barrier of about 5 MeV. This results in partial-half life for spontaneous fission of 10^5 year [1]. This nucleus decays by emitting α particle with half-life of 0.1～10 ms [1,2], long enough to be detected. For the actinide nuclei with N=126, the isotopes up to uranium (^{218}U) has been produced.
The purpose in this study is to produce neutron-deficient actinide nuclei around N=126 with element heavier than uranium and investigate the role of the shell on the stability of the nuclei. Firstly, we have started the production of a new isotope ^{220}Pu in the fusion-evaporation reaction of ^{82}Kr + ^{140}Ce at the JAEA tandem facility.

In order to separate the ^{220}Pu from the ^{82}Kr beams the JAEA recoil mass separator was used. Recent development of ECR ion source at the tandem facility succeeded in the production of high intensity beams, making such experiments more efficient. We also developed a system to reduce background particles which pass through the separator, as explained below. We found that most of the scattered particles are generated when the beams hit the edge of the frame used to support the thin target foil on the rotating disk. The number of background particle transported to the focal plane is shown in fig. 1(a) obtained in the reaction of ^{82}Kr + ^{140}Ce with the ^{82}Kr energy of 380 MeV. Intensive background particles are generated when the beam hits the frames (we have two frames). In order to prevent the scattering of the projectiles at the frames, we developed a beam chopper system synchronized with the target rotation. The location of the frame on the wheel is monitored by a photo-sensor. The signal was fed to the high voltage generator to operate an electro-static stirer to kick the beams. Figure 1 (b) shows the spectrum of background particles under the operation of the chopper. With this method, the background rate was suppressed to be 5 % of the value before.

We have carried out the experiment ^{82}Kr + ^{140}Ce with suppressed background condition. The ^{140}Ce target was made by sputtering the Ce metal on a 1.2 μm aluminum foil with the thickness of 400 μg/cm^2. The sputtered material was covered by a carbon layer (20～30 μg/cm^2) to prevent oxidization. The target was irradiated by 55 pnA ^{82}Kr beams with the center-of-mass energy 228 MeV at the middle of the Ce target layer. With totally 29 hour irradiation (net), we did not observed any indication of the production of ^{220}Pu.

[1] Japan Atomic Energy Agency (JAEA)
[2] High Energy Accelerator Research Organization (KEK)

The upper limit cross-section was 70 pb, and the value is compared with the fusion-evaporation calculation in fig. 2, where the calculations have uncertainty arising from the estimation of fusion hindrance from the data obtained in refs. [3] and [4].

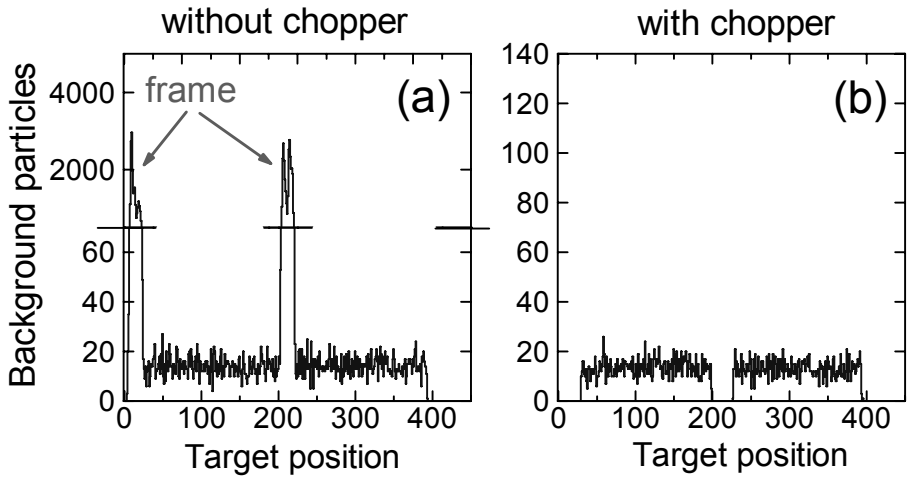

Fig. 1 Background particles transported to the focal plane of the JAEA recoil mass separator plotted as a function of the location of the target wheel irradiated by the ^{82}Kr beam.

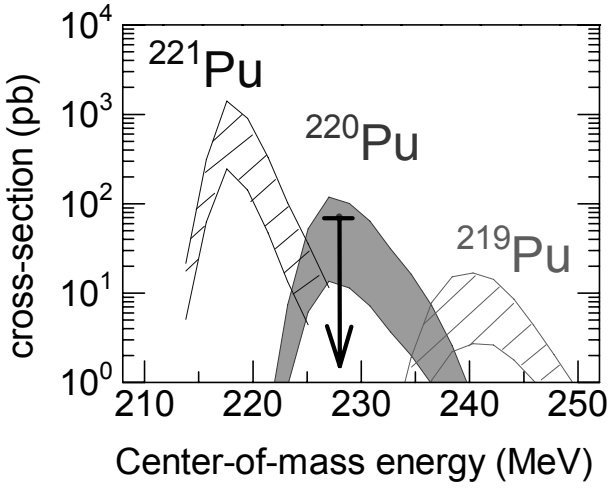

Fig. 2 Cross-sections for Pu isotopes estimated in the reaction ^{82}Kr + ^{140}Ce. The upper limit cross-sections for ^{220}Pu obtained in this experiment is shown by the arrow.

References

[1] H. Koura, private communication.

[2] P. Moller, At. Data and Nucl. Data Table, 66 (1997) 131-343.

[3] K. Nishio *et al*., Phys. Rev., C63 (2001) 044610.

[4] K. Satou *et al*., Phys. Rev., C73 (2006) 034609.

3. 5 R&D for a test of time reversal symmetry experiment using polarized nuclei

J. Murata[1], T. Akiyama[1], M. Hata[1], Y. Hirayama[2], Y. Ikeda[1], T. Ishii[3], D. Kameda[4], H. Kawamura[1], S. Mitsuoka[3], H. Miyatake[2], D. Nagae[3], K. Ninomiya[1], M. Nitta[1], E. Seitaibashi[1], and T. Toyoda[1]

Time reversal symmetry is one of the most fundamental symmetries in the nature. This project is aiming to test the time reversal symmetry using polarized ^{8}Li nuclei produced at TRIAC by tilted foil technique. Final goal of this project is to examine an existence of transverse polarization of electrons emitted from the polarized ^{8}Li nuclei in beta decay. For non-zero value of the transverse electron polarization violates the time reversal symmetry, which is almost held in the standard model, it can be said that this project is aiming to test the standard model in a highest precision in a nuclear system. We have developed an electron polarimeter using a drift chamber, and have performed a test experiment using ^{8}Li nuclei at TRIAC in April 2008, confirming its high enough performance as a polarimeter. The experiment was performed from April 14th to 16th, 2008 using 178keV/u ^{8}Li beam in 10-100kpps intensities, produced from 60MeV ^{7}Li primary beam (~1.3e μ A) from TANDEM accelerator with ^{13}C target via ^{13}C(^{7}Li, ^{8}Li)^{12}C reaction. This report is a short description about the test experiment.

Cabbibo-Kobayashi-Maskawa (CKM) mechanism, which is consistent with all the observed CP-violating phenomena in K-meson and B-meson system, predicts a negligible effect on u-d quark systems. On the other hand, numbers of models based on physics beyond the standard model, predict visible size of CP-violating effects, i.e. T-violating effects in normal nuclear system. Therefore, observation of a non-zero T-violating effect directly implies the evidence for a new physics beyond the standard model. A triple vector correlation between nuclear spin, electron spin and momentum is a T-odd variable, therefore, assuming time reversal symmetry, beta decay rate must not depends on the correlation named *R*-correlation, defined as; $\vec{\sigma}_e \cdot \frac{\langle \vec{J}_I \rangle}{J_I} \times \frac{\vec{p}_e}{E_e}$. In the standard model, *R* is almost zero. If non-zero *R*-correlation exists, electrons emitted from the polarized nuclei would have non-zero transverse polarization. Therefore, experimental investigation of time reversal symmetry can be accomplished by the measurement of electron momentum and its transverse polarization, using polarized beta unstable nuclei [1,2].

Polarized nuclei are illuminated on the surface of solid material. In the present experiment, in order to focus on the performance test of the polarimeter system, unpolarized ^{8}Li are used. A thin cupper foil with 37mm diameter, 10 micron thickness is used as the stopper. Electrons are emitted from the stopped nuclei, and then inject towards the polarimeter, set outside of the vacuum chamber. The polarimeter utilizes the transverse analyzing power in a Mott scattering of electrons from heavy nuclei. By measuring hitting ratio between upward and downward scattered electrons, the transverse polarization can be determined.

[1] Department of Physics, Rikkyo University
[2] High Energy Accelerator Research Organization (KEK)
[3] Japan Atomic Energy Agency (JAEA)
[4] The Institute of Physical and Chemical Research (RIKEN)

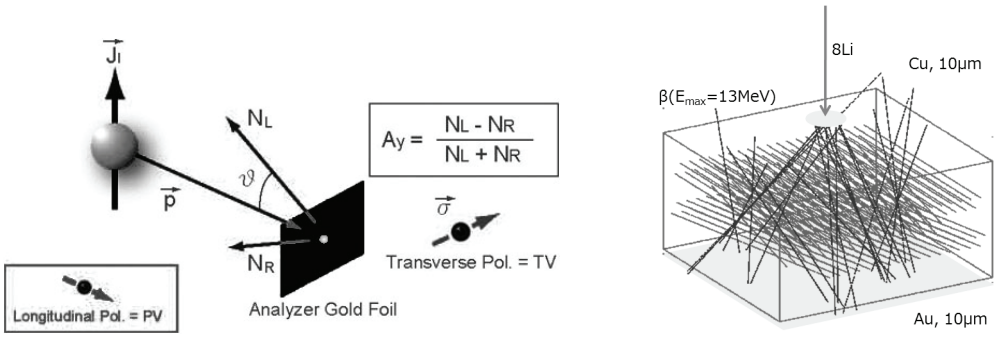

Fig. 1 [Left] Principle of determining electron transverse polarization by observing up-down asymmetry in backward scattering angular distribution. [Right] Reconstructed "V-track"s obtained in the TRIAC experiment using ^{8}Li (Real Data).

On this purpose, our polarimeter is designed to observe not only the tracks of the incident electrons, but also the second tracks of backward scattered electrons which originate from a thin metal analyzer foil, set behind the electron tracking detector. Our polarimeter consists of trigger scintillation counters, planer drift chamber, and the analyzer foil. We have built a planer multi-wire drift chamber and present experiment is aimed to test the performance as a polarimeter at TRIAC, yielding successful determination of the "V-track" events scattered from the thin gold foil (10 micron foil, 300mm x 500mm). Obtained results on the Mott scattering angular distribution is good agreement with a Mont-Carlo simulation including full detector simulation.

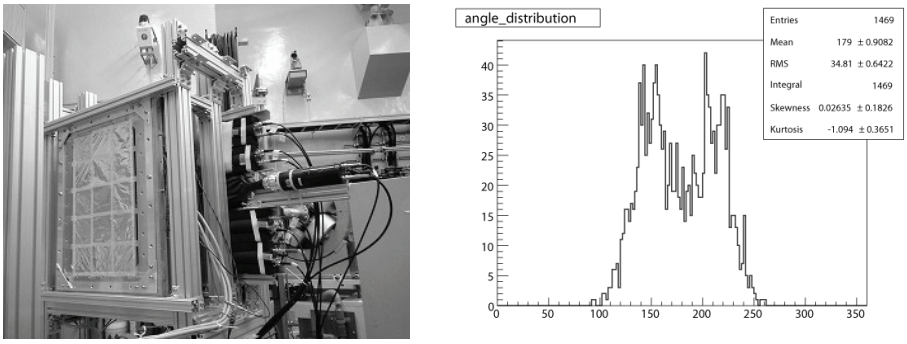

Fig. 2 [Left] Experimental setup in the TRIAC experiment. [Right] Reconstructed scattering angular distribution of the Mott scattering electrons, obtained in the TRIAC experiment.

In the next experiment at TRIAC, we are going to take first physics results on *R*-correlation using full tracking measurement with minimum systematic errors from background events.

References

[1] J. Sromicki *et al*., Phys. Rev., C 83 (1996) 932-955.

[2] R. Huber *et al*., Phys. Rev. Lett., 90 (2003) 202301.

This is a blank page.

CHAPTER 4

Nuclear Chemistry

This is a blank page.

4. 1 Oxidation of divalent nobelium (No) to the trivalent state using an electrochemistry apparatus

A. Toyoshima[1], Y. Kasamatsu[1], K. Tsukada[1], Y. Kitatsuji[1], H. Haba[2], M. Aasi[1], Y. Ishii[1], H. Toume[1], K. Akiyama[3], K. Ooe[4], W. Sato[4], A. Shinohara[4], and Y. Nagame[1]

It is interesting and challenging to elucidate oxidation-reduction (redox) properties of the heaviest elements with atomic numbers $Z > 100$, such as stable oxidation states and redox potentials in aqueous solutions. Such redox properties show relative stabilities of the oxidation states, and thus redox studies of the heaviest elements give us valuable information on binding energy of valence electrons for those elements that would be influenced by relativistic effects. Redox properties of the heaviest elements are, however, little known because these need to be studied based on atom-at-a-time chemistry. So far performed were the redox experiments using chemical oxidizing or reducing agents. These methods are, however, unsuitable for precise determination of the redox potentials because of the irregular experimental conditions and the slow kinetics. An electrochemical approach is, therefore, of essential importance to examine the redox properties of the heaviest elements. Recently, we have developed a new electrochemical apparatus using a flow-electrolytic column combined with a chromatographic separation technique available for a tracer scale [1]. In this report, we present successful electrochemical oxidation of nobelium (No) in 0.1 M α-hydroxyisobutyric acid (α-HIB) solution using the apparatus on single-atom scale.

The isotopes ^{255}No (3.1 min) and ^{162}Yb (18.9 min) were produced in the ^{248}Cm(^{12}C,5*n*) and Gd(^{12}C,*xn*) reactions, respectively, at the JAEA tandem accelerator. Ytterbium-162 was used to monitor its elution behavior as a trivalent ion. Reaction products transported by a He/KCl gas-jet method were deposited on a collection site of a chemical device for 10 min. The products were then dissolved with 0.1 M α-HIB (pH 3.9) and subsequently fed into a column working-electrode of the electrochemistry apparatus through a thin Teflon capillary. The working electrode was made by glassy-carbon fibers packed into a porous Vycor-glass tube, and the surface of the carbon fibers was chemically modified with a polyelectrolyte material of Nafion perfluorinated ion-exchange resin. Thus the working electrode serves just as a cation-exchange column. An electric potential applied to the electrode was adjusted to be 0.2 - 1.2 V versus an Ag-AgCl reference electrode using a potentiostat. Details of the electrochemistry apparatus are found in ref. [1]. The effluents from the working electrode were fractionated into six 180 μL aliquots which were collected on separate 6 Ta discs. The products adsorbed on the electrode were then stripped with 280 μL of 3 M HCl and the effluent was collected on another 2 Ta discs. These eight fractions were evaporated to dryness with helium gas and halogen heat lamps, and were subjected to α-spectrometry equipped with eight 600 mm^2 PIPS detectors. After the α-particle measurement, γ-rays of ^{162}Yb were measured with Ge detectors. Elution behaviour of ^{81}Sr (22.2 min) and ^{162}Yb produced by the Ge(^{12}C,*xn*) and Gd(^{12}C,*xn*) reactions, respectively,

[1] Japan Atomic Energy Agency (JAEA)
[2] The Institute of Physical and Chemical Research (RIKEN)
[3] Tokyo Metropolitan University
[4] Osaka University

was also measured in separate experiments under the same conditions as those of ^{255}No in order to verify the difference in elution behavior between the divalent (Sr^{2+}) and trivalent (Yb^{3+}) ions.

In fig. 1(a), the elution behavior of $^{81}Sr^{2+}$ and $^{162}Yb^{3+}$ used as the indicators for the oxidation states is shown by triangles and squares, respectively. Open symbols represent the behavior under the applied potential of 0.2 V and the closed symbols are of 1.2 V. Independently of the applied potentials, $^{162}Yb^{3+}$ was eluted in 0.1 M α-HIB, while $^{81}Sr^{2+}$ was stripped with 3 M HCl, showing clear separation of the different oxidation states under the present conditions. In figs. 1(b) and (c), elution behavior of ^{255}No is shown under the applied potentials of 0.2 V and 1.2 V, respectively. At the low potential of 0.2 V, ^{255}No was observed only in 3 M HCl, indicating that No is bound in the most stable divalent state. On the other hand, at the higher potential of 1.2 V, ^{255}No was unambiguously detected in 0.1 M α-HIB, showing that No exists as a trivalent ion. These results demonstrate that the electrochemical oxidation of No^{2+} to No^{3+} is successfully performed.

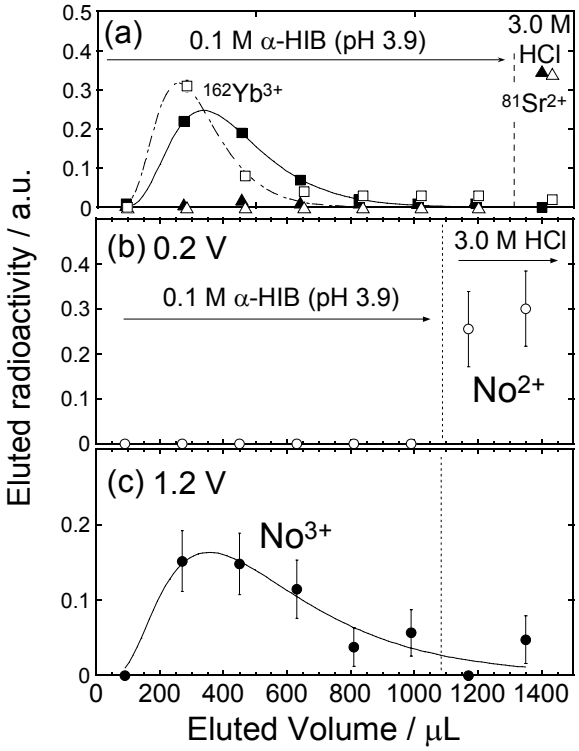

Fig. 1 (a) Elution behavior of $^{81}Sr^{2+}$ (Δ, ▲) and $^{162}Yb^{3+}$ (□, ■); open symbols show the behavior under the applied potential of 0.2 V, while closed symbols are of 1.2 V. (b) Elution behavior of No^{2+} (○) under the applied potential of 0.2 V and (c) No^{3+} (●) under the potential of 1.2 V.

Reference

[1] A. Toyoshima *et al*., Radiochim. Acta, 96 (2008) 323-326.

4. 2 Adsorption of element 105, Db, on the anion-exchange resin in HF/HNO_3 media

Y. Kasamatsu[1], A. Toyoshima[1], M. Asai[1], K. Tsukada[1], Y. Ishii[1], H. Toume[1], I. Nishinaka[1], T.K. Sato[1], Y. Nagame[1], H. Haba[2], H. Kikunaga[2], K. Akiyama[3], S. Goto[4], T. Ishikawa[4], H. Kudo[4], W. Sato[5], K. Ooe[5], T. Kuribayashi[5], A. Shinohara[5], N. Kinoshita[6], M. Arai[6], A. Yokoyama[6], M. Sakama[7], Z. Qin[8], and Ch.E. Düllmann[9]

The aqueous phase chemistry of the group-5 elements Nb, Ta, and element 105 (dubnium, Db) has been studied by several research groups by chromatographic methods, and the similarity of the chemical behavior of Db to those of its lighter homologues has been discussed [1-3]. For deeper understanding of the chemical properties of Db, more detailed systematic studies are required. To systematically investigate fluoride complexation of Db as a function of the fluoride ion concentration and the nitrate ion concentration, we previously studied the anion-exchange behavior of the homologues Nb, Ta, and also the pseudo homologue Pa in HF/HNO_3 solutions by a batch method [4, 5]. Furthermore, we also conducted on-line anion-exchange experiments with Nb and Ta produced at the JAEA tandem accelerator and confirmed that distribution coefficients of Nb and Ta obtained by the batch experiments and those by the on-line experiments agree with each other [6]. In the present work, we performed on-line anion-exchange experiments with Db together with Ta.

Dubnium-262 was produced in the $^{248}Cm(^{19}F, 5n)$ reaction at the JAEA tandem accelerator. Tantalum isotopes were simultaneously produced by using 32 μg/cm^2 of ^{152}Gd contained in the 540-μg/cm^2 ^{248}Cm target to monitor the elution behavior and chemical yield of Ta during the experiment. The reaction products were continuously transported by a He/KCl gas-jet system to the collection site of the AIDA (automated ion-exchange separation apparatus coupled with the detection system for alpha-spectroscopy). After the collection for 73 s, the products were dissolved in 120 μL of 0.89 M HF/0.3 M HNO_3 solution and were fed onto the column (ϕ1.0 × 3.5 mm) filled with the anion-exchange resin MCl GEL CA08Y at a flow rate of 1.2 mL/min. The effluent was collected on a tantalum disk as fraction 1, which was followed by the evaporation to dryness with hot helium gas and a halogen heat lamp. The remaining Db and Ta on the resin were stripped with 150 μL of 0.015 M HF/6 M HNO_3. The effluent was collected on another disk as fraction 2 and evaporated to dryness in the same way. The both disks were automatically transferred to the α-spectroscopy station of AIDA, where α particles were detected with eight passivated ion-implanted planar silicon (PIPS) detectors. After the α-particle measurement, some of the samples were subjected to

[1] Japan Atomic Energy Agency (JAEA)
[2] The Institute of Physical and Chemical Research (RIKEN)
[3] Tokyo Metropolitan University
[4] Niigata University
[5] Osaka University
[6] Kanazawa University
[7] University of Tokushima
[8] Institute of Modern Physics (IMP)
[9] Gesellschaft fur Schwerionenforschung (GSI)

the γ-ray measurement with Ge detectors to monitor the γ-ray intensity of ^{169}Hf which is a daughter nuclide of ^{169}Ta. The anion-exchange procedure was repeated about 4000 times with AIDA.

Alpha spectra observed in the both fractions are shown in fig. 1. The number of α counts ascribed to the decay of 34-s ^{262}Db and its daughter 3.9-s ^{258}Lr was 5.6 in fraction 1 and 0.8 in fraction 2. Alpha counting in the energy region of interest was almost free from interfering events from other product nuclides. In the evaluation of the α counts, a little interfering events and the background from such as electronic noise were subtracted. The percent adsorption (%*ads*) is defined by the equation of $100 \times A_2 / (A_1 + A_2)$, where A_1 and A_2 are radioactivities in the fractions 1 and 2, respectively. The %*ads* value of Db on the anion-exchange resin was less than 80% (99% confidence level) under the studied conditions in which 76% of Nb and more than 99% of Ta adsorb on the resin [6]. It is found that the adsorption of Db on the anion-exchange resin is considerably weaker than that of Ta in 0.89 M HF/0.3 M HNO_3.

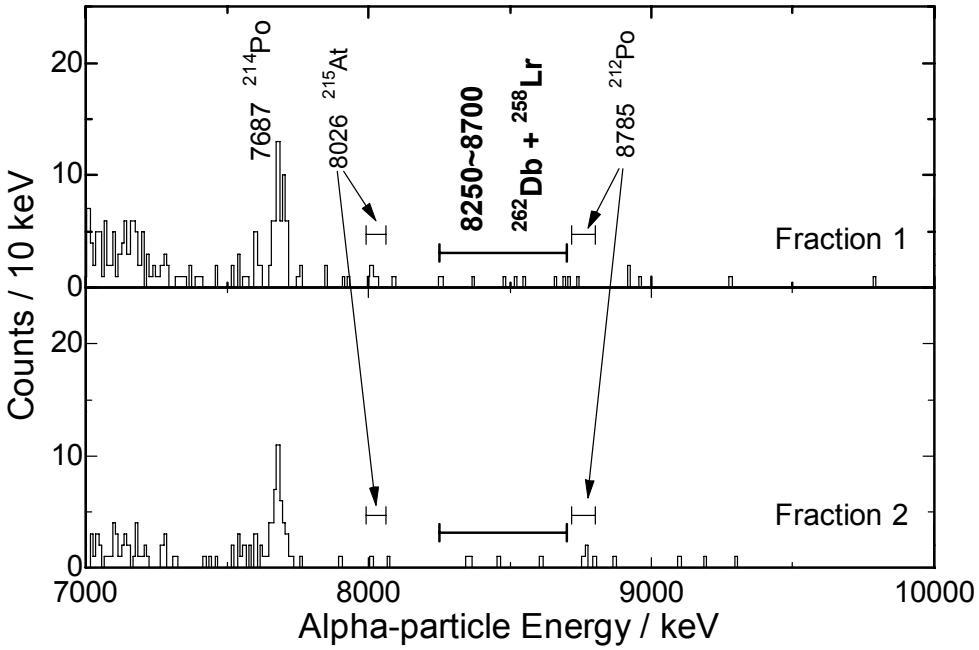

Fig. 1 Alpha spectra measured for the fraction 1 and 2.

References

[1] M.K. Gober *et al*., Radiochim. Acta, 57 (1992) 77-84.

[2] H.P. Zimmermann *et al*., Radiochim. Acta, 60 (1993) 11-16.

[3] W. Paulus *et al*., Radiochim. Acta, 84 (1999) 69-77.

[4] Y. Kasamatsu *et al*., J. Nucl. Radiochem. Sci., 8 (2007) 69-72.

[5] Y. Kasamatsu *et al*., J. Radioanal. Nucl. Chem., in press.

[6] Y. Kasamatsu *et al*., JAEA-Tokai TANDEM Ann. Rep. 2006, JAEA-Review 2007-046 (2008) 65-66.

4. 3 New apparatus AIDA-II for the study of aqueous chemistry of the transactinide elements

K. Tsukada[1], Y. Kasamatsu[1], M. Asai[1] A. Toyoshima[1], Y. Ishii[1], H. Toume[1], and Y. Nagame[1]

In order to carry out chemical experiments on the heaviest elements with single atoms, we developed an automated rapid ion-exchange separation apparatus based on high performance liquid chromatography (HPLC) coupled to an on-line α-particle detection system, AIDA (Automated Ion-exchange separation apparatus coupled with the Detection system for Alpha-spectroscopy). AIDA enables us to perform cyclic discontinuous column chromatographic separations of short-lived nuclides in aqueous solutions and automated detection of α-particles within a typical cycle of 80 - 110 s. Chemical properties of element 104, rutherfordium (^{261}Rf: $T_{1/2}$ = 78 s), have been successfully studied with AIDA in acidic solutions [1].

Aqueous chemistry of element 105, dubnium (Db), is now being performed at JAEA [2]. The nuclide 34-s ^{262}Db is produced in the ^{248}Cm(^{19}F, 5n) reaction with the cross section of 1.5 nb. This results in the production rate of about 0.25 atoms per min. To obtain more accurate data with high statistics, we need to develop a new device to shorten the time for the preparation of α sources. A new apparatus based on a continuous sample preparation and detection system, i.e., continuous collection and evaporation of effluent,

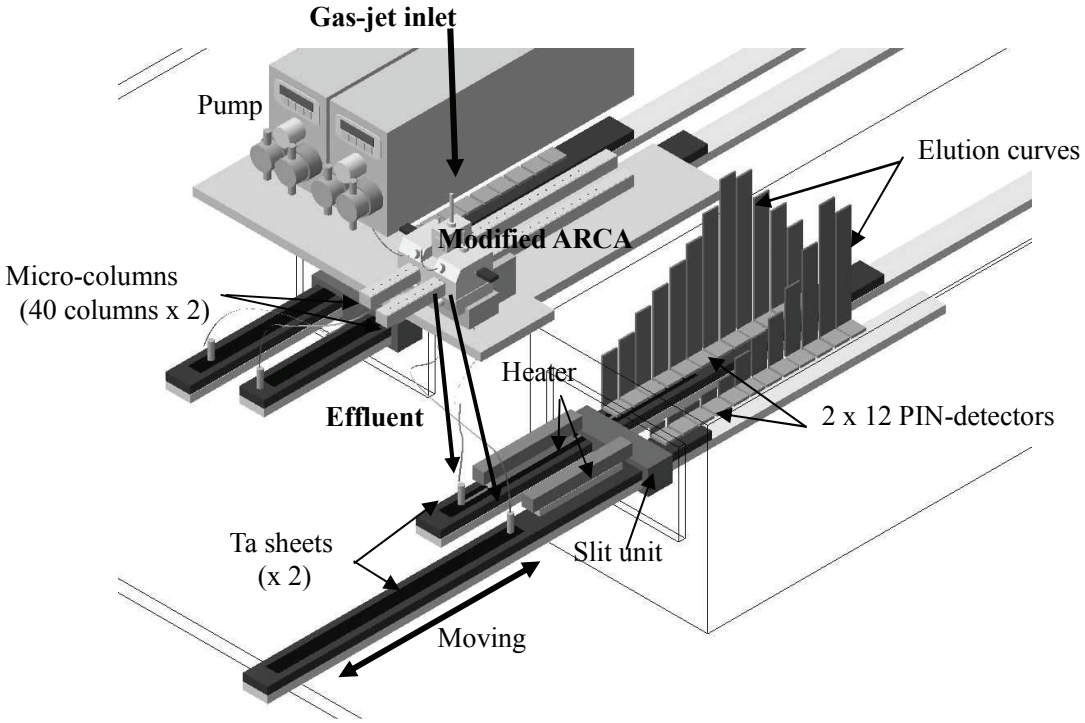

Fig. 1 Schematic view of AIDA-II.

[1] Japan Atomic Energy Agency (JAEA)

and successive α-particles measurement, has been developed. Figure 1 shows the schematic view of the new apparatus AIDA-II. For the HPLC system, we modified the ARCA [3]. As shown in fig. 1, there are two pairs of sampling and detection systems, each has two sample transport arms on which thin Ta sheets (30 cm long) are placed. Each arm continuously moves into the detection chamber filled with helium gas. The effluent is continuously collected on this moving Ta sheet and evaporated with halogen heat lamps. The dried sample is successively going into the α-particle detection chamber where an array of 12 PIN-detectors is installed for each arm. The sample preparation is accomplished within 20 s. Further, from the measurement of radioactivities in each detector, we can measure an elution curve of a nuclide for each condition. The remaining nuclides in the column are stripped with other solution and collected on another Ta sheet.

References

[1] Y. Nagame *et al*., Radiochim. Acta, 93 (2005) 519.
[2] Y. Kasamatsu *et al*., separated paper in this report (ref. contents No. 4.2).
[3] M. Schädel *et al*., Radiochim. Acta, 48 (1989) 171.

4. 4 Production of radioactive tracers for chemistry of transactinide elements

S. Goto[1], T. Ishikawa[1], T. Kawasaki[1], T. Hasegawa[1], H. Kudo[1],
K. Tsukada[2], M. Asai[2], A. Toyoshima[2], and Y. Nagame[2]

Since a transactinide element has a very short life and its production cross-section is very small, only a very little quantity — usually one atom — is handled for a chemistry experiment at a time. To investigate the chemical property of such transactinide element, it is necessary that many repetition experiments in terms of a rapid chemistry method are performed until sufficient statistics are obtained. In other words, it takes very long time to even one experimental condition. Thus, the off-line experiment using a light homologue will be valid for an efficient on-line experiment. The aim of this work is to produce the non-carrier tracer for carrying out such off-line chemical experiments.

For the rapid chemistry experiments of Db, the radioactive isotopes ^{95g}Nb ($T_{1/2}$ = 35 d) and ^{179}Ta ($T_{1/2}$ = 665 d) were selected as a tracer because measuring their gamma-ray (or x-ray) is possible and the half life is long enough. The tracers were produced using the ^{96}Zr(p, $2n$)^{95g}Nb, ^{179}Hf(p, n)^{179}Ta and ^{180}Hf(p, $2n$)^{179}Ta reactions with JAEA tandem accelerator. The ^{nat}Zr foils (130 mg cm^{-2}) and the ^{nat}Hf foils (133 mg cm^{-2}) covered with aluminum foils were stacked and placed at the end of the R2 beam line. The Zr foils were put on the front of the target stack to make the proton energy optimal to the intended nuclear reactions. The proton beam energies on the Zr and Hf target were determined to be about 14 MeV and 11 MeV, respectively, according to the energy loss calculation. The irradiation time was about 17 hours, and the average beam current was about 1.7 μA. The irradiated targets were brought to Niigata University after cooling down the activity of the by-products such as ^{90g}Nb ($T_{1/2}$ = 14.6 h), ^{92m}Nb ($T_{1/2}$ = 10.15 d) , ^{96}Nb ($T_{1/2}$ = 23.4 h), and ^{177}Ta ($T_{1/2}$ = 56.6 h). The activities of ^{95g}Nb and ^{179}Ta were 1.3 MBq and 530 kBq, respectively, after 1 month from the end of bombardment. Those were enough to perform the experiment for a few months.

Each tracer nuclide was separated from the target material using an anion-exchange method. The tracers have been used in different experiments to develop newer solvent extraction technique for 5th-group elements at Niigata University.

[1] Niigata University
[2] Japan Atomic Energy Agency (JAEA)

This is a blank page.

CHAPTER 5

Nuclear Theory

This is a blank page.

5. 1 Single-particle property of unstable nuclei around N=28 from the spectroscopic factor calculated with a new shell model interaction

Y. Utsuno[1], B.A. Brown[2], T. Otsuka[3], M. Honma[4], and T. Mizusaki[5]

Spectroscopic factor represents how the single-particle orbit is occupied in a designated orbit. It is thus quite useful to explore the single-particle structure in nuclei. Recently, the spectroscopic factor of nuclei far from the β-stability line has been accessible by using the so-called knockout reaction [1]. It would provide key information on how the single-particle structure changes driven, for instance, by the spin-isospin property of the nucleon-nucleon interaction [2]. In the present study, we investigated a possible exotic shell structure in the neutron-rich region around N=28 by means of probing the spectroscopic factor. The study is based on a new shell model interaction for the sd-pf shell model space incorporating the shell evolution mechanism due to the tensor force [3].

The effective interaction used in the present study is constructed as follows. The inner-shell interactions, i.e., the sd-shell and pf-shell interactions are taken from standard ones: USD [4] for the sd shell and GXPF1A [5] for the pf shell. Since the cross shell interaction has not been explored in detail before, we develop a new one. The tensor part is fixed to be the π+ρ meson-exchange interaction with cutoff at 0.7 fm [3], and the two-body spin-orbit force is taken from the M3Y interaction [6]. We propose a new way to construct the central force of high reliability. Adopting a simple Gaussian force whose parameters are determined so that its monopole interaction becomes as close to that of the GXPF1 interaction as possible, the central force of the cross shell interaction is calculated. The new interaction successfully reproduces low-lying levels in K isotopes from N=20 to 28 systematically.

The spectroscopic factor of nuclei in the sd-pf shell is calculated with a new shell model code NuShellX [7]. It enables to reach the J-scheme shell-model dimension up to the order of 10^7, which is large enough to calculate low-lying states in this region. One of the authors (B.A.B.) is developing the code to have a similar user interface to the well-known shell-model code OXBASH [8]. It will thus replace OXBASH in a near future.

Figure 1 compares the distribution of the experimental and calculated spectroscopic factors for a single proton-hole state in ^{48}Ca. From a good agreement between them, descriptive power of the present interaction is confirmed. In particular, we excellently reproduced a characteristic feature that the $d_{5/2}$ hole state is distributed over some states in the 3-8 MeV region. We next apply the calculation to the spectroscopic factor for a neutron pickup reaction on ^{42}Si. Figure 2 shows a strong dependence on the

[1] Japan Atomic Energy Agency (JAEA)
[2] Michigan State University
[3] University of Tokyo
[4] University of Aizu
[5] Senshu University

strength of the tensor force. Without the tensor force, the ground state of the N=29 isotope ^{43}Si is 3/2$^-$ as expected from the naïve shell model configuration of a $p_{3/2}$ neutron on top of the ^{42}Si core. On the other hand, when the tensor force is included, the ground state is predicted to be 1/2$^-$ having a large spectroscopic factor with regard to the $p_{1/2}$ orbit. Hence, that spectroscopic factor should be a good measure to probe the exotic shell structure around ^{42}Si caused by the tensor force.

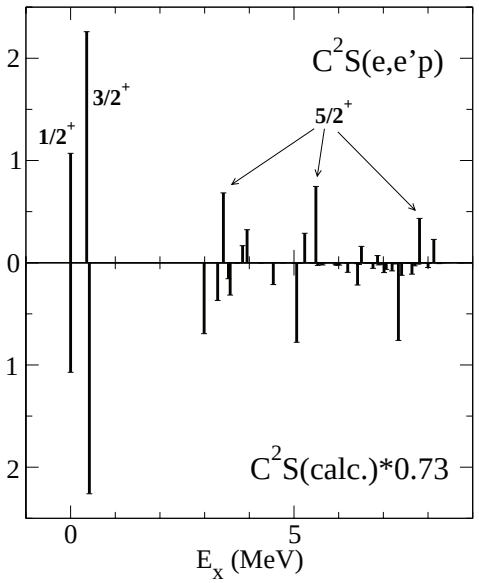

Fig. 1 Distribution of the spectroscopic factor in a proton removal reaction from ^{48}Ca compared between experiment (upper) and the present calculation (lower). For the calculation, all of the spectroscopic factors are quenched by a factor 0.73.

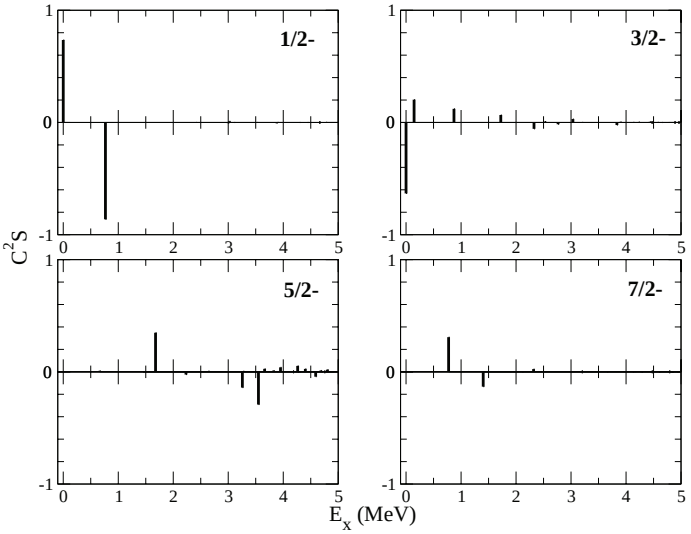

Fig. 2 Distribution of the spectroscopic factor in a neutron pickup reaction on ^{42}Si compared between interactions with tensor (upper) and without tensor force (lower).

References

[1] P.G. Hansen and J.A. Tostevin, Ann. Rev. Nucl. Part. Sci., 53 (2003) 219-261.

[2] T. Otsuka *et al*., Phys. Rev. Lett., 87 (2001) 082502-1-4.

[3] T. Otsuka *et al*., Phys. Rev. Lett., 95 (2001) 232502-1-4.

[4] B.A. Brown and B.H. Wildenthal, Ann. Rev. Nucl. Part. Sci., 38 (1988) 29-66.

[5] M. Honma *et al*., Phys. Rev. C, 69 (2004) 034335-1-34.

[6] G. Bertsch *et al*., Nucl. Phys., A284 (1977) 399-419.

[7] W.D.M. Rae, Home of NuShellX & NuShell (2007), http://knollhouse.org/ (accessed 2008-05-15).

[8] B.A. Brown, A. Etchegoyen and W.D.M. Rae, OXBASH, MSU-NSCL report No. 524 (1988).

5. 2 Analysis of inclusive (K^-, K^+) reaction with semi-classical distorted wave model

S. Hashimoto[1], M. Kohno[2], K. Ogata[3], and M. Kawai[3]

Interactions between baryons play an important role in hadronic many-body systems with strangeness. Hypernuclear physics has been disclosing characteristic features of the interactions through analyses of experimental data on hyperon production reactions, and the Λ-N interaction has been fairly well explored. However, because of inadequate data the Ξ-N interaction is very ambiguous despite the fact that its knowledge is the most important for understanding the physics of octet baryons as a probe of the strangeness S=-2 sector.

The (K^-, K^+) reaction with production of a Ξ^- hyperon is a principal source of information on the single-particle potential U_Ξ felt by the Ξ hyperon in the final hypernucleus that reflects the properties of the underlying Ξ-N interaction. The K^+ spectra of the (K^-, K^+) reaction were measured [1], and the Distorted Wave Impulse Approximation (DWIA) analyses of the data evaluated the strength of the real part of the Ξ-nucleus potential to be about -14 MeV. However, the value was not conclusive because of the limited statistics and resolution of the experiments and several simplifying approximations used in the DWIA calculations. The former may be resolved in the future, since accurate experimental data of (K^-, K^+) reactions will be measured by the Japan Proton Accelerator Research Complex (J-PARC) project.

The data of Iijima et al. [2] were analyzed by Tadokoro *et al.* [3] or by Nara et al. [4]. The calculation in ref. [3] was based on DWIA with the Green's function method using a simplifying approximation that the differential cross section for the elementary process K^-+p -> K^++Ξ^- was replaced by a constant value ignoring the variation of the elementary cross section due to the Fermi motion of the target nucleons. The analysis in ref. [4] was carried out by means of the intra-nuclear cascade (INC) model. The INC model took account of the Fermi motion with an empirical formula of elementary cross sections. In the calculations, however, the asymptotic momenta of the Ξ and $K^\pm$ were used to calculate the matrix element of the elementary process with neglecting the effects of the Ξ- and $K^\pm$-distorting potentials.

We analyzed the (K^-,K^+) reaction with Ξ^- production by means of the semiclassical distorted wave (SCDW) model and examined the validity of the assumptions in the previous works. The SCDW model has been successful in quantitatively describing (p, p'x) and (p, nx) inclusive cross sections [5]. In the recent paper [6], the SCDW model was applied to the analysis of the inclusive spectra of the (π^-, K^+) reaction with $\sum^-$ formation.

[1] Japan Atomic Energy Agency (JAEA)
[2] Kyushu Dental College
[3] Kyushu University

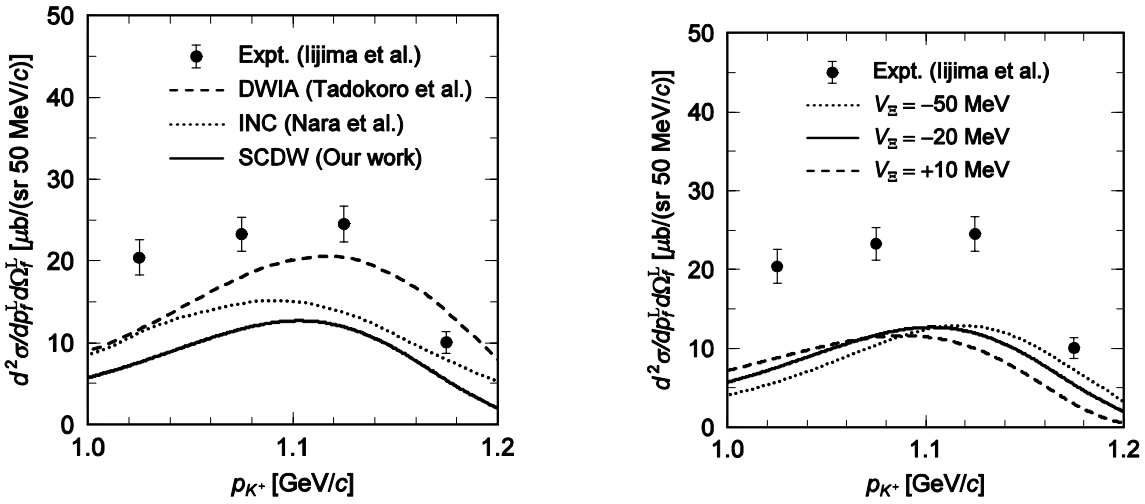

Fig. 1 Momentum spectrum of K^+ in $^{12}C(K^-, K^+)$ at incident momentum p_{K^-}=1.65 GeV/c.

In the left panel of fig. 1 we show the result of the SCDW model with V_Ξ= -20 MeV (solid line) for the inclusive (K^-, K^+) momentum, which is compared with the result of the previous DWIA calculation [3] (dashed line) and the one-step contribution evaluated with the INC model [4] (dotted line). The KEK data [2] are shown in the figure. Since the data are average over the emission angles θ_{K+} between 1.7° and 13.6°, the values calculated with the SCDW and INC models are correspondingly averaged. On the other hand, the result of ref. [3] corresponds to θ_{K+}=0°.The disagreement between the results of the SCDW model and the Green's function method is due to the difference in the dependence of the spectrum on θ_{K+}; the spectrum calculated with the SCDW model has very strong θ_{K+}-dependence which is due to the change of the two-body kinematics of the elementary process in the nuclear medium. The result of the SCDW model calculation is similar to that of the INC calculation. However, the peak positions of the two spectra deviate from each other, and the deviation is due to neglecting the Ξ potential. The right pane shows the dependence of the SCDW result on the V_Ξ. One sees that the V_Ξ-dependence of the angle-averaged spectrum is not very strong, and one hardly determines the value of V_Ξ from the present analysis.

In conclusion, it is obvious that the accurate treatment of the kinematics of the elementary process by means of the SCDW model is important to analyze the (K^-, K^+) reaction. The result of this study suggests that more accurate evaluation is necessary such as the contribution from multi-step processes.

References

[1] P. Khaustov *et al*., Phys. Rev., C61 (2000) 054603.
[2] T. Iijima *et al*., Nucl. Phys., A546 (1992) 588-606.
[3] S. Tadokoro, H. Kobayashi, and Y. Akaishi, Phys. Rev., C51 (1995) 2656.
[4] Y. Nara *et al*., Nucl. Phys., A614 (1997) 433-460.
[5] Y. Watanabe *et al*., Phys. Rev., C59 (1999) 2136.
[6] M. Kohno *et al*., Phys. Rev., C74 (2006) 064613.

5. 3 Hyperon suppression in hadron-quark mixed phase

T. Maruyama[1], S. Chiba[1], T. Tatsumi[2], and H.-J. Schulze[3]

It is well known that hyperons appear at several times normal nuclear density and lead to a strong softening of the equation of state (EOS) with a consequent substantial reduction of the maximum neutron star mass. Actually the microscopic Brueckner-Hartree-Fock approach gives much lower masses than current observation values of ~1.5 $M_{\rm sol}$. On the other hand, the hadron-quark deconfinement transition is believed to occur in hot and/or high-density matter. Taking EOS of quark matter within the MIT bag model, the maximum mass can increase to the Chandrasekhar limit once the deconfinement transition occurs in hyperon matter [1,2]. Since the deconfinement transition from hadron to quark phase may occur as a first-order phase transition, the hadron-quark mixed phase should appear.

The bulk Gibbs calculation of the mixed phase, without the effects of the Coulomb interaction and surface tension, leads to a broad region of the mixed phase (MP) [3] and large softening of the EOS. However, if one takes into account the geometrical structures of the mixed phase, one may find that MP is considerably limited and thereby EOS approaches to the one given by the Maxwell construction (MC) [4]. In this report we explore the EOS and the structure of the mixed phase during the hyperon-quark transition, properly taking account of the Gibbs conditions together with the geometrical structure of the MP.

The numerical procedure to determine the EOS and the geometrical structure of the MP is similar to that explained in detail in ref. [4]. We employ the Wigner-Seitz approximation in which the whole space is divided into equivalent cells with a given geometrical symmetry like a sphere for three dimension (3D), cylinder for 2D, and slab for 1D. A lump portion made of one phase is embedded in the other phase and thus the quark and hadron phases are separated in each cell. A sharp boundary is assumed between the two phases and the surface energy is taken into account in terms of a surface-tension parameter. The energy density of the mixed phase is thus written as

$$\varepsilon = \frac{1}{V_{\rm W}}\left[\int_{V_{\rm H}} d^3r\varepsilon_{\rm H}(\mathbf{r}) + \int_{V_{\rm Q}} d^3r\varepsilon_{\rm Q}(\mathbf{r}) + \int_{V_{\rm W}} d^3r\left(\varepsilon_{\rm e}(\mathbf{r}) + \frac{(\nabla V_{\rm C}(\mathbf{r}))^2}{8\pi e^2}\right) + \sigma S\right] \qquad (1)$$

where the volume of the Wigner-Seitz cell $V_{\rm W}$ is the sum of those of hadron and quark phases $V_{\rm H}$ and $V_{\rm Q}$, S the quark-hadron interface area. $\varepsilon_{\rm H}$, $\varepsilon_{\rm Q}$ and $\varepsilon_{\rm e}$ are energy densities of hadrons, quarks and electrons, which are $\boldsymbol{r}$-dependent since they are functions of local densities $a(\boldsymbol{r})$ ($a = n, p, \Sigma^-, \Lambda, u, d, s, e$). The Coulomb potential $V_{\rm C}$ is obtained by solving the Poisson equation. For a given density B, the optimum dimensionality of the cell, the cell size $R_{\rm W}$, the lump size R, and the density profile of each component are searched for to give the minimum energy density. We employ σ= 40 MeV/fm^2 in the present study. To calculate $\varepsilon_{\rm H}$ in the hadron phase, we use the nonrelativistic BHF approach [1] based on microscopic NN

[1] Japan Atomic Energy Agency (JAEA)
[2] Kyoto University
[3] Istituto Nazionale Fisica Nucleare (INFN)

and NY potentials that are fitted to scattering phase shifts. Nucleonic three-body forces are included in order to (slightly) shift the saturation point of purely nucleonic matter to the empirical value. For the quark phase, we use the MIT bag model with massless u and d quarks and massive s quark with m_s = 150 MeV. We here use the bag constant B=100 MeV/fm^3 and the QCD fine structure constant α_s = 0 to get the quark EOS which crosses the hadronic one at an appropriate baryon density.

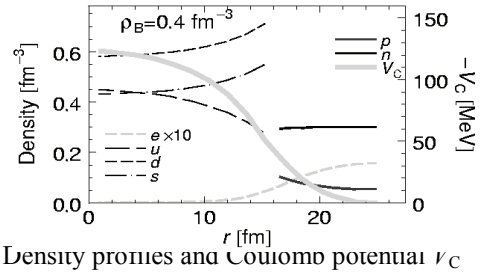

Fig. 1 Density profiles and Coulomb potential V_C within a 3D (quark droplet) Wigner-Seitz cell at ρ_B = 0.4 fm^{-3}.

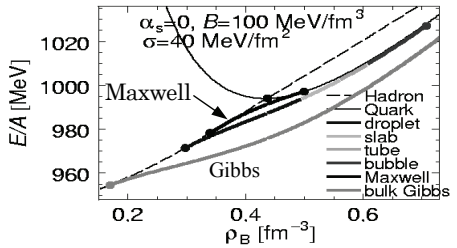

Fig. 2 EOS of the MP (thick curves) in comparison with pure hadron and quark phases (thin curves).

Figure 1 illustrates an example of the density profile in a 3D cell. One can see the nonuniform density distribution of each particle species together with the finite Coulomb potential; charged particle distributions are rearranged to screen the Coulomb potential. The quark phase is negatively charged, so that *d* and *s* quarks are repelled to the phase boundary, while *u* quarks gather at the center. The protons in the hadron phase are attracted by the negatively charged quark phase, while the electrons are repelled.

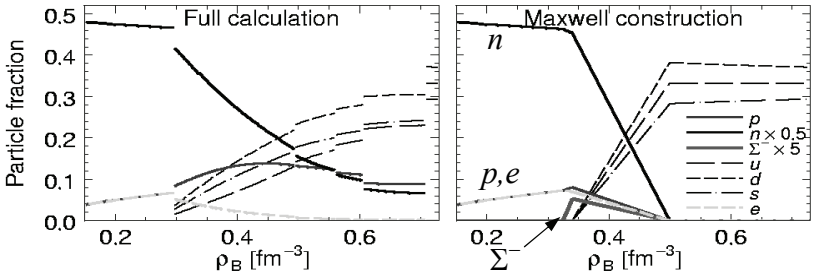

Fig. 3. Particle fractions in the MP by the full calculation (left) and the MC (right).

Figure 2 compares the resulting EOS with that of the pure hadron and quark phases. The thick black curve indicates the case of the MC, while the colored line indicates the MP starting with a quark droplet structure and ending with a bubble structure. Note that the charge screening effect, combined with the surface tension, makes the EOS of the MP close to that of the MC. However, the structure and the composition of the MP are very different from those of the MC, as shown in fig. 3. In particular, a relevant hyperon (Σ^-) fraction is only present in the MC. Non-uniform structure and suppression of hyperons in the mixed phase should have some implications on the neutrino transport and cooling of pulsars.

References

[1] M. Baldo, G.F. Burgio, and H.-J. Schulze, Phys. Rev., C61 (2000) 055801.

[2] O.E. Nicotra *et al.*, A& A, 451 (2006) 213.

[3] N.K. Glendenning, Phys. Rep., 342 (2001) 393.

[4] T. Maruyama *et al.*, Recent Res. Devel. Phys., 7 (2006) 1.

5. 4 Decay modes and limit of existence of nuclei in the superheavy nuclidic region

H. Koura[1], T. Tachibana[2,1], and S. Chiba[1]

Nucleus is a composite system consisting of protons and neutrons, and approximately 3000 nuclides have been identified experimentally. However, the existence of much more nuclides is postulated theoretically. How far the area of nuclei extends is an essential and important question in nuclear physics.

We have developed an original model based on the macroscopic and mean-field models to describe the global feature of nuclear masses, called the KTUY (Koura-Tachibana-Uno-Yamada) nuclear mass model [1]. The standard deviation from known masses is 0.67 MeV, and below 0.4 MeV from some separation energies.

By using the KTUY model, we have studied decay modes for α-decay, β-decay, proton emission and spontaneous fission ranging from light nuclei to superheavy nuclei. In the previous report [2], we estimated dominant decay modes and pointed out a possibility of existence of next "island of stability" in the region of superheeavy nuclei along neutron number N=228 in a considered region of N<250 due to the limit of calculation. After that work we extend the region of calculated nuclei to the much heavier region.

Figure 1 is a chart of estimated nuclear decay modes with longer lives than one nanosecond. In the heavier nuclear mass region, a large amount of nuclei placed over N=308 is shown. This is due to the strong magicity of N=308. The region of nuclei with longer lives than 1ns ends or is disconnected at N≈334. A solid curve as a fissility line is also drawn in the figure. This represents a macroscopic limit against spontaneous fission, and the curve and the neutron-drip line, which is shown as a comb-tooth shape here and determines the border in the neutron-side, is across each other at N≈334. Our calculation by using the KTUY model seems to be consistent with this macroscopic consideration. This calculation over Z>174 is not shown in the figure because of the limitation in our β-decay calculation. From the consideration of the macroscopic fissility line, however, the upper region seems to be not so extended or to be vanished quickly. Figure 2 shows calculated total half-lives. In this calculation we determined the number of nuclei depending on the half-life range. For example, the total number of nuclei with more than one nanosecond is estimated to be approximately eleven thousands. Some of other cases are shown in table 1.

Table 1. Number of nuclides with a certain half-lives or longer.

Shorter limit of half lives	1 s	1 ms	1 μs	1 ns
Number of nuclei	~4,000	~8,000	~10,000	~11,000

[1] Japan Atomic Energy Agency (JAEA)
[2] Waseda University Senior High School

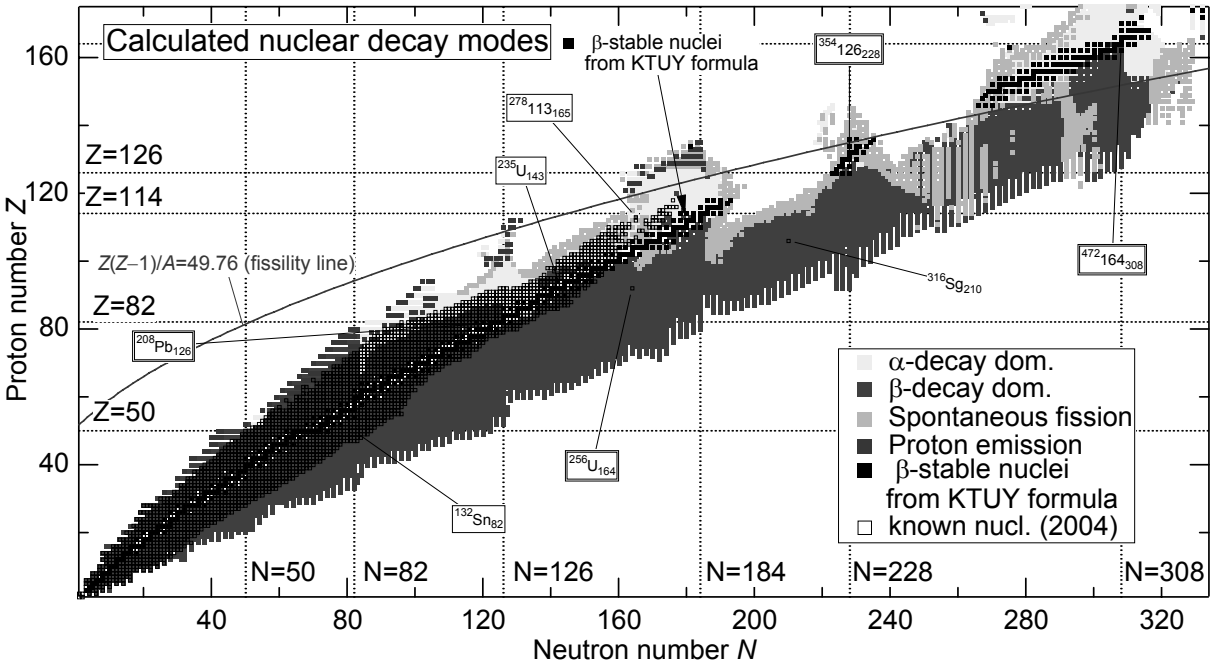

Fig. 1 Chart of the nuclides with half-lives of one nanosecond or longer. Dominant decay modes among α-decay, β-decay, proton emission and spontaneous fission are indicated.

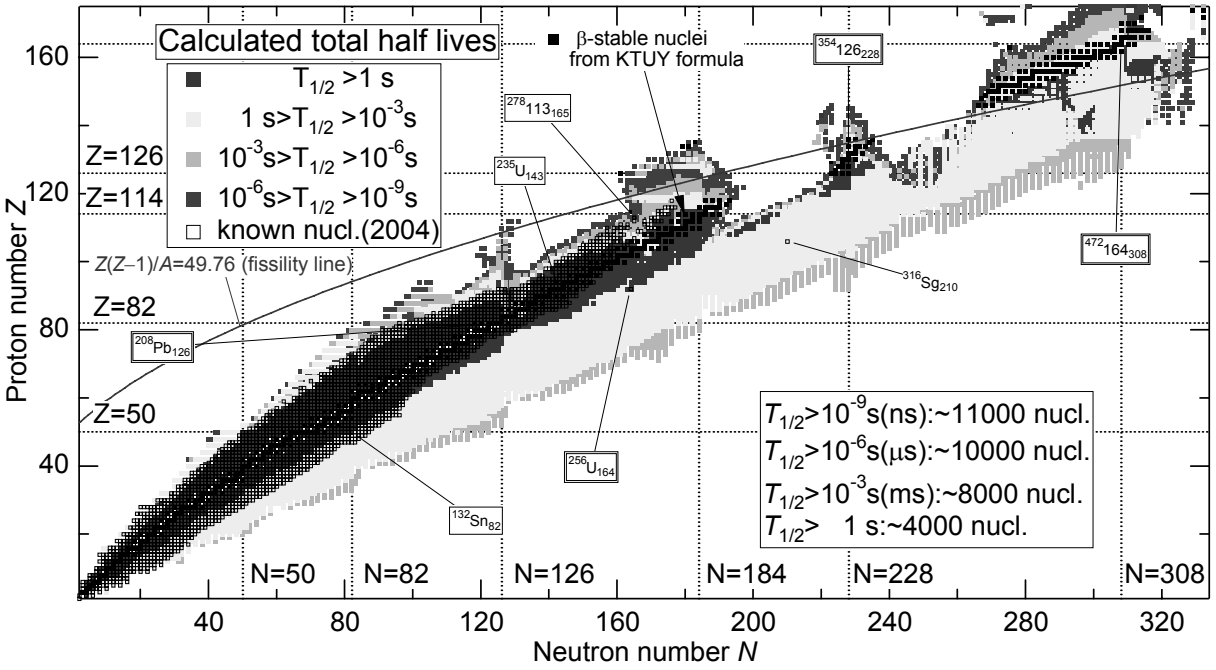

Fig. 2 Calculated total half-lives of the nuclides with half-lives of one nanosecond or longer.

References

[1] H. Koura, *et al*., Prog. Theor. Phys., 113 (2005) 305-325.

[2] H. Koura and T. Tachibana, JAEA-Tokai TANDEM Ann. Rep. 2005, JAEA-Review 2006-029 (2006) 67-68.

5. 5 Direct and semi-direct capture in the low-energy (n,γ) reactions of neutron-rich Tin isotopes and its implications for the r-process nucleosynthesis

S. Chiba[1], H. Koura[1], T. Hayakawa[1], T. Maruyama[1], T. Kawano[2], and T. Kajino[3]

The neutron capture reaction rates on neutron-rich unstable isotopes far from the β-stability line are essential for understanding the rapid neutron capture nucleosynthesis (r-process), which is considered to occur in supernova explosions. The neutron magic numbers affect the final mass distribution of products in the r-process, where the capture cross sections have minima. Astronomical observations of metal-deficient stars reported a "universal" abundance distribution of the r-nuclei in a certain mass region but that relative abundances between different mass regions separated by the neutron magic number N=82 are different[1]. Therefore, an unstable nucleus ^{132}Sn (N=82) is a key for understanding the r-process.

Rauscher *et al*. presented clearly the role of the direct neutron capture reaction on Tin and Lead isotopes [2]. They have employed three different models to calculate the single-particle energies (SPE), namely, Hartree-Fock-Bogoliubov model, relativistic mean field theory, and macroscopic-microscopic finite-range droplet model. Predictions of the direct capture cross sections based on different models sometimes disagree up to several orders of magnitude, showing a significance of the nuclear structure effect on direct neutron capture and hence a clear need of a search for single-particle potential (SPP) that can reproduce the SPE accurately and systematically.

We carried out a systematic calculation of both direct and semi-direct (DSD) cross sections to improve the prediction of the neutron capture reaction rate on the Tin isotopes. The semi-direct process was included here to calculate the capture cross section up to 20 MeV to cover an energy range wide enough for many other applications consistently. In the present study, we adopt a single-particle potential that gives a good reproduction of the known single-particle energies over a wide mass region. We also perform Hauser-Feshbach (HF) model calculations and consider whether the inversion of the HF and direct cross sections occurs or not at the neutron-rich isotopes [3].

We employed Koura-Yamada SPP [4] (KY-SPP). Figure 1 shows neutron single-particle levels in the vicinity of ^{132}Sn. The single-particle energies above the N=82 gap are obtained as the neutron separation energy necessary to bring the nucleus from the corresponding single-particle states of ^{133}Sn to the ground state ^{132}Sn, while those below the N=82 gap are given as the neutron separation energy from the ground state of ^{132}Sn to the corresponding single-hole states of ^{131}Sn. Calculated binding energies are compared to the corresponding experimental values. The levels calculated

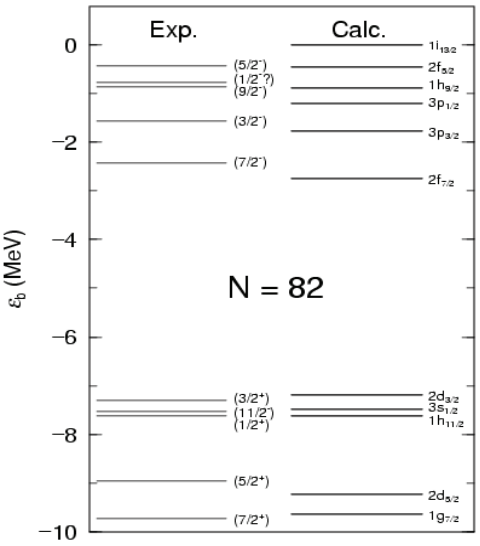

Fig. 1 Observed (left) and calculated neutron SPEs in the vicinity of ^{132}Sn.

[1] Japan Atomic Energy Agency (JAEA)
[2] Los Alamos National Laboratory
[3] National Astronomical Observatory of Japan

predict somewhat narrower gap at N=82, but the single-particle energies of the unfilled levels are reproduced with an accuracy of about 300 keV on the average. It is especially important to predict the energy and presence of $3p_{3/2}$ and $3p_{1/2}$ states which can couple to the s-wave of the incoming scattering wave function, that gives a dominant contribution to the low-energy direct capture cross section relevant to the r-process.

The DSD neutron capture cross sections are calculated for a series of even-even Tin isotopes at 30 keV, which are shown in fig. 2. The HF cross section is decreasing as the mass number increases, and shows a drastic decrease when going from ^{130}Sn to ^{132}Sn. This trend is completely correlated with the values of neutron separation energies. On the other hand, the DSD cross section decreases only modestly, and it exceeds the HF cross section at ^{132}Sn. Therefore, we see that the inversion of the HF and DSD cross section indeed occurs at the border of the N=82 magic for the neutron-rich Tin isotopes (and probably its vicinity). The gradual decrease of the direct cross sections in our calculation is different from the more-rapid mass-number dependence of the calculation by Rauscher *et al.* [2] due, probably, to the stability of the single-particle energies calculated by KY-SPP. The cross symbol denotes a result calculated by Rauscher *et al***.** [2] by using experimental level energies as their best estimate of the direct (n, γ) cross section of ^{132}Sn. Our result, without adjustment, is in a fair agreement with this value.

We compared the r-process abundance of ^{132}Sn nuclei, by considering the HF (n,γ) rate alone and both the HF + DSD rates. We notice that the difference in these reaction rate gives rise to a difference of more than a factor of 3 in the initial abundance of ^{132}Sn nuclei as shown in fig. 3, but the difference diminishes as time passes..

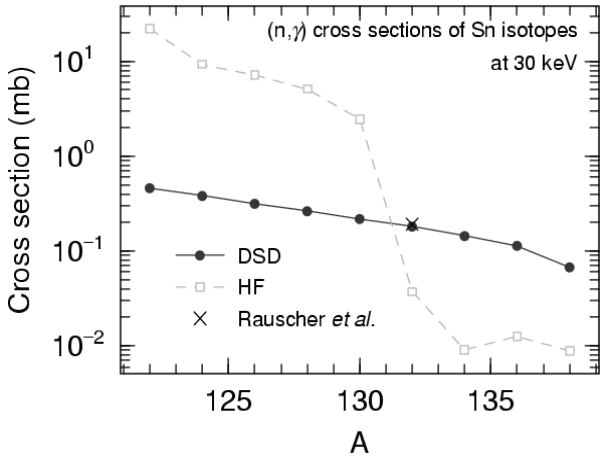

Fig. 2 Calculated DSD and HF cross sections for a series of even-even Tin isotopes at 30 keV.

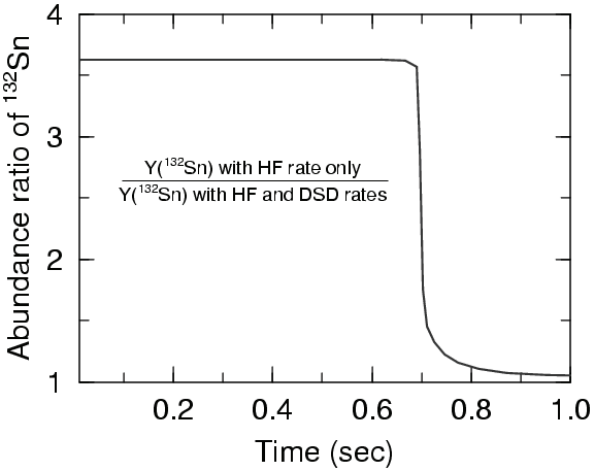

Fig. 3 Time-dependence of the abundance ratio of ^{132}Sn without and with the contribution of DSD process.

References

[1] C. Sneden *et al*., Astrophys. J., 533 (2000) L139-L142.
[2] T. Rauscher *et al*., Phys. Rev., C 57 (1998) 2031-2039.
[3] S. Chiba *et al.*, Phys. Rev., C 77 (2008) 015809-1-7.
[4] H. Koura and Y. Yamada, Nucl. Phys., A671 (2000) 96-118.

5. 6 Soft-rotator model analysis for medium-heavy nuclei and systematics of the Hamiltonian parameters

S. Kunieda[1], S. Chiba[1], K. Shibata[1], A. Ichihara[1], O. Iwamoto[1], N. Iwamoto[1], and E.Sh. Sukhovitskii[2]

The equilibrium non-axial deformation may exist as a general feature of atomic nuclei [1]. The soft-rotator model (SRM) [2] is a phenomenological nuclear model which is designed to describe the low-lying collective level structures of even-even nuclei in terms of the asymmetric-rotation and vibration picture. In this study, we tried to estimate a complete SRM Hamiltonian parameter set for a wide range of even-even medium-heavy nuclei in order to investigate the isotopic differences and/or systematic behaviors of the parameter values.

The SRM Hamiltonian parameters such as the equilibrium deformation and elasticity constant parameters were deduced from experimentally known low-lying level structure which involves the ground-state, γ-, β_2- and β_3-bands in the context of the model. We also carried out the SRM coupled-channels (SRM-CC) [2] optical model analysis for inelastic scattering cross sections of protons in order to predict the equilibrium quadrupole deformation parameter β_{20} (and rigid hexadecapole deformation parameter β_4 for deformed nuclei). The global CC optical model potential developed by us [3] was employed in the SRM-CC calculation. Figures 1 and 2 show typical results in descriptions of the measured data for ^{152}Sm. Those analyses enabled us to obtain a complete Hamiltonian parameter set for various even-even nuclei such as ^{56,58}Fe, ^{60,62,64}Ni, $^{64\text{-}70}$Zn, $^{70\text{-}76}$Ge, $^{74\text{-}82}$Se, ^{86}Sr, ^{96,98,100}Mo, ^{102}Ru, $^{104\text{-}110}$Pd, $^{106\text{-}116}$Cd, $^{116\text{-}124}$Sn, $^{122\text{-}130}$Te, ^{144,150}Nd, $^{148\text{-}154}$Sm, ^{160}Gd, ^{166}Dy, ^{166,168}Er, ^{174,176}Yb, ^{178,180}Hf, ^{182,184}W, ^{192}Os, ^{194}Pt, ^{232}Th and ^{238}U.

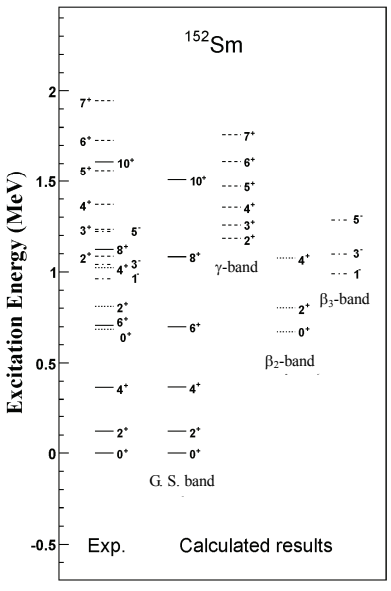

Fig. 1 (left panel)
Low-lying level structure given by the SRM analysis which is compared with measured data for ^{152}Sm.

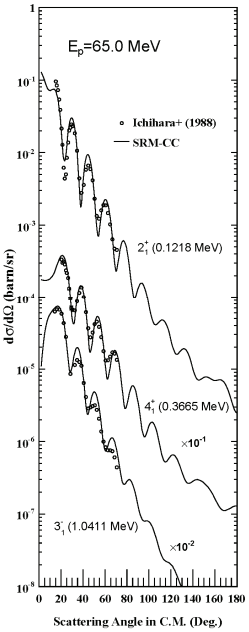

Fig. 2 (right panel)
Inelastic proton scattering differential cross sections at 65 MeV which were described by the SRM-CC optical model calculations, together with those by the measurement [4] for ^{152}Sm.

[1] Japan Atomic Energy Agency (JAEA)
[2] Joint Institute for Energy and Nuclear Research (Belarus)

The estimated quadrupole and octupole equilibrium deformation parameters, i.e., β_{20} and β_{30} are listed in table 1 for Ge isotopes as an example. We can clearly see a possible shape transitional phenomenon between ^{72}Ge and ^{74}Ge. It is consistent with the existence of a sub-shell closure N=40. The same phenomenon is seen between ^{74}Se and ^{76}Se. The effective deformations β^{eff}_2 and β^{eff}_3 describe the strengths of exciting 2_1^+ and 3_1^- states, respectively. The SRM-CC results agree with values derived from the experimental B(E2) and B(E3) data [5,6]. Big differences between the equilibrium and effective deformations on ^{70,72}Ge are due to their strong vibrational properties.

Table 1. The equilibrium and effective deformations for ^{70,72,74,76}Ge.

	SRM-CC				Exp.	
	β_{20}	β_{30}	$\beta^{eff.}_2$	$\beta^{eff.}_3$	$\beta^{eff.}_2$	$\beta^{eff.}_3$
^{70}Ge	0.063	0.084	0.215	0.259	0.225	0.274
^{72}Ge	0.044	0.069	0.219	0.217	0.242	0.264
^{74}Ge	0.245	0.114	0.295	0.129	0.283	0.145
^{76}Ge	0.265	0.115	0.279	0.120	0.262	0.144

Figure 3 shows the deduced quadrupole non-axial equilibrium deformation parameter $\gamma_0\beta_{20}$ as a function of β_{20} for all nuclei of our interests. As presented separately in this figure, the obtained results can be classified into at least three groups. The nuclei which possess (near) magic (sub-)shell tend to exhibit γ_0~30º even if they have large β_{20} value as illustrated in fig. 3-a). It is interesting that another group is positioned along with a line which is slightly shifted towered the prolate shape as plotted in fig. 3-b). Typical deformed heavy nuclei are characterized by $\gamma_0\beta_{20}$~0.04 though no regular behavior is seen as shown in fig. 3-c). Those findings infer that the non-axiality parameter strongly depends on the shell structure of nuclei.

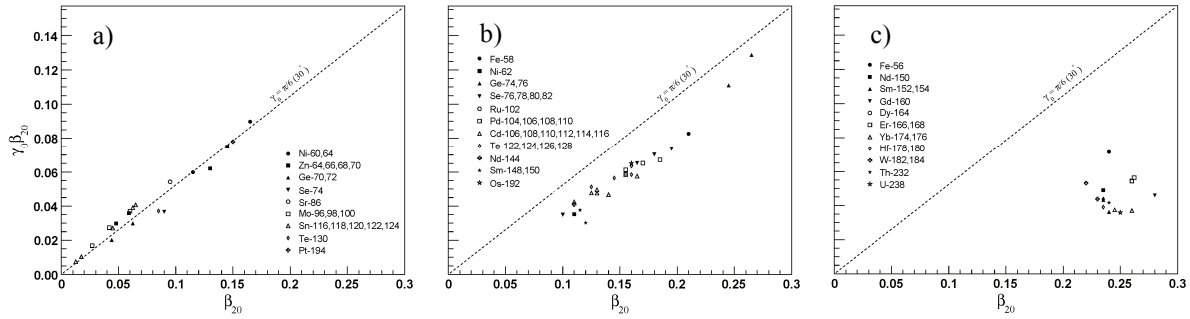

Fig. 3 The obtained quadrupole non-axial equilibrium deformation parameters as a function of β_{20}. They can be classified at least into three groups as shown in a), b) and c) separately.

References

[1] L. Guo, J.A. Maruhn, and P.-G. Reinhard, Phys. Rev., C76 (2007) 034317, 1-11.

[2] S. Chiba *et al*., Nucl. Phys., A624 (1997) 305-327.

[3] S. Kunieda *et al*., J. Nucl. Sci. Technol., 44 (2007) 838-852.

[4] T. Ichihara *et al*., Phys. Rev., C36 (1987) 1754-1776.

[5] S. Raman, C.W. Nestor, Jr. and P. Tikkanen, At. Data. Nucl. Data. Tables, 78, (2001) 1-128.

[6] T. Kibedi and R.H. Spear, At. Data. Nucl. Data. Tables, 80, (2002) 35-82.

CHAPTER 6

Atomic Physics and Solid State Physics

This is a blank page.

6. 1 Coster-Kronig electrons from N^{3+} Rydberg states produced in high-energy collisions with He

K. Kawatsura[1], K. Takahiro[1], M. Sataka[2], M. Imai[3], H. Sugai[2], K. Ozaki[1], H. Shibata[3], and K. Komaki[4]

High Rydberg states in low-energy highly charged ions are produced by electron capture processes, especially double electron capture (DEC). Most of the studies on DEC process have been made on He-like ions such as C^{4+} and O^{6+} [1,2] and N^{5+} [3]. Those from dielectronic recombination (DR) processes have been measured with modest resolution for Li-like ions such as C^{3+}, F^{6+}, Ne^{7+} and Ar^{15+}. Coster-Kronig (C-K) electrons from $1s^22pnl$ states were observed from DEC and DR processes. For high-energy collisions with He, highly excited states are formed mainly by single-electron excitation of metastable $1s^22s2p$ for Be-like ions such as O^{4+} [4] and S^{12+} [5]. We have found with high-resolution measurements that $1s^22pnl$ states with relatively lower angular momenta are produced, while high angular momenta are produced in DEC and DR processes. Recently, the DR spectrum for Li-like N^{4+} $1s^22s$, which recombines into Be-like N^{3+} $1s^22pnl$ ($n \geq 5$) has been measured with high resolution using heavy-ion storage-ring facilities [6]. The experimental DR spectrum is in agreement with the calculations and also with the optical values. It is also found that high angular momenta are produced in DR processes. In the present study, to compare with the DR data [6] and previous results obtained from 32 MeV/u O^{4+} + He [4], we have measured Coster-Kronig electrons ejected at zero-degree in 21 MeV N^{3+} + He collisions with high resolution and systematically investigated high-Rydberg states of Be-like four-electron N and O ions, where the highly excited states are formed by electron excitation/ionization.

The experiments were performed at the tandem accelerator facility at the Japan Atomic Energy Agency (JAEA) of Tokai. The Coster-Kronig electrons ejected at zero degree in the beam direction were measured using a tandem-type 45° parallel plate electron spectrometer. The primary N^{3+} ion beams were produced by using ECRTIS (Super-Nanogan) installed at the high-energy terminal of the tandem accelerator, and then accelerated up to 21 MeV for N^{3+} ions. The projectile N^{3+} ions penetrated the He gas target under single collision conditions. The beam currents were 0.3~10 nA and were collected in the Faraday cup placed right after the spectrometer. All spectra were normalized to the same gas-cell target pressure and ion charge.

Figure 1 shows zero-degree ejected electron spectrum around the cusp energy region. The observed electron spectrum was dominated by the so-called cusp peak at around 0.832 keV and a series of C-K electron peaks was superposed on the low and high energy wings of the cusp, corresponding to the backward and forward ejected electrons from the moving projectiles, respectively. Figure 2 shows the ejected electron spectrum of autoionization lines from N^{3+} Rydberg states, where energy scale refers to the projectile rest frame transferred from the laboratory frame as shown in fig. 1. The representative peaks are

[1] Kyoto Institute of Technology
[2] Japan Atomic Energy Agency (JAEA)
[3] Kyoto University
[4] National Center for University Entrance Examinations

assigned to a series of $1s^22p(^2P)nl$ -$1s^22s(^2S)\varepsilon l'$ (n = 5-9) C-K transitions as indicated by the vertical bars. Vertical bars indicate line positions obtained by,

$$E_n = \Delta E - Q^2 R_y/n^2, \qquad (1)$$

where E_n is the C-K electron energy, n is the principal quantum number, ΔE is the energy difference between the initial and final states of the ion core configuration, taken from the compiled transition energy tables, Q is the effective charge of the N^{4+} $1s^22p(^2P)$ ion core (assumed to be +4 for this case), and R_y is the Rydberg energy (13.606 eV). In this case, ΔE is 10.0 eV for $1s^22p(^2P)$. A detailed analysis of the C-K spectra for N^{3+} and O^{4+} ions, and of the electron-excitation process is underway [7].

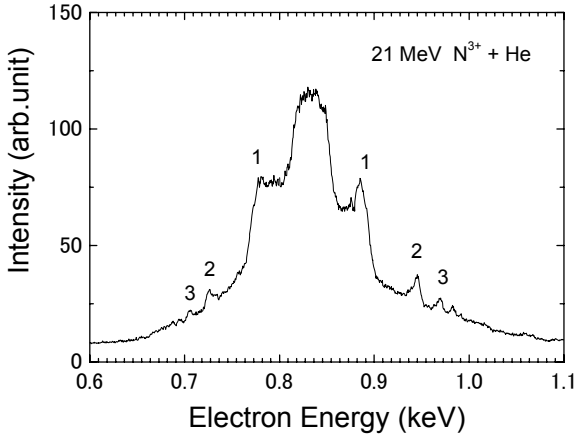

Fig. 1 Zero-degree electron spectrum around the cusp energy (t = 0.832 keV) in the collisions of 21 MeV N^{3+} + He. Energy scale refers to the laboratory frame.

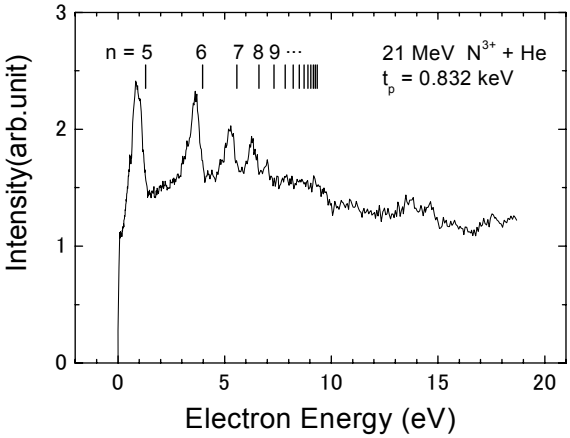

Fig. 2 High-resolution Coster-Kronig electron spectrum ejected at 0^o from the moving projectile in collisions of 21 MeV N^{3+} + He. Energy scale refers to the projectile rest frame.

References

[1] N. Stolterfoht *et al*., Phys. Rev. Lett., 57 (1986) 74-77.

[2] F.W. Meyer *et al*., Phys. Rev. Lett., 60 (1988) 1821-1824.

[3] M. Mack and A. Niehaus, Nucl. Instrum. Methods Phys. Res., B23 (1987) 116-119.

[4] K. Kawatsura *et al*., Nucl. Instrum. Methods Phys. Res., B205 (2003) 528-532.

[5] M. Sataka *et al*., Phys. Rev., A65 (2002) 052704 (1-11).

[6] P. Glans *et al*., Phys. Rev., A64 (2001) 043609 (1-11).

[7] K. Kawatsura *et al*., submitted to Nucl. Instrum. Methods Phys. Res. B.

6. 2 Charge state distribution of sulfur ions after penetration of C-foil targets (V)

M. Imai[1], M. Sataka[2], K. Nishio[2], H. Sugai[2], K. Kawatsura[3],
K. Takahiro[3], K. Komaki[4], and H. Shibata[1]

Charge state is one of the most important aspects to study ion-solid interactions. Various interactions, such as electron capture, ionization and excitation of projectile and/or target electrons, and consequent phenomena like energy deposition into targets, i.e., stopping of projectile, are closely related with projectile charge state and its evolution in target. Equilibrium charge state distributions for various collision systems after passing through gaseous or solid target have been extensively investigated and compiled [1], although charge state distributions somewhat change upon exiting target foil. As has been presented in the previous annual report [2], we measured the exit charge state distributions for penetrations of 2.0 MeV/u S^{10+}, S^{11+} and S^{13+} ions through C-foil targets of $0.9\tilde{}10$ μg/cm^2 in thickness and performed calculations by ETACHA code [3] to succeed in reproducing the experimental results sufficiently, where ETACHA has been designed for higher energy (>10MeV/u) region [4]. We have also started another simulation for S^{q+} ion fractions, in which electron transfer cross sections $\sigma_{qq'}$ are calculated with codes applicable to the present collision energy [5]. In this report, results of our extensive measurements on thicker targets to observe real equilibrium charge state distribution for 2.0 MeV/u S ions are presented.

The present experiments were performed at the LIR1-3 beam line of the 20UR Tandem Accelerator Facility. A beam of 2.0 MeV/u (64 MeV) S^{7+} ions was provided from the tandem accelerator within 0.1% of energy accuracy, using a calibrated energy analyzing magnet. A post-stripper C-foil of ~20 μg/cm^2 in thickness was placed after the energy analyzing magnet to produce higher charge state projectile ions. Energy losses at the post-stripper foil were estimated to be at most 0.7% by our separate measurement of cusp electron energies with zero-degree electron spectroscopy [6]. The primary S^{7+} or post-stripped S^{q+} (q = 12, 14) ion beam was directed by a switching magnet to self-support carbon target foil of 54 and 98 μg/cm^2 in thickness. The charge state distributions after foil penetration were measured using the heavy ion magnetic spectrometer ENMA and a position-sensitive gas chamber detector. The vacuum condition inside the spectrometer was maintained below $10\tilde{}^6$ Pa to eliminate background charge exchange collisions with residual gas, which was confirmed by measurements without target foil.

Measured charge state fractions for 2.0 MeV/u S^{q+} (q = 7, 12, 14) ion incidences are shown in fig. 1. The statistical errors are less than 1% for almost all the points. Typical total error values are estimated as 20% for the smallest fractions around 1.0×10^{-5} and less than 0.5% for the largest fractions around 0.3.

[1] Kyoto University
[2] Japan Atomic Energy Agency (JAEA)
[3] Kyoto Institute of Technology
[4] National Center for University Entrance Examinations

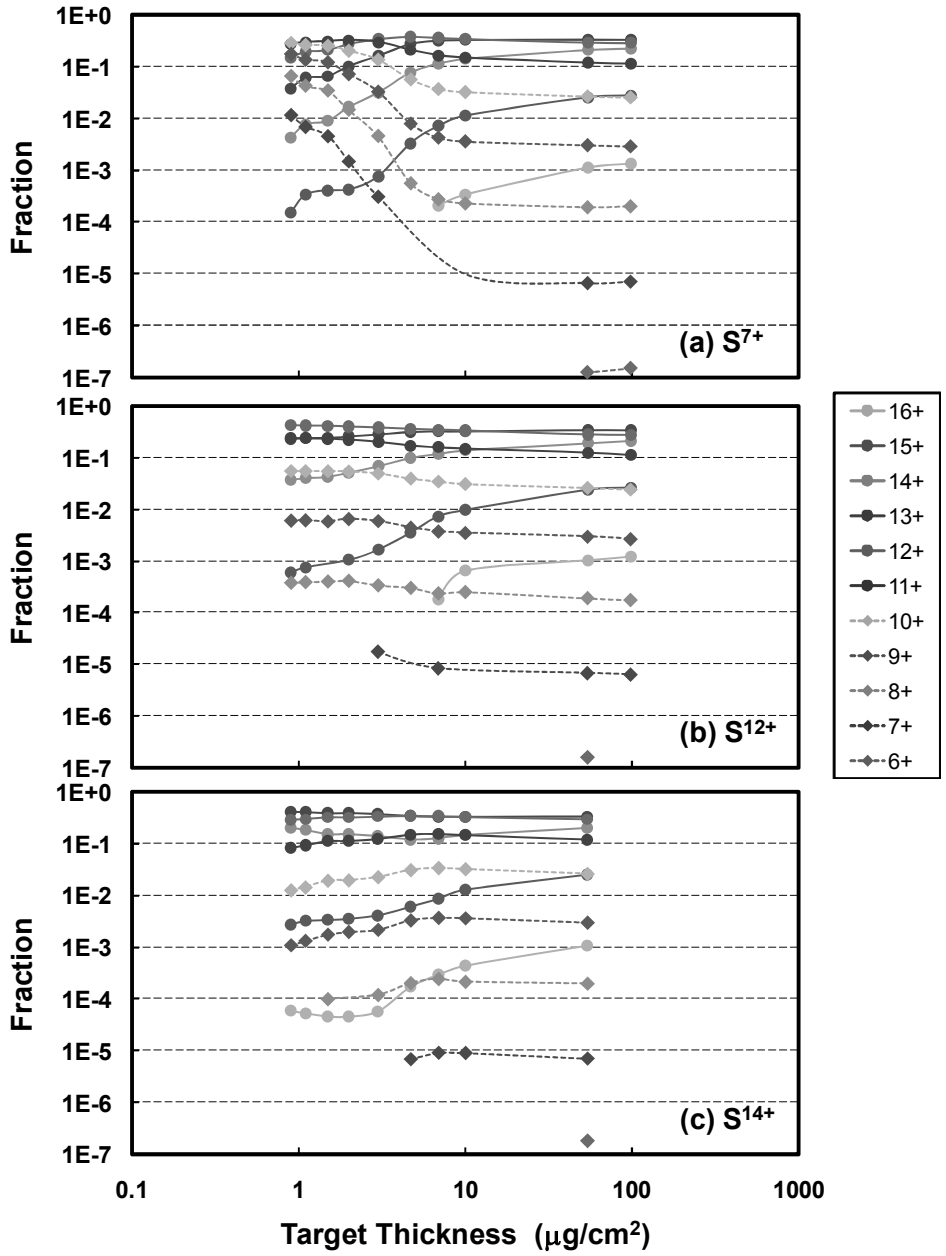

Fig. 1 Charge state evolution for 2.0 MeV/u S^{7+}, S^{12+} and S^{14+} projectiles penetrated through C-foil targets of 0.9, 1.1, 1.5, 2.0, 3.0, 4.7, 6.9, 10, 54 and 98 μg/cm^2 in thickness. Charge state evolution for targets of 0.9 – 10 μg/cm^2 has already been presented in the previous annual report [2].

References

[1] A.B. Wittkower and H.D. Betz, At. Data Nucl. Data Tables, 5 (1973) 5; K. Shima *et al*., At. Data Nucl. Data Tables, 51 (1992) 173; K. Shima *et al*., Nucl. Instrum. Methods Phys. Res., B33 (1988) 212.

[2] M. Imai *et al*., JAEA-Tokai TANDEM Ann. Rep. 2006, JAEA-Review 2007-046 (2008) 87-88.

[3] J. P. Rozet *et al*., J. Phys., B22 (1989) 33; Nucl. Instrum. Methods Phys. Res., B107 (1996) 67.

[4] M. Imai *et al*., Nucl. Instrum. Methods Phys. Res., B230 (2005) 63.

[5] M. Imai *et al*., Nucl. Instrum. Methods Phys. Res., B256 (2007) 11.

[6] M. Sataka *et al*., Phys. Rev. A65 (2002) 052704; M. Imai *et al*., Nucl. Instrum. Methods, B67 (1992) 142.

6. 3 Diffusion of ^{8}Li short-lived radiotracer in Li ionic conductors of NaTl-type intermetallic compounds

H. Sugai[1], M. Sataka[1], S. Okayasu[1], S. Ichikawa[1], K. Nishio[1], S. Mitsuoka[1], T. Nakanoya[1], A. Osa[1], T.K. Sato[1], T. Hashimoto[1], S.C. Jeong[2], I. Katayama[2], H. Kawakami[2], Y.X. Watanabe[2], H. Ishiyama[2], N. Imai[2], Y. Hirayama[2], H. Miyatake[2], Takanori Hashimoto[3], and M. Yahagi[3]

Non-destructive and on-line Li diffusion experiments in Li ionic conductors are conducted using the short-lived α-emitting radiotracer of ^{8}Li. Li-8 decays through β-emission to ^{8}Be with a half lifetime of 0.84s, which immediately breaks up into two α-particles with energies broadly distributed around 1.6MeV with a full width at half maximum (FWHM) of 0.6MeV. The radiotracers produced as an energetic and pulsed ion beam from TRIAC [1] (Tokai Radioactive Ion Accelerator Complex) are implanted into a structural defect mediated Li ionic conductor of NaTl-type intermetallic compounds (β-LiGa and β-LiIn). The experimental time spectra of the yields of α-particles are compared with simulated results and Li diffusion coefficients in the intermetallic compounds [2] are extracted with an accuracy of ±10%. The diffusion coefficients obtained for β-LiGa [3] with Li content of 43-54 at.% are discussed in terms of the interaction between Li-ion and the structural defects in the specimen, compared with the cases of β-LiAl and β-LiIn [4].

The crystal structure of β-phase (β-LiAl, β-LiGa and β-LiIn) is NaTl-type (or Zintl phase) [4], which is composed of two interpenetrating diamond sublattices such that each atom has eight nearest neighbors: four like and four unlike atoms. The characteristic defect structure of the compound consists of two types of defects at room temperature, i.e., vacancies in the Li sublattice (V_{Li}) and Li antistructure atoms in the Ga sublattice (Li_{Ga}). The concentrations of the point defects, [V_{Li}] and [Li_{Ga}], strongly depends on Li content; with increasing the Li content from 43 to 54%, [V_{Li}] decreases from 11.4 to 2.8%, while [Li_{Ga}] increases from 0 to 5.1%. V_{Li} is the dominant defect for the Li-deficient region, Li_{Ga} is the dominant defect for the Li-rich one. The coexistence V_{Li} of Li_{Ga} is expected to form V_{Li}- Li_{Ga} complex defects as reported for the defect structure of β-LiAl, which would play an important role in reducing the strain energy caused by the point defects in the real cystal. Especially, almost the same amounts of V_{Li} and Li_{Ga} exist around the content of 51 at.% Li.

As shown in fig. 1, the Li diffusion coefficients of β-LiGa around the Li content of 48 at.% have maximum. The results is quite different from those observed for β-LiAl and β-LiIn (the Li-content of β-phase: 48-54at.%) [4], although they are iso-structural with the β-LiGa. In the cases of β-LiAl and β-LiIn, the Li diffusion coefficients, the corresponding diffusion constants and activation energies, decrease monotonically with increasing the lithium content with a minor modification due to the coexistence of V_{Li}

[1] Japan Atomic Energy Agency (JAEA)
[2] High Energy Accelerator Research Organization (KEK)
[3] Aomori University

and Li_{Ga}. Since the vacancy concentration in the Li sublattice decreases with increasing lithium content, this monotonic behavior can be associated with the Li vacancy. The motion of Li is slightly suppressed or assisted depending on the kinds of anti-site atoms; Li diffusion rather slows down in β-LiAl, while becomes rather faster in β-LiIn around the stoichiometric region. Such a slight modification in the monotonic behavior of Li diffusion has suggested the possibility of an interaction between vacancies and lithium anti-structure atoms; the interaction must be attractive in β-LiAl and repulsive in β-LiIn [4]. The difference in the interactions has been understood by the atomic size effect. The lithium anti-structure atom, Li_{Al}, in β-LiAl produces compressional strain (expanded lattice), since the radius (0.68Å) for the Li ion in a closed shell configuration is larger than that (0.50 Å) for the Al ion, while the anti-structure atom, Li_{In}, in β-LiIn induces dilatational strain (contracted lattice) because of ionic radius (0.8 Å) for In larger than that of the substitutional Li ion. On the other hand, the vacancy, V_{Li}, always produces dilatational strain. On the basis of the atomic size effect, the interaction between V_{Li} and Li_{Ga} in β-LiGa is supposed to be attractive as in β-LiAl, because the radius (0.62 Å) of Ga ion is slightly smaller than that of Li ion. The strength of the interaction can be considered to be weaker than observed in β-LiAl and β-LiIn, since the radii of the constituent ions are quite close to each other.

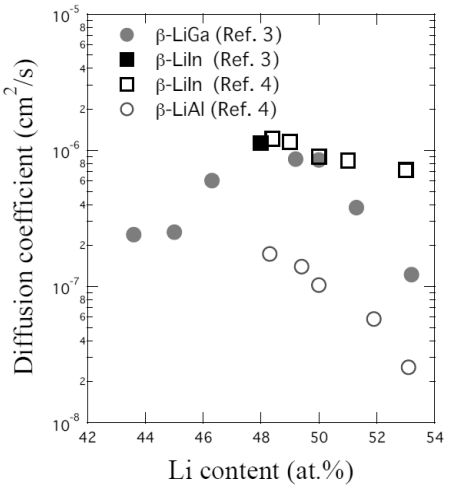

Fig. 1 Li-content dependence of the diffusion coefficients for β-LiGa (Ref. 3), β-LiIn (Ref. 4) and β-LiAl (Ref. 4).

As mentioned in the former paragraph, the Li diffusion around the stoichiometric region is faster than in the most Li-rich region and Li-deficient one, demonstrating that the Li diffusion through the vacancies on the Li atomic site seems to be strongly promoted by the coexistence of V_{Li} and Li_{Ga}. This suggests that the interaction between V_{Li} and Li_{Ga} would be unexpectedly large and repulsive as same as observed in β-LiIn [4]. On the other hand, it is also suggested that the motion of Li ion for the Li-deficient region could be quenched by the formation of the defects complex such as V_{Li}-Li_{Ga}-V_{Li} and /or V_{Li}-V_{Li}, since the concentration of V_{Li} defects is much (almost three times) larger in the Li-deficient side as compared to the cases in β-LiAl and β-LiIn. It should be noted that the number of vacant Li sites in a unit cell volume (8 for Li and 8 for Ga) is about two for the most Li-deficient β-LiGa, whereas there exist about one vacant Li site in every two unit cells for the most Li-deficient β-LiAl and β-LiIn [4] by assuming the random distribution of the vacancies over the entire volume.

References

[1] Information on http://www.srim.org/

[2] S.C. Jeong *et al*., Nucl. Instrum. Methods Phys. Res., B230 (2005) 596-600.

[3] H. Sugai *et al*., Defect and Diffusion Forum, 273-276 (2008) 667-672.

[4] J.C. Tarczon *et al*., Mater. Sci. and Eng., A 101 (1988) 99-108.

CHAPTER 7

Radiation Effects in Materials

This is a blank page.

7. 1 Character and accumulation effects of ion tracks in $UO_2$and CeO_2 under irradiation with high energy ions

T. Sonoda[1], N. Ishikawa[2], M. Sataka[2], K. Yasunaga[3], M. Kinoshita[1], and A. Iwase[4]

In order to extend the burnup of LWR fuels, formation and growth mechanism of a crystallographic re-structuring in the periphery region of high burnup fuel pellets, namely “rim structure” [1] should be clarified. This structure is characterized by the existence of highly dense small sub-grains whose size is approximately 200 nm, and the accumulation of small pores with average size around 1 μm. The structure can be formed by the accumulation and mutual interactions of radiation damages, fission products (FPs) and electronic excitations deposited partially by nuclear fissions [2-4]. In order to clarify the character and the accumulation effects of ion tracks that are formed by highly dense electronic excitation, 210 MeV Xe^{+14} ions irradiation examinations on UO_2 and CeO_2 have been done at JAEA-Tokai tandem accelerator facility. Microstructure evolutions in the irradiated samples are observed in a FE-SEM (JSM-6340F) and a FE-TEM (HF-3000) at CRIEPI. This study was financially supported by the Budget for Nuclear Research of the Ministry of Education, Culture, Sports, Science and Technology, based on the screening and counseling by the Atomic Energy Commission.

Figure 1(a) shows the SEM image of irradiation surface of CeO_2 under irradiation with 210 MeV Xe^{+14} ions to a fluence of $2x10^{15}$ ions/cm^2 at 300 °C. This figure indicates that the drastic change of the surface condition is occurred under accumulation of ion tracks. In order to observe the change of inner structure of this sample, cross-sectional TEM observations have been done. Figure 1 (b) and (c) show the bright field image and dark field image of the same area of the cross-section, respectively. In these figures, many smaller grains whose size is around 1~2 μm are observed and they are smaller than the mean grain size of non-irradiated samples (~6 μm). Moreover, sub-grains whose size is around 0.1 μm are also observed (white allows in fig. 1(c) and (d)). These results suggest that the grain sub-division has been occurred in CeO_2 whose irradiation surface was drastically changed under irradiation with Xe^{+14} ions. In addition to these results, the other results such as non-drastic surface changes have been occurred under irradiation with low energy Xe ions irradiations (~100 dpa) and high energy Xe^{+14} ions irradiations up to 800°C, suppose that the accumulation of ion tracks will accelerate the grain sub-divisions.

Figure 2 shows the typical SEM images of irradiated surfaces of UO_2 under irradiation with 210 MeV Xe^{+14} at 300°C to a fluence of (a) un-irradiated, (b) $1x10^{13}$ ions/cm^2, (c) $1x10^{14}$ ions/cm^2, (d) $5x10^{14}$ ions/cm^2 and (e) $8x10^{14}$ ions/cm^2. These figures indicate that the irradiation surface is not changed up to $1x10^{14}$ ions/cm^2, and the drastic change is observed to a fluence between $5x10^{14}$ ions/cm^2 and $8x10^{14}$ ions/cm^2. In case of 210 MeV Xe^{+14} ion irradiation, the fluence to change the irradiation surface of UO_2

[1] Central Research Institute of Electric Power Industry (CRIEPI)
[2] Japan Atomic Energy Agency (JAEA)
[3] Kyushu University
[4] Osaka Prefecture University

(~5x10^{14} ions/cm^2) tends to be almost same of CeO_2's. Figure 3 indicates a cross-sectional TEM image of UO_2 under irradiation with 210 MeV Xe^{+14} at 300°C to a fluence of 5x10^{14} ions/cm^2, and the ion tracks are clearly observed.

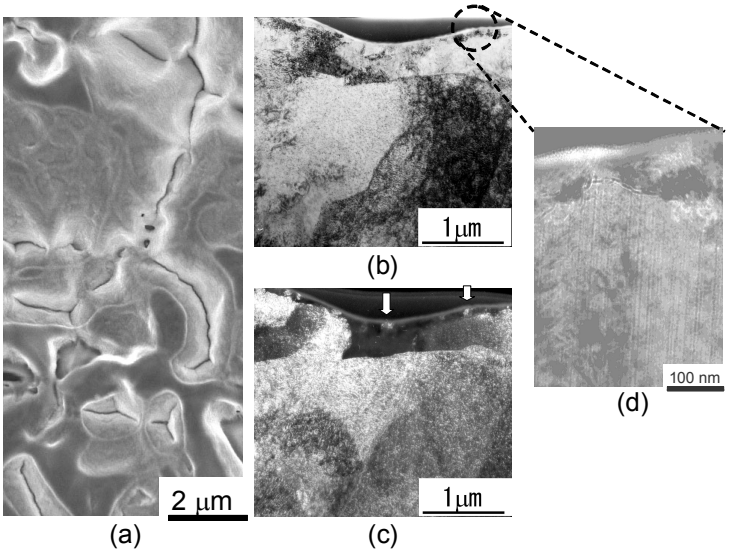

Fig. 1 SEM and TEM Images in CeO_2 under irradiation with 210 MeV Xe^{+14} to a fluence of 2x10^{15} ions/cm^2 at 300°C, (a) SEM image of irradiation surface, (b) a cross-sectional TEM (bright field) image, (c) a cross-sectional TEM (dark field) image, (d) the high magnification image of (b).

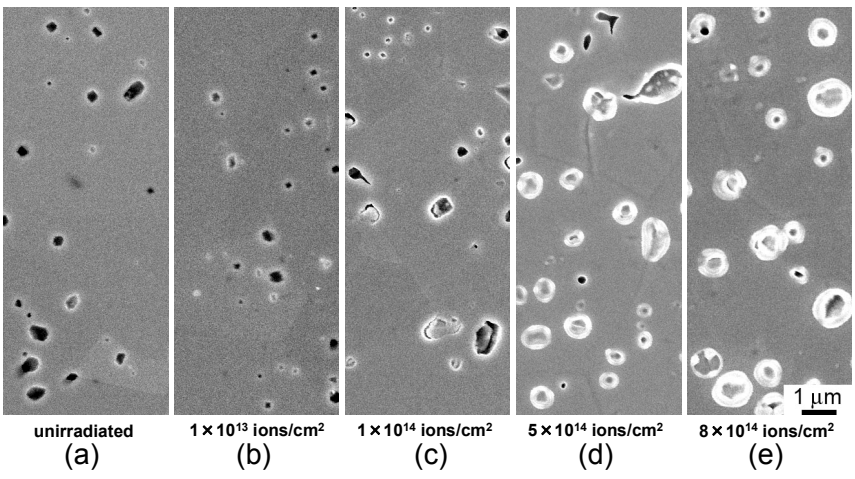

Fig. 2 SEM images of irradiated surface in UO_2 under irradiation with 210 MeV Xe^{+14} to a fluence of (a) unirradiated, (b) 1x10^{13} ions/cm^2, (c) 1x10^{14} ions/cm^2, (d) 5x10^{14} ions/cm^2, and (e) 8x10^{14} ions/cm^2 at 300°C.

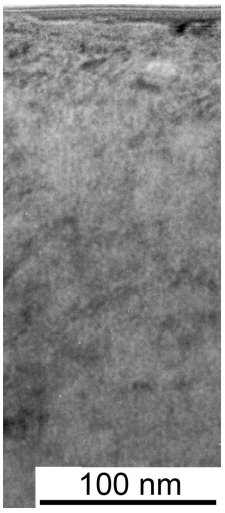

Fig. 3 Cross-sectional TEM images of UO_2 under irradiation with 210 MeV Xe^{+14} to a fluence of 5x10^{14} ions/cm^2 at 300 °C.

References

[1] J.O. Barner *et al*., HBEP-61, 1990, Battelle Pacific Northwest Laboratories.

[2] T. Sonoda *et al*., Nucl. Instrum. Methods Phys. Res., B191 (2002) 622-628.

[3] T. Sonoda *et al*., Nucl. Instrum. Methods Phys. Res., B250 (2006) 254-258.

[4] T. Sonoda *et al*., Nucl. Instrum. Methods Phys. Res., B266 (2008) 2882-2886.

7. 2 Evaluation of radiation damage in CeO_2 created by high-density electronic energy deposition

N. Ishikawa[1]

Radiation damage in nuclear fuel in fast breeder reactor can be classified into various types in term of its defect structure, such as 1) point-like defects created by relatively low energy particle irradiation, 2) continuous damage region (ion-track) created by high energy particle irradiation, and 3) strain fields created by accumulation of fission gas. In this study, in order to simulate irradiation damage by high energy fission fragments in MOX (mixed oxide) fuel, oxide ceramic material (CeO_2) with fluorite crystallographic structure is irradiated with high energy particles using tandem accelerator at Tokai Research and Development Center, Japan Atomic Energy Agency (JAEA-Tokai). The evaluation of radiation damage is done by X-ray diffraction method, by which quantitative evaluation of radiation damage is possible.

Thin films of CeO_2 were prepared on single crystal sapphire substrates by sputtering methods. The film thickness was about 300 nm. The films were irradiated at various temperatures (room temperature, 400°C and 800°C) with 120MeV Xe from the tandem accelerator at JAEA-Tokai. Irradiation with 120MeV Xe particles is to simulate creation of high energy fission fragments. The high temperature irradiation experiment is performed in order to simulate the damage creation in ceramic fuel at high temperature. In order to investigate the degradation of crystal structure, X-ray diffraction (XRD) patterns were measured before and after the irradiation. A sharp XRD peak corresponding to (002) reflection is observed before irradiation. In this study irradiation-induced change of the (002) peak intensity is investigated.

Figure 1 shows (002) diffraction peaks observed for CeO_2 irradiated with 120MeV Xe at 800°C. The decrease in peak intensity after the irradiation is observed, indicating that radiation damage is induced by the irradiation even at very high temperature of 800°C. The fluence dependence of the intensity is shown in fig. 2. Here, the intensity of (002) peak after the irradiation (I) is normalized by the peak intensity before irradiation (I_o). The change in the normalized intensity for 800°C irradiation is less than that for room temperature and 400°C irradiation. The decrement of the normalized intensity corresponds to radiation damage. The figure indicates that the irradiation damage induced at room temperature is nearly the same as that induced at 400°C, while the irradiation damage induced at 800°C is relatively less than that induced at room temperature and 400°C. The less damage for 800°C irradiation is probably due to thermal annihilation of radiation damage. Thermal energy corresponding to 400°C is not sufficient to annihilate the damage, while thermal energy corresponding to 800°C is high enough to annihilate part of radiation damage.

[1] Japan Atomic Energy Agency (JAEA)

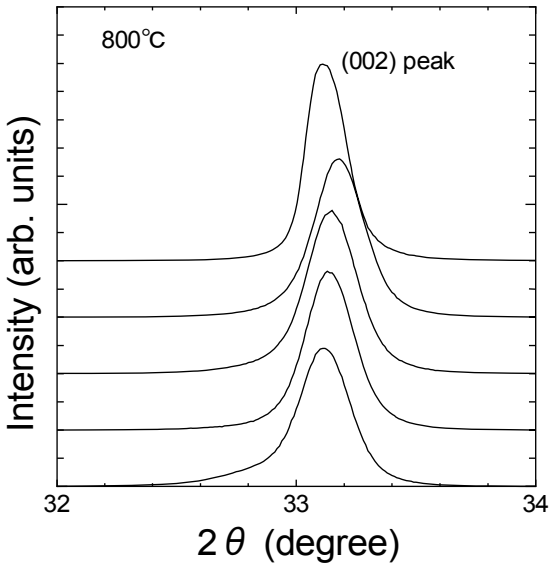

Fig. 1 X-ray diffraction patterns observed for CeO_2 irradiated with 120MeV Xe at 800°C. The fluence is, from up to bottom, 0 ions/cm^2, 3.0x10^{11}ions/cm^2, 1.0x10^{12}ions/cm^2, 1.0x10^{13} ions/cm^2, 1.0x10^{14}ions/cm^2.

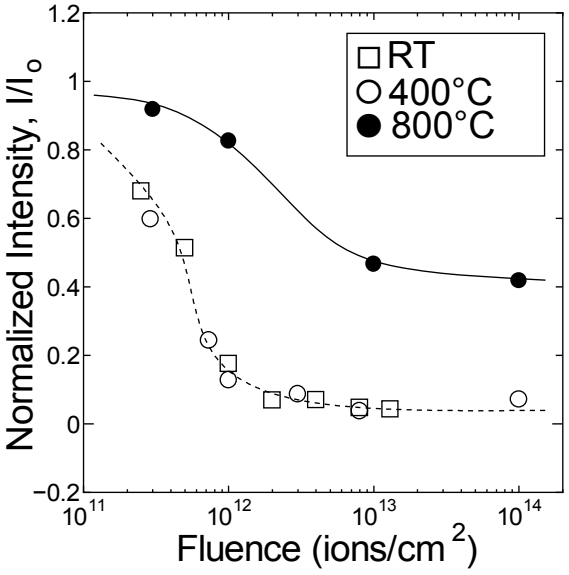

Fig. 2 Intensity of (002) peak normalized by the peak intensity before irradiation plotted as a function of fluence for CeO_2 irradiated with 120MeV Xe at room temperature (RT), 400°C and 800°C.

Here, the effect of overlapping of ion-tracks is discussed. The coverage of ion-tracks can be defined by the fraction of ion-tracks which designates the ratio of volume of ion-tracks to the whole sample volume. The fraction, δ, can be estimated by the Poisson law δ(Φ)=1-exp(-SΦ), which is the function of the fluence, Φ. Here S is the cross section of ion-tracks. Figure 3 is the fraction plotted as a function of fluence, where the diameter of the ion-track is assumed as a typical value of 15nm. The figure shows that, after irradiation up to 3x10^{12} ions/cm^2, the whole sample is covered with ion-tracks. Further irradiation means further overlapping of ion-tracks. From the figures shown above, overlapping of ion-track causes severe damage for room temperature and 400°C irradiation,, while that for 800°C the overlapping results in less damage.

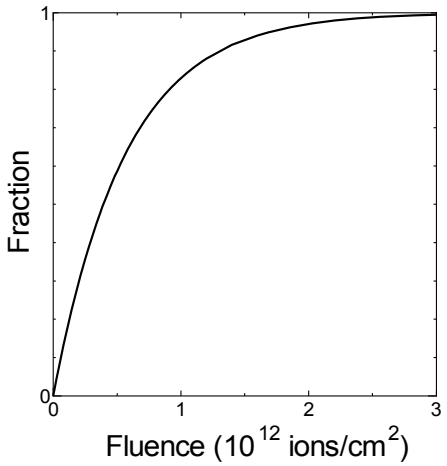

Fig. 3 The fraction of ion-tracks plotted against fluence.

7. 3 Evaluation of radiation damage in CeO_2 created by Xe-implantation

N. Ishikawa[1] and M. Matsuda[1]

Radiation damage in nuclear fuel in fast breeder reactor can be classified into various types in term of its defect structure, such as 1) point-like defects created by relatively low energy particle irradiation, 2) continuous damage region (ion-track) created by high energy particle irradiation, and 3) strain fields created by accumulation of fission gas. In this study, in order to simulate irradiation damage by accumulation of high-density fission gas in nuclear ceramic fuel, oxide ceramic material (CeO_2) with fluorite crystallographic structure is irradiated with intense beam of gas atoms using nanogan at Tokai Research and Development Center, Japan Atomic Energy Agency (JAEA-Tokai). Nanogan with electron cyclotron resonance (ECR) ion source produces intensive positive ion beams from gaseous atoms and molecules. This is suitable for implanting high-density gaseous atoms into ceramic materials, and is thus adopted in this study to simulate damage behavior due to high-density accumulation of fission gas. The evaluation of radiation damage is done by X-ray diffraction method, by which quantitative evaluation of radiation damage is possible.

Thin films of CeO_2 were prepared on single crystal sapphire substrates by sputtering methods. The film thickness was about 0.1μm. The films were irradiated at room temperature and at 400°C with 140keV Xe^{7+} from the ECR ion source. From the ion range calculation by SRIM-code, it can be confirmed that all of the irradiated Xe atoms are implanted in the materials. The high temperature irradiation is performed in order to simulate the damage creation in ceramic fuel at high temperature. In order to investigate the degradation of crystal structure, X-ray diffraction (XRD) patterns were measured before and after the irradiation. A sharp XRD peak corresponding to (002) reflection is observed before irradiation. In this study irradiation-induced change of the (002) peak intensity is investigated.

Figure 1(A) shows (002) diffraction peaks observed for CeO_2 irradiated with 140keV Xe at room temperature. In the figure, the fluence values are, from top to bottom, 0 ions/cm^2, $1.9x10^{15}$ions/cm^2, $3.8x10^{15}$ions/cm^2, $5.5x10^{15}$ions/cm^2, $1.2x10^{16}$ions/cm^2, $1.7x10^{16}$ions/cm^2 and $2.3x10^{16}$ions/cm^2. Figure 2(B) shows (002) diffraction peaks observed for CeO_2 irradiated with 140keV Xe at 400°C. In the figure, the fluence values are, from top to bottom, 0 ions/cm^2, $1.9x10^{15}$ions/cm^2, $5.5x10^{15}$ions/cm^2, $1.2x10^{16}$ions/cm^2 and $2.3x10^{16}$ions/cm^2. Both results indicate that intensity of X-ray diffraction peak decreases by implanting Xe gas. This means that accumulation of Xe gas increases damage of the ceramic sample.

Figure 2 shows the fluence dependence of X-ray diffraction intensity for CeO_2 implanted with 140keV Xe. The vertical axis is the normalized intensity, I/I_o, which is defined by the peak intensity after implantation (I) normalized by the peak intensity before irradiation (I_o). From the figure it is found that, for low fluence region (low gas density region) of the order of 10^{13}-10^{14} ions/cm^2, damage is very small. However, for high

[1] Japan Atomic Energy Agency (JAEA)

fluence region (high gas density region) of the order of 10^{16} ions/cm^2, damage increases as increasing fluence. From the figure, there is no difference (within the experimental error) in damage between CeO_2 implanted at room temperature and that implanted at 400°C. The damage recovery due to thermal energy corresponding to 400°C is found to be negligible.

Part of the present study is the result of "Research of highly accurate evaluation of radiation damage in advanced nuclear reactor fuel ceramics" entrusted to "Japan Atomic Energy Agency" by the Ministry of Education, Culture, Sports, Science and Technology of Japan (MEXT).

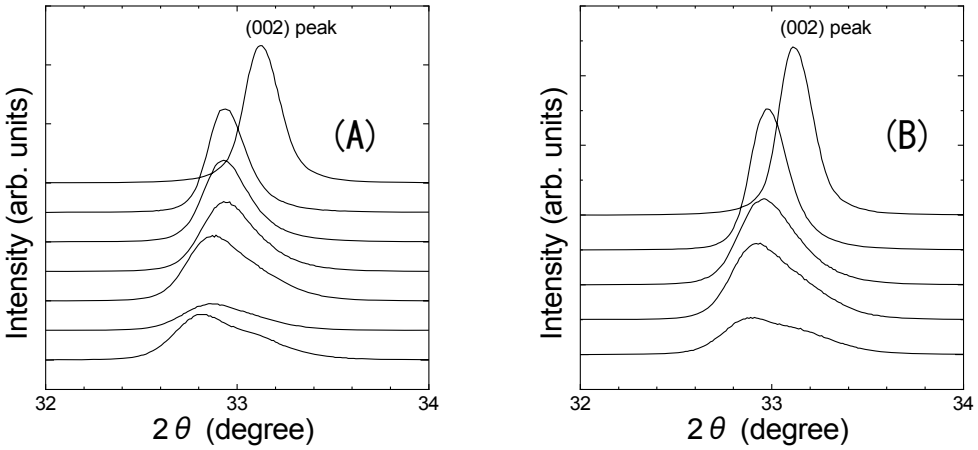

Fig. 1 X-ray diffraction peaks for CeO_2 thin films implanted with 140keV Xe at room temperature (A) and at 400°C (B). X-ray diffraction pattern for unimplanted sample is also shown in the same figure. The fluence is designated in the text.

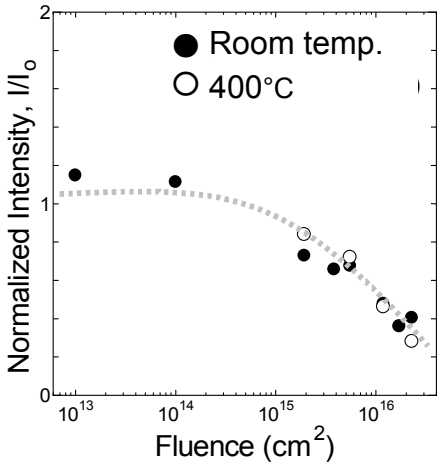

Fig. 2 Normalized intensity of X-ray diffraction peak plotted against fluence for CeO_2 implanted with 140keV Xe at room temperature (closed circles) and at 400°C (open circles).

7. 4 Atomic structure of ion tracks in magnesium aluminate spinel irradiated with swift heavy ions

K. Yasuda[1], T. Yamamoto[1], S. Kawasoe[1], M. Eto[1], S. Matsumura[1], and N. Ishikawa[2]

Numerous investigations of radiation effects have shown that magnesium aluminate spinel, $MgAl_2O_4$, is highly resistant to radiation damage caused by energetic particles, such as electrons, ions and neutrons. $MgAl_2O_4$ is, therefore, a promising candidate for the host of inert matrix fuels in light water reactors and the transmutation target for minor actinides and/or long life fission products. We have investigated radiation response of $MgAl_2O_4$ under a variety of radiation environments [1,2], including swift heavy ion irradiation, with which one can simulate the radiation damage caused by fission fragments.

Atomic resolution transmission electron microscopy (TEM) observations and analyses have been undertaken on single crystals of $MgO{\cdot}1.1Al_2O_3$. Swift heavy ions of 200 MeV Xe ions and 350 MeV Au ions were irradiated at the Tandem Accelerator Facility of JAEA-Tokai at an ambient temperature to fluence of ranging from $1x10^{15}$ to $1x10^{17}$ ions/m^2. The irradiated specimens were prepared for electron transparent thin foils with the cross sectional technique, which allows us to observe/analyze irradiated specimens as a function of the penetrating depth of incident ions. TEM techniques, such as high resolution (HR) and bright-field (BF) imaging, high angular resolution electron channeling spectroscopy (HARECXS), were utilized for the evaluation of the atomic structure of ion tracks.

Figure 1 (a) shows a BF image of the cross section specimen. Continuous traces of ion tracks are seen as diffraction contrast up to a depth of 11 μm, which corresponds to $(dE/dx)_e$=12 keV/nm. Elastic displacement damage induced by 350 MeV Au ions with a fluence of $5x10^{15}$ ions/m^2 is estimated to be $1x10^{-4}$ dpa from SRIM simulation at a depth of 11 μm. The cation disordering observed in the present study is, therefore, due to the high density of the electronic excitation. Figure 1 (b)-(d) are HARECXS profiles of $MgO{\cdot}1.1Al_2O_3$ obtained from the unirradiated specimen (b), and those obtained from the cross section specimen shown in fig.1 (a) at a depth of 2 μm (c) and 8 μm (d), in which normalized x-ray intensity is plotted as a function of incident electron-beam direction in k/g_{400}, where k refers to the intersection of the Ewald sphere with the [001] zone axis along 400 systematic reflections. Figure 1 shows that the HARECXS profiles obtained from the irradiated region differ from those of unirradiated specimens. The change is seen more distinctly for the profile obtained at 2 μm than that at 8 μm, indicating greater disordering with higher values of $(dE/dx)_e$. Those HARECXS profiles were analyzed to obtain the size of disordered zone induced by one incident ion [3]. Figure 2 shows the size of disordered region as a function of $(dE/dx)_e$. The disordered region is formed with a value of $(dE/dx)_e$ higher than around 10 keV/nm, and that it increases with $(dE/dx)_e$, which provides useful information for the evaluation of disordered zone induced by fission fragments.

[1] Kyushu University
[2] Japan Atomic Energy Agency (JAEA)

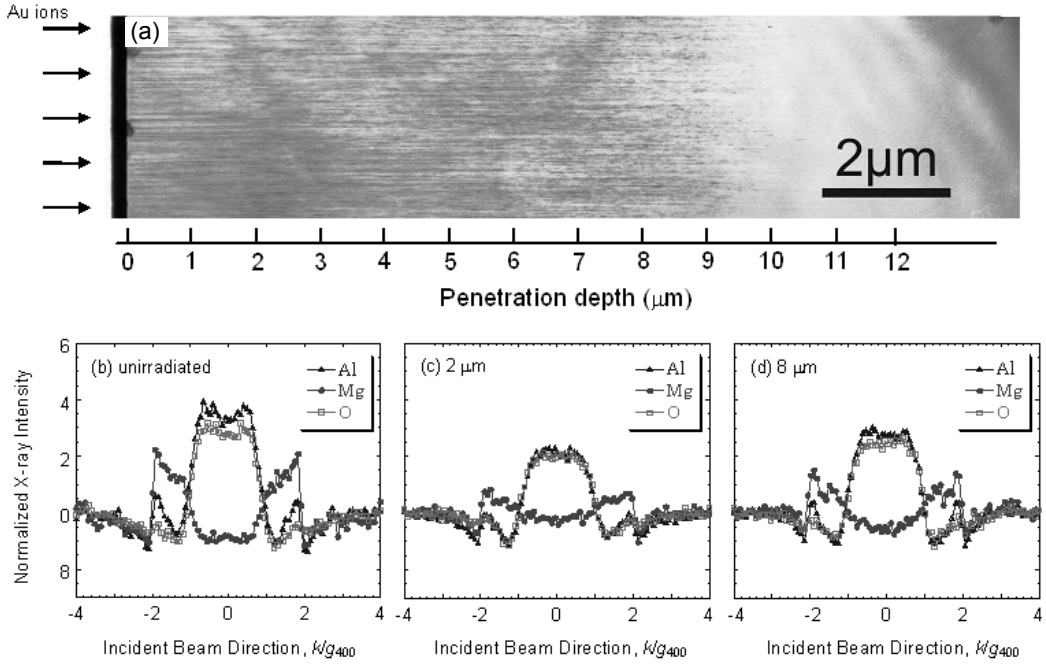

Fig. 1 BF cross section view of $MgO{\cdot}1.1Al_2O_3$ (a) irradiated at 300 K with 350 MeV Au ions to a fluence of $5x10^{15}$ ions/m^2, and HARECXS profiles taken from an unirradiated specimen (b), and from a depth of 2 μm (c) and 8 μm (d) of the irradiated specimen. Characteristic x-ray intensities of Al-K, Mg-K and O-K signals normalized by the those under the kinematic condition are plotted against k/g_{400}.

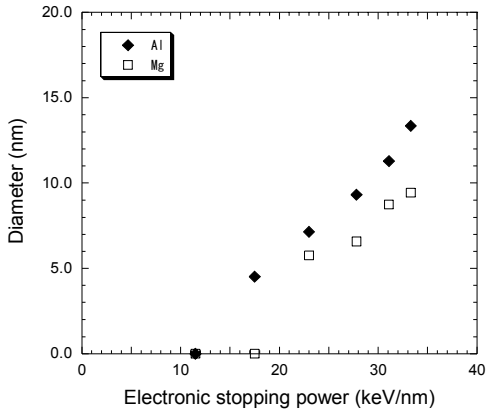

Fig. 2 Diameter of the disordered region induced by one 350 MeV Au ion in $MgO{\cdot}1.1Al_2O_3$ as a function of electronic stopping power, $(dE/dx)_e$. The diameters were evaluated from analysis of HARECXS profiles under the assumption that the disordered region is fully disordered.

The present study includes the result of 'Study on radiation damage in oxide ceramics for the transmutation of long life radio isotopes' entrusted to Kyushu University by the Ministry of Education, Culture, Sports, Science and Technology of Japan (MEXT).

References

[1] K. Yasuda *et al*., Defect and Diffusion Forum, 206-207 (2002) 53-74.
[2] K. Yasuda *et al*., Nucl. Instrum. Methods. Phys. Res., B250 (2006) 238-244.
[3] K. Yasuda *et al*., Nucl. Instrum. Methods. Phys. Res., B266 (2008) 2834-2841.

7. 5 Surface amorphization in single crystalline α-Al_2O_3 induced by swift heavy ion

N. Okubo[1], T. Nakazawa[1], M. Sataka[1], and S. Jitsukawa[1]

Aluminum oxide (α-Al_2O_3) is expected as functional materials in a field of nuclear energy e.g. an insulating material, window used for plasma diagnosis in a fusion reactor and an inert matrix material of geological disposal of high level radioactive waste. Recently, amorphization in ceramics such as α-Al_2O_3, which affects the physical and mechanical properties, is attracted as a phenomenon induced by swift heavy ion irradiations [1]. In previous studies, we reported that amorphous phase was caused in polycrystalline aluminum oxide by ion irradiation with high-density electronic energy depositions (S_e), although lattice structure of aluminum oxide is stable against nuclear energy depositions (S_n) [2]. The amorphization behaviors caused by high-density S_e indicated dependences on the specimen depth and grain orientation around the amorphized-crystalline region. Detailed mechanism of amorphization induced by high energy ion irradiation has not been clearly understood.

Single crystalline α-Al_2O_3 specimens with (0001) surface were irradiated with several energies of Xe ions at ambient temperature, by using the Tandem Accelerator of JAEA. The irradiation energy was from about 160 to 70 MeV by using aluminum foil energy degrader. The specimens used were 10 x 10 mm^2 plates with 0.5 mm thickness. The fluences were in the range of from 1.0 x 10^{13} to 1.0 x 10^{15} ions/cm^2. In the case of 160 MeV, the projected range (R_p) of the Xe ions in the α-Al_2O_3 was calculated to be 10.7 μm with the SRIM2000 code [3]. The electronic energy deposition (S_e) and nuclear energy deposition (S_n) at the surface were also calculated to be 24.5 keV/nm and 0.1 keV/nm, respectively. Cross sectional transmission electron microscope (TEM) observation was conducted after normal focused ion beam sample making process, where 30 keV-Ga^+ was used for sputtering and specimen was deposited by platinum, carbon and tungsten to protect surface and suppress the charge up.

In previous studies, by inferring the result of XRD measurements, the amorphization was considered to take place above the fluence of 1.0 x 10^{14} ions/cm^2 in the case of 160 MeV-Xe ion irradiation [4]. Then, the α-Al_2O_3 specimens irradiated at 3.5 x 10^{14} ions/cm^2 was observed by TEM in order to confirm the cross sectional structure. The cross sectional TEM images of region between surface and 3 μm depth and high magnitude image, which is expanded from inset as a doted rectangular, are shown in fig.1 (1) and (2), respectively. In fig.1 (1), obvious boundary is observed around 800 nm depth. The crystal structure of surface region above the boundary was identified to be amorphous and deeper region to be single crystal by electron diffraction patterns. In fig. 1 (2), distinct ion tracks induced by passing of high energy particles are vertically observed in the region of single crystal. This result indicates that amorphization could be caused by overlapping of ion tracks. The amorhization depth of 800 nm is rather short from the case of polycrystalline aluminum oxide [2] in spite of almost same S_e and S_n. This difference implies that

[1] Japan Atomic Energy Agency (JAEA)

amorhization induced by high energy ion irradiation depends on crystal direction.

In summery, cross sectional TEM measurements demonstrated that amorphization was appeared in surface region with high S_e in single crystalline α-Al_2O_3 irradiated by swift heavy ions above the fluence expected from XRD measurements. Ion track formation, which could cause amorhization by its overlapping, was observed in depth of crystalline region.

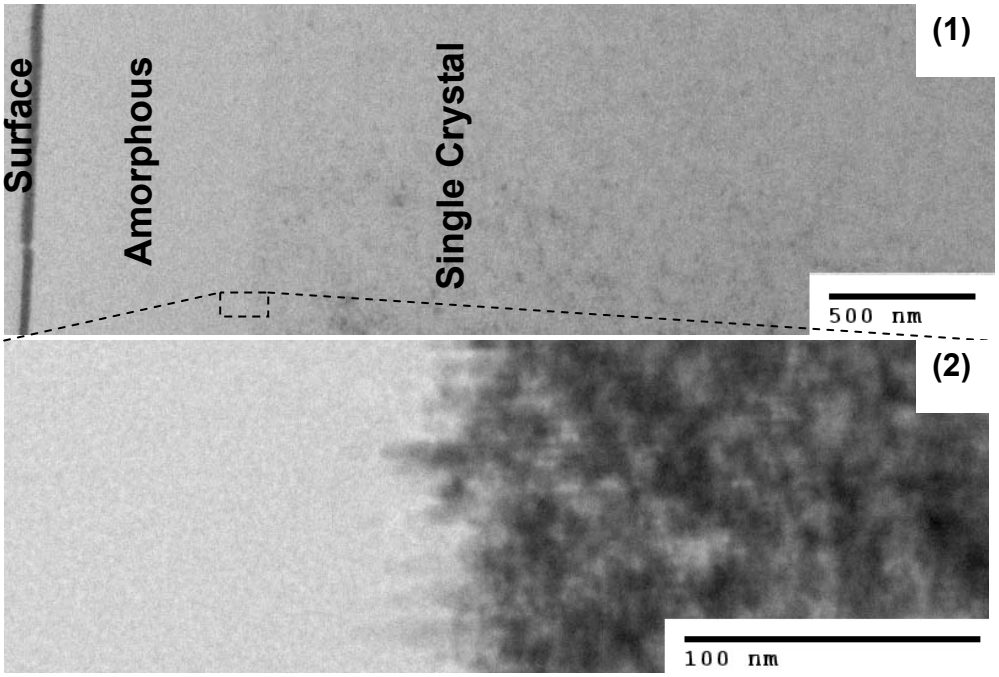

Fig. 1 Cross sectional TEM images of Al_2O_3 specimens irradiated by 160 MeV Xe ions. Total fluence was 3.5×10^{14} ions/cm^2.

References

[1] G. Szenes, J. Nucl. Mater., 336 (2005) 81-89.

[2] T. Aruga e*t al*., Nucl. Instrum. Methods Phys. Res., B166-167 (2000) 913-919.

[3] J.F. Ziegler, J.P. Biersack, and U. Littmark, The Stopping and Range of Ions in Solids, (Pergamon Press, New York, 1985), Chap 8.

[4] N. Okubo *et al*., JAERI TANDEM Ann. Rep. 2004, JAEA-Review 2005-004 (2006) 90-91.

7. 6 Modifications of atomic structure and optical properties of cuprite by high-energy ion impact

N. Matsunami[1], M. Sataka[2], S. Okayasu[2], N. Ishikawa[2],
M. Tazawa[3], and H. Kakiuchida[3]

We have investigated high-energy ion irradiation effects on atomic structure and optical properties of cuprite (Cu_2O). Cuprite is known as a p-type semiconductor with bandgap of ~2 eV [1-3]. The present study is a step towards a study of doped-cuprite and comparison with ion irradiation effects on n-type semiconductors such as ZnO [4,5]. Furthermore, the band-gap dependence of the electronic sputtering is of interest [6].

Cu_2O films were prepared on MgO-substrates at 700 ºC by using an RF-magnetron-sputter-deposition (off-axis) method with a Cu disk target of 99.99 % purity in Ar and O_2 gas (total pressure was ~10 Pa and the O_2 flow rate was approximately one-tenth of Ar) [7]. By means of Rutherford backscattering spectroscopy (RBS), the film thickness and composition are evaluated to be ~100 nm and nearly stoichiometric, using the stopping power in ref. [8] and film density of 5.0×10^{22} Cu cm^{-3} (6.0 gcm^{-3}). X-ray diffraction (XRD) and optical absorption measurements were performed before and after high-energy heavy ion irradiation. Sputtering yields were obtained using the carbon-foil collector method [7].

XRD shows that the film has (111) preferential orientation of cubic structure. For 100 MeV Xe and 90 MeV Ni ion irradiation up to $1 \times 10^{13} cm^{-2}$, the diffraction intensity and the lattice constant decrease with the ion fluence, indicating disordering of the crystal structure (see table 1). It is found that the disordering depends on the electronic stopping power more strongly than the electronic sputtering yields described below, and that the change in lattice constant does much weaker.

No appreciable change in the optical absorption was observed under 100MeV Xe ion irradiation at $3 \times 10^{12} cm^{-2}$. It also appears that the bandgap (2.54 eV) is unchanged under the ion irradiation as shown in fig. 1, in contrast with the increase in the bandgap of Al-doped ZnO [5]. Here, the wavelength calibration was made (the spectra and bandgap slightly differ from those in ref. [7]).

Preliminary results of the electronic sputtering are given in table 1 together with the electronic and nuclear stopping powers, and the calculated sputtering yields Y_c based on the elastic collisions. The measured sputtering yields Y are much larger than Y_c and this confirms that the electronic sputtering plays a dominant role. It is noticed that the sputtering yields by 100 MeV Xe and 90 MeV Ni differ by a factor of ~4, while the decease of the XRD intensity is much more pronounced. This may indicate that the radiation effects in the film are much more effective than near the surface-region. The electronic sputtering yield is interpolated as 11 at the electronic stopping power of 15 keV/nm and this is somewhat larger than the estimated value of 5 at E_g=2.54 [6]. The discrepancy is under investigation, considering a problem in bandgap determination (oscillation seen in fig. 1), disordering effect mentioned above, modification of the suggested bandgap dependence of the electronic sputtering yield [6] etc.

[1] Nagoya University
[2] Japan Atomic Energy Agency (JAEA)
[3] National Institute of Advanced Industrial Science and Technology (AIST)

Table 1. Electronic (S_e) and nuclear (S_n) stopping powers in Cu_2O (keV/nm), XRD intensity (I_{XRD}) normalized to that of unirradiated, lattice constant change (Δa) in % at $6x10^{12}$ cm^{-2}, sputtering yield Y, calculated yield Y_c based on the elastic collision cascade and Y/Y_c.

Ions	S_e	S_n	I_{XRD}	Δa	Y	Y_c	Y/Y_c
90 MeV Ni	14.7	0.032	0.95	-0.8	10	0.21	48
100 MeV Xe	22.0	0.20	0.5	-1.1	38	1.3	29
200 MeV Xe	26.4	0.114			48	0.75	64

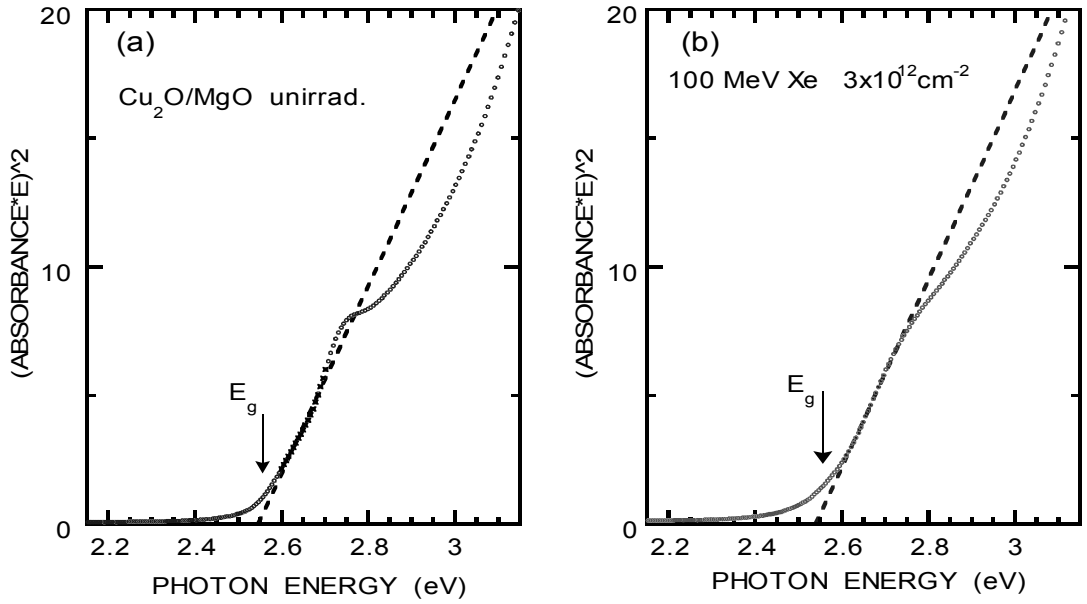

Fig. 1 (a) Square of absorbance times photon energy E versus photon energy illustrating the bandgap (indicated by the vertical arrow) for as-deposited film. The dotted line is the least square fit to the data in the photon energy of 2.6-2.7 eV. (b) Similar to Fig. 1(a) except for irradiated film with 100 MeV Xe ions at $3x10^{12}$ cm^{-2}.

References

[1] A. Roos and B. Karlsson, Solar Energy Mater., 7 (1983) 467-480.

[2] J. Ghijsen *et al*., Phys. Rev., B38 (1988) 11322-11330.

[3] M.T.S. Nair *et al*., Appl. Surf. Sci., 150 (1999) 143-151.

[4] H. Sugai *et al*., Nucl. Instrum. Methods Phys. Res., B250 (2006) 291-294.

[5] O. Fukuoka *et al*., Nucl. Instrum. Methods Phys. Res., B250 (2006) 295-299.

[6] N. Matsunami *et al*., Nucl. Instrum. Methods Phys. Res., B256 (2007) 333-336.

[7] N. Matsunami *et al*., Nucl. Instrum. Methods Phys. Res., B266 (2008) 2986-2989.

[8] J.F. Ziegler, J.P. Biersack, and U. Littmark, The Stopping and Range of Ions in Matter, Pergamon Press, New York (1985).

7. 7 Magnetic domains induced by swift heavy ion irradiation in FeRh alloys

A. Iwase[1], Y. Zushi[1], N. Fujita[1], T. Matsui[1], F. Hori[1], N. Ishikawa[2], and S. Seki[3]

Recently, we have reported that swift heavy ion irradiation induces ferromagnetic state in Fe-50at.% Rh alloys at low temperatures[1-4]. Although the origin of the irradiation-induced ferromagnetism in FeRh alloy has been gradually clarified, magnetic domain structure for the irradiated FeRh alloys has never been reported. In this report, we show the domain structure of the ion-irradiated FeRh alloys.

Alloys of Fe-50 at.%Rh were irradiated with 200 MeV Xe ions by using a tandem accelerator at JAEA-Tokai. The ion-fluences were $2x10^{12}$, $5x10^{12}$, $1x10^{13}$ and $5x10^{13}/cm^2$. After the irradiations, magnetic domain structures at the surface of the irradiated samples were observed by using a magnetic force microscope (MFM) at room temperature.

The result of the MFM observation is shown in fig. 1. In the unirradiated sample, no obvious domain structure can be seen in the scanned area (25 μm x 25 μm). In the irradiated samples, the dark and bright contrasts are observed in the MFM image, which indicate the existence of small magnetic domains in the scanned area. With increasing the ion-fluence, the magnetic domain structures transform from a monochromatic structure on a scale of 5 μm into segmentalized ones on a scale of less than 1 μm. The magnetic domain structures reveal a fractal-like development with increasing ion-fluence.

The present observation can be explained as follows; the energy parameter (e.g., exchange energy, magnetostatic energy, magnetocrystalline energy and so on) at the surface are varied by the irradiation-induced local fluctuations of composition and/or strains, which contribute to the development of the fractal-like domain structures.

References

[1] M. Fukuzumi *et al*., Nucl. Instrum. Methods Phys. Res., B230 (2005) 269-273.
[2] M. Fukuzumi *et al*., Nucl. Instrum. Methods Phys. Res., B245 (2006) 161-165.
[3] A. Iwase *et al*., Nucl. Instrum. Methods Phys. Res., B 256 (2007) 429-433.
[4] Y. Zushi *et al*., Nucl. Instrum. Methods Phys. Res., B 256 (2007) 434-437.

[1] Osaka Prefecture University
[2] Japan Atomic Energy Agency (JAEA)
[3] Osaka University

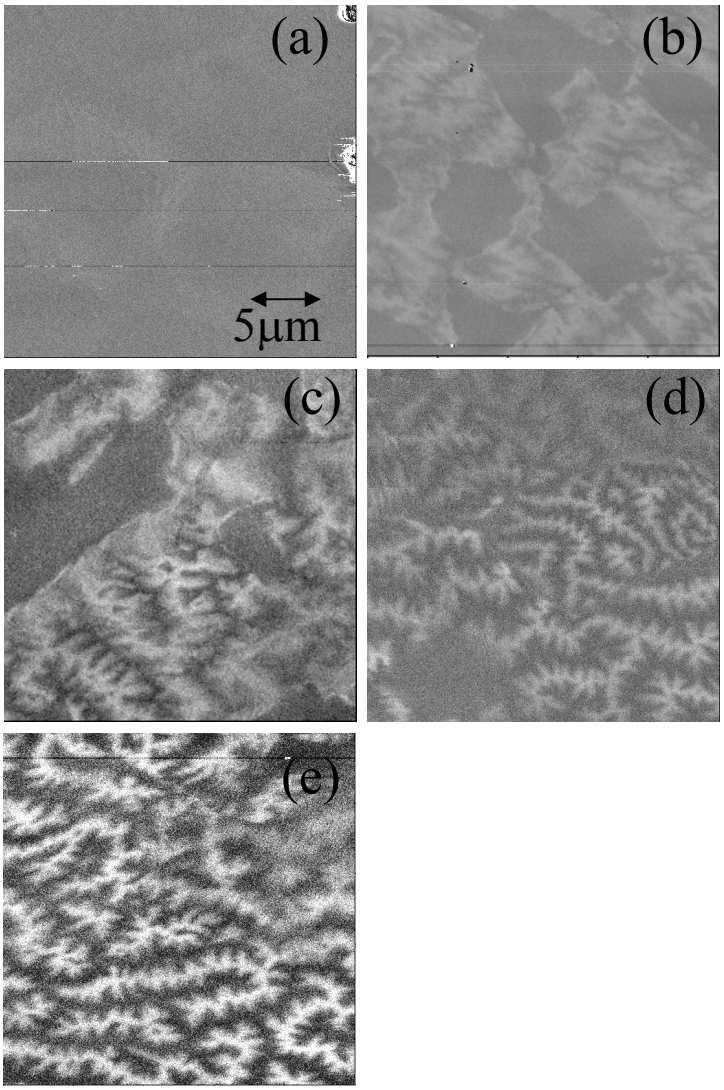

Fig. 1 MFM images at room temperature for (a) unirradiated Fe-50at.% Rh and those irradiated to the ion-fluence of (b) $2x10^{12}$, (c) $5x10^{12}$, (d) $1x10^{13}/cm^2$ and (e) $5x10^{13}cm^{-2}$. The scanned area is 25μm x 25μm.

7. 8 Nanostructural changes of iron disilicides (β-$FeSi_2$) thin films by high-energy heavy ion irradiation

M. Sasase[1] and S. Okayasu[2]

β-$FeSi_2$ was irradiated by various ions with a fluence of 1.0 x 10^{12} ion/cm^2 at room temperature using the Tandem accelerator. The size of the columnar defects as a function of the deposited energy (S_e) has been investigated. The present experiments shows that the size of the columnar defects depends on the S_e into the specimens. The deposited energy contributed to the columnar defects formation.

Iron disilicide (β-$FeSi_2$) is one of the candidates of compound semiconductor, which contains harmless elements to the human bodies, natural resources and the environment [1]. Another attractive feature of β-$FeSi_2$ is transformation to the metal phase α-$FeSi_2$ when heated above 1246 K. Since the bulk α-$FeSi_2$ has electric resistivity as low as 2.5 x 10^{-4} Ω cm, one may consider if a small part of β-$FeSi_2$ can be transformed into α-$FeSi_2$ selectively, it can be used as the electrode of a β-$FeSi_2$ based device.

When high-energy heavy ions are irradiated into materials, most of their energies are dissipated through an electronic excitation [2]. This leads to strong localization of the dissipated energy along the projectile path. The density of energy deposition is high enough, compared with bond or displacement energy of the target materials, so that nanostructural changes take place such as amorphization and phase transition etc. We attempted to perform phase transition from β-$FeSi_2$ into other phase by the high-energy heavy ion irradiation.

The specimens used in this study were β-$FeSi_2$ films fabricated with the ion beam sputter deposition method by depositing Fe on Si(100) substrates at certain temperatures [3]. The specimens were irradiated by 180 MeV Fe^{11+}, 200 MeV Xe^{14+} and 240 MeV Au^{24+} ions at room temperature with a fluence of 1.0 x 10^{12} ions/cm^2 using the Tandem accelerator at Japan Atomic Energy Agency (JAEA). The projected ranges and deposited energies, $S_{e,}$ through the electronic excitation process of these ions in β-$FeSi_2$/Si(100) are estimated by using the TRIM code calculations [4]. Cross sectional observations were performed with β-$FeSi_2$/Si(100) by using a transmission electron microscope (TEM, JEOL JEM-3000F) with a field emission gun operated at 300 keV.

If the phase transition of β-$FeSi_2$ to α phase takes place by the high-energy heavy ion irradiation, it is expected that nanostructural changes are observed in TEM images. Typical defect nanostructures of β-$FeSi_2$ thin films irradiated with 240 MeV Au^{24+} ions are shown as a TEM image in fig. 1. The lines are observed in this image along the direction perpendicular to the a-axis of β-$FeSi_2$. These lines can be interpreting as the columnar defects from the higher magnification images. The arrows indicate the columnar defect produced by the ion passing along this direction. The amorphization of the damaged

[1] The Wakasa-wan Energy Research Center (WERC)
[2] Japan Atomic Energy Agency (JAEA)

area is clearly visible in the samples.

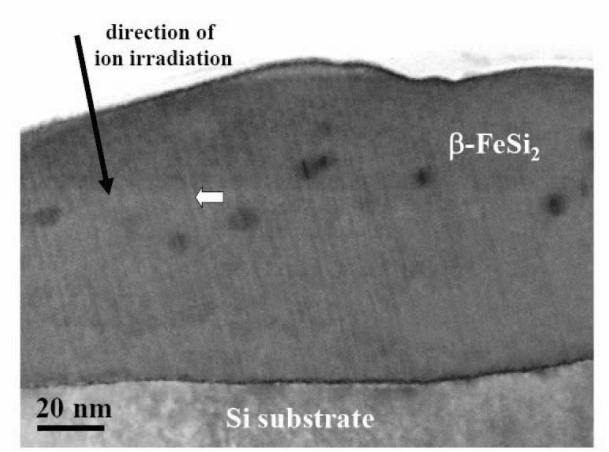

Fig. 1 Columnar defects introduced with 240 MeV Au^{24+} in β-$FeSi_2$ thin films.

Table 1. The relationship between irradiation condition and diameter of columnar defects.

Ion	Energy(MeV)	S_e (keV/nm)	Diameter of defect size (nm)
Fe	180	12.3	2
Xe	200	26.5	4
Au	240	34.0	6

From these TEM micrographs, the size of each columnar defect was estimated. The most probable diameter of the columnar defects was 2 nm for 180 MeV Fe^{11+} ion irradiation, while 4 nm for 200 MeV Xe^{14+} and 6 nm for 240 MeV Au^{24+} irradiation, respectively. At these experimental conditions, the deposited energies S_e were calculated to be 12.3 – 34 keV/nm, corresponding to 180 Fe^{11+} – 240 MeV Au^{24+} irradiation. These values are listed in table 1 for each ion irradiation condition. The diameter of the columnar defects becomes larger with the energy of irradiated heavy ions. This tendency shows that 240 MeV Au^{24+} ions cause more severe lattice damage compared with 180 MeV Fe^{11+} and 200 MeV Xe^{14+} ion irradiation.

It can be considered that the diameter of the columnar defects depends both on the atomic number and on the energy of irradiated ions, which is strongly correlated to S_e, from a previous study [5]. As listed in table 1, the size of the columnar defects increases with S_e. Therefore, defect formation takes place with thermal spike due to the energy dissipation through electron excitation.

Although the phase transition of β-$FeSi_2$ to α phase is not confirmed yet, our results showed the structural change by high energy heavy ion irradiation. We will intend to observe the microstructure of defects and phase transitions in the irradiated films precisely by using both high resolution TEM and micro-diffraction.

References

[1] K. Yamaguchi and K. Mizushima, Phys. Rev. Lett., 86 (2001) 6006-6009.
[2] M. Toulemonde, S. Bouffard, and F. Studer, Nucl. Instrum. Methods Phys. Res., B91 (1994) 108-123.
[3] M. Sasase *et al*., Thin Solid Films, 401 (2001) 73-76.
[4] J.F. Ziegler, Handbook of Stopping Cross Section for Energetic Ions in All Elements, Pergamon Press, New York (1980).
[5] Y. Zhu *et al*., Phys. Rev., B48 (1993) 6436-6450.

CHAPTER 8

Publication in Journal and Proceedings, and Contribution to Scientific Meetings

This is a blank page.

8. 1 Accelerator Operation and Development

Journal / Proceedings

M. Matsuda, M. Sataka, S. Takeuchi, Y. Tsukihashi, S. Hanashima, S. Abe, A. Osa, N. Ishizaki, H. Tayama, T. Nakanoya, H. Kabumoto, M. Nakamura, K. Kutsukake, Y. Otokawa, and I. Ohuchi
Present Status of JAEA-Tokai Tandem Accelerator
JAEA-Conf 2008-005 (2008) 42-45.

M. Matsuda, T. Nakanoya, K. Kutsukake, and S. Takeuchi
Development of the heavy ion injector in the high voltage terminal
Proc. of the 4th Annual Meeting of Particle Accelerator Society of Japan and the 32nd Linear Accelerator Meeting in Japan, Wako, Japan (Aug. 1-3, 2007) 736-738.

H. Kabumoto, S. Takeuchi, N. Ishizaki, and Y. Otokawa

Performance test of low beta superconducting twin quarter wave resonator
Proc. of the 4th Annual Meeting of Particle Accelerator Society of Japan and the 32nd Linear Accelerator Meeting in Japan, Wako, Japan (Aug. 1-3, 2007) 469-471.

H. Kabumoto, S. Takeuchi, N. Ishizaki, and Y. Otokawa

Development of low beta superconducting twin quarter wave resonator
JAEA-Conf 2008-005 (2008) 137-140.

A. Osa
Status of JAEA-KEK radioactive ion beam facility, TRIAC
Nucl. Instrum. Methods Phys. Res., B261 (2007) 1048.

Meetings

M. Matsuda, M. Sataka, S. Takeuchi, Y. Tsukihashi, S. Hanashima, S. Abe, A. Osa, N. Ishizaki, H. Tayama, T. Nakanoya, H. Kabumoto, M. Nakamura, K. Kutsukake, Y. Otokawa, and I. Ohuchi
Present Status of JAEA-Tokai Tandem Accelerator
The 20th Meeting for Tandem Accelerators and their Associated Technologies, Tokai, Japan (Jul. 12, 2007).

M. Matsuda, T. Nakanoya, K. Kutsukake, and S. Takeuchi
Development of the heavy ion injector in the high voltage terminal
The 4th Annual Meeting of Particle Accelerator Society of Japan and the 32nd Linear Accelerator Meeting in Japan, Wako, Japan (Aug. 3, 2007).

H. Kabumoto, S. Takeuchi, N. Ishizaki, and Y. Otokawa

Performance test of low beta superconducting twin quarter wave resonator
The 4th Annual Meeting of Particle Accelerator Society of Japan and the 32nd Linear Accelerator Meeting in Japan, Wako, Japan (Aug. 2, 2007).

H. Kabumoto, S. Takeuchi, N. Ishizaki, and Y. Otokawa

Development of low beta superconducting twin quarter wave resonator
The 20th Meeting for Tandem Accelerators and their Associated Technologies, Tokai, Japan (Jul. 12, 2007).

A. Osa, S. Ichikawa, M. Matsuda, T.K. Sato, and S.C. Jeong

Ion source development for the on-line isotope separator at JAEA
15th International Conference on Electromagnetic Isotope Separators and Techniques Related to their Applications (EMIS2007), Deauville, France (Jun. 26, 2007).

A. Osa, M. Matsuda, T.K. Sato, and S. Ichikawa

Release and efficiencies of radioactive ion beams from the JAEA-ISOL target/ion source systems
15th International Conference on Electromagnetic Isotope Separators and Techniques Related to their Applications (EMIS2007), Deauville, France (Jun. 25, 2007).

8. 2 Nuclear Structure

Journal / Proceedings

Y.H. Zhang, S. Guo, X. H. Zhou, L. Ma. W. T. Guo, M. Oshima, Y. Toh, M. Koizumi, A. Osa, A. Kimura, Y. Hatsukawa, M. Sugawara, and H. Kusakari
Identification of a new band and its signature inversion in ^{174}Re
Chin. Phys. Lett., 24 (2007) 1203-1206.

T. Shizuma, T. Ishii, H. Makii, T. Hayakawa, S. Shigematsu, M. Matsuda, E. Ideguchi, Y. Zheng, M. Liu, and T. Morikawa
Evidence for a $K^{\pi}=1/2^{+}$ isomer in neutron-rich ^{185}Ta
Eur. Phys. J., A34 (2007) 1-4.

T. Shizuma, T. Ishii, H. Makii, T. Hayakawa, S. Shigematsu, M. Matsuda, E. Ideguchi, Y. Zheng, M. Liu, T. Morikawa, and M. Oi
One-quasiparticle bands in neutron-rich ^{187}W
Phys. Rev., C77 (2007) 047303 (1-4).

Y. Liu, X.H. Zhou, Y.H. Zhang, M.L. Liu, Y.X. Guo, M. Oshima, Y. Toh, M. Koizumi, A. Osa, Y. Hatsukawa, and Y. Sun
Prolate and oblate shape coexistence in ^{188}Pt
Chin. Phys. Lett., 25 (2008) 1633-1635.

H. Makii, T. Ishii, M. Asai, K. Tsukada, A. Toyoshima, M. Matsuda, A. Makishima, J. Kaneko, H. Toume, S. Ichikawa, S. Shigematsu, T. Kohno, and M. Ogawa
Z dependence of the N = 152 deformed shell gap: In-beam γ-ray spectroscopy of neutron-rich $^{245, 246}Pu$
Phys. Rev. C 76 (2007) 061301(R) (1-5).

T. Ishii, H. Makii, M. Asai, H. Koura, S. Shigematsu, K. Tsukada, A. Toyoshima, M. Matsuda, A. Makishima, J. Kaneko, H. Toume, I. Hossain, T. Shizuma, S. Ichikawa, T. Kohno, and M. Ogawa
Ground-state bands of neutron-rich ^{236}Th and ^{242}U nuclei and implication of spherical shell closure at N=164
Phys. Rev., C76 (2007) 011303(R) (1-5).

H. Iimura, T. Horiguchi, Y. Ishida, M. Ito, M. Koizumi, M. Miyabe, and M. Oba
Production of ^{186m}Re from proton bombardment of enriched ^{186}W
J. Phys. Soc. Jpn., 77 (2008) 025004 (1-2).

H. Iimura and F. Buchinger
Charge radii in macroscopic-microscopic mass models of axial asymmetry

Phys. Rev., C76 (2007) 057302 (1-4).

H. Hayashi, Y. Akita, O. Suematsu, M. Shibata, M. Asai, T. K. Sato, S. Ichikawa, I. Nishinaka, Y. Nagame, A. Osa, K. Tsukada, T. Ishii, Y. Kojima, and A. Taniguchi
Q_β measurements of ^{158,159}Pm, ^{159,161}Sm, $^{160\text{-}165}$Eu, ^{163}Gd and ^{166}Tb using a total absorption BGO detector
Eur. Phys. J., A34 (2008) 363-370.

Meetings

E. Ideguchi, M. Liu, T. Morikawa, Y. Toh, M. Koizumi, M. Oshima, A. Kimura, K. Furutaka, Y. Hatsukawa, B. Cederwall, Y. Zheng, H. Kusakari, M. Sugawara, and S. Mitarai
Study of high-spin states in A～30 region via ^{18}O+^{24}Mg reaction
2007 Fall Meeting of the Physical Society of Japan, Sapporo, Japan (Sep. 24, 2007).

T. Morikawa, E. Ideguchi, M. Liu, Y. Zheng, M. Oshima, M. Koizumi, Y. Toh, A. Kimura, A. Osa, H. Harada, K. Furutaka, S. Nakamura, F. Kitatani, Y. Hatsukawa, M. Sugawara, H. Kusakari, and S. Mitarai
High-spin spectroscopy of neutron-rich ^{38}Cl nucleus
2007 Fall Meeting of the Physical Society of Japan, Sapporo, Japan (Sep. 24, 2007).

T. Morikawa, M. Nakamura, T. Sugimitsu, H. Kusakari, S. Mitarai, M. Oshima, Y. Toh, Y. Hatsukawa, J. Katakura, M. Koizumi, A. Osa, A. Kimura, J. Goto, E. Ideguchi, M. Liu, Y. Zheng, and M. Sugawara
Spectroscopy of ^{33}P and high-spin study of neutron-rich nuclei via fusion evaporation reactions
International Nuclear Physics Conference 2007 (INPC2007), Tokyo, Japan (Jun. 6, 2007).

T. Shizuma, T. Ishii, H. Makii, T. Hayakawa, S. Shigematsu, M. Matsuda, E. Ideguchi, Y. Zheng, M. Liu, T. Morikawa, P.M. Walker, and M. Oi
Spectroscopy of neutron-rich ^{187,188}W produced in neutron transfer reactions
International Nuclear Physics Conference 2007 (INPC2007), Tokyo, Japan (Jun. 4, 2007).

H. Makii, T. Ishii, M. Asai, K. Tsukada, A. Toyoshima, M. Matsuda, A. Makishima, J. Kaneko, H. Toume, S. Ichikawa, S. Shigematsu, T. Kohno, and M. Ogawa
In-beam γ-ray spectroscopy of neutron-rich 245, 246Pu and properties of N = 152 deformed shell closure
Nuclear Structure: New Pictures in the Extended Isospin Space, Kyoto, Japan (Jun. 14, 2007).

T. Ishii, H. Makii, M. Asai, H. Koura, S. Shigematsu, K. Tsukada, A. Toyoshima, M. Matsuda, A. Makishima, T. Shizuma, J. Kaneko, H. Toume, I. Hossain, S. Ichikawa, T. Kohno, and M. Ogawa
In-beam γ-ray spectroscopy of neutron-rich nuclei in the uranium region through the heavy-ion transfer reaction
International Nuclear Physics Conference 2007 (INPC2007), Tokyo, Japan (Jun. 4, 2007).

T. Ishii, H. Makii, M. Asai, K. Tsukada, A. Toyoshima, M. Matsuda, T. Shizuma, A. Makishima, H. Toume, S. Shigematsu, T. Kohno , Ogawa, and I. Hossain
High-j quasi-particle states in ^{249}Cm
2008 Spring Meeting of the Physical Society of Japan, Osaka, Japan (Mar. 23, 2008).

T. Ishii
In-beam γ-ray spectroscopy of neutron-rich nuclei in the uranium region
4th Meeting on Nuclear Physics of Slow and Stop Radio Isotope (SSRI4), Sendai, Japan (Dec. 21, 2007).

M. Asai
Gamma-ray spectroscopy of the heaviest nuclei
International Workshop on Nuclear Structure: New Pictures in the Extended Isospin Space (NS07), Kyoto, Japan (Jun. 13, 2007).

M. Asai, K. Tsukada, M. Sakama, Y. Ishii, A. Toyoshima, T. Ishii, I. Nishinaka, Y. Nagame, Y. Kasamatsu, H. Haba, Y. Kojima, M. Shibata, H. Hayashi, and K. Sueki
Alpha-gamma spectroscopy N = 155 and 157 nuclei using a gas-jet transport technique
The 3rd International Conference on the Chemistry and Physics of the Transactinide Elements (TAN07), Davos, Switzerland (Sep. 27, 2007).

M. Asai, K. Tsukada, Y. Ishii, A. Toyoshima, T. Ishii, I. Nishinaka, and Y. Nagame
Alpha fine structure spectroscopy for heavy- and transactinide nuclei
The 3rd International Conference on the Chemistry and Physics of the Transactinide Elements (TAN07), Davos, Switzerland (Sep. 25, 2007).

H. Schuessler, F. Buchinger, T. Cocolios, J.E. Crawford, S. Gulick, H. Iimura, J.K.P. Lee, C.D.P. Levy, M. Pearson, V. Lioubimov, F. Zhu, J. Rikovska, S.D. Rosner, R. Thompson, and R. Wyss
Nuclear moments of the radioactive isotope ^{131}La determined by collinear fast-beam laser spectroscopy
International Nuclear Physics Conference 2007 (INPC2007), Tokyo, Japan (Jun. 4, 2007).

H. Iimura and F. Buchinger
Nuclear charge radii calculated with mass models taking axially asymmetric deformation into consideration
63rd Annual Meeting of the Physical Society of Japan, Higashiosaka, Japan (Mar. 24, 2008).

Y. Hirayama
Nuclear Spectroscopy with polarized radioactive beam by tilted foil technique
4th Meeting on Nuclear Physics of Slow and Stop Radio Isotope (SSRI4), Sendai, Japan (Dec. 20, 2007).

M. Asai

Alpha fine structure spectroscopy for the heaviest nuclei
4th Meeting on Nuclear Physics of Slow and Stop Radio Isotope (SSRI4), Sendai, Japan (Dec. 21, 2007).

8. 3 Nuclear Reaction

Journal / Proceedings

S. Mitsuoka, H. Ikezoe, K. Nishio, K. Tsuruta, S.C. Jeong, and Y. Watanabe
Barrier distributions derived from quasielastic backscattering of ^{48}Ti, ^{54}Cr, ^{56}Fe, ^{64}Ni and ^{70}Zn projectiles on a ^{208}Pb target
Phys. Rev. Lett. 99, 182701 (2007).

Z. Muhammad, K. Hagino, S. Mitsuoka, and H. Ikezoe
Coupled-channels analyses for large-angle quasi-elastic scattering in massive systems
Phys. Rev. C77, 034604 (2008).

K. Nishio, S. Hofmann, H. Ikezoe, F.P. Hessberger, D. Ackermann, S. Antalic, V.F. Comas, Z. Gan, S. Heinz, J.A. Heredia, J. Khuyagbaatar, B. Kindler, I. Kojouharov, P. Kuusiniemi, B. Lommel, R. Mann, M. Mazzocco, S. Mitsuoka, Y. Nagame, T. Ohtsuki, A.G. Popeko, S. Saro, H.J. Schött, B. Sulignano, A. Svirikhin, K. Tsukada, K. Tsuruta, and A.V. Yeremin
Measurement of evaporation residue and fission cross-sections of the reaction ^{30}Si + ^{238}U at subbarrier energies
J. Nucl. and Rad. Sci., 8 (2007) 73-78.

J. Murata, K. Asahi, D. Kameda, H. Kawamura, D. Nagae, K. Narita, K. Shimada, T. Shimoyama, T. Suehiro, T. Toyoda, M .Uchida, H. Ueno, and A. Yoshimi
Beta neutrino correlation and T-violation experiment in nuclear beta decay
AIP Conference Proceedings, 915 (2007) 218.

Meetings

Y. Watanabe, S. Mitsuoka, K. Nishio, S.C. Jeong, T. Hashimoto, Y. Hirayama, N. Imai, H. Ishiyama, H. Miyatake, and H. Ikezoe
Measurement of quasi-elastic back-scattering of ^{64}Ni+^{118}Sn and ^{58}Ni+^{124}Sn
63rd Annual Meeting of the Physical Society of Japan, Osaka, Japan (Mar. 23, 2008).

Y. Watanabe
Experiments for possible effect of neutron transfer on fusion process
4th Meeting on Nuclear Physics of Slow and Stop Radio Isotope (SSRI4), Sendai, Japan (Dec. 21, 2007).

S. Mitsuoka, H. Ikezoe, K. Nishio, K. Tsuruta, S.C. Jeong, and Y. Watanabe
Barrier distributions for quasi-elastic back-scattering of ^{48}Ti, ^{54}Cr, ^{56}Fe, ^{64}Ni and ^{70}Zn projectiles on ^{208}Pb target

International Workshop on Nuclear Structure, Kyoto, Japan (Jun.13, 2007).

S.Mitsuoka, H.Ikezoe, K.Nishio, T. Hashimoto, S.C. Jeong, Y. Watanabe, H. Miyatake, H. Ishiyama, N. Imai, and Y. Hirayama
Barrier distribution for sub-barrier fusion of deformed nuclei
Annual Meeting of the Physical Society of Japan, Sapporo, Japan (Sep. 24, 2007).

K. Nishio, H. Ikezoe, S. Mitsuoka, I. Nishinaka, Y. Watanabe, Y. Nagame, T. Ohtsuki, and K. Hirose
Effects of nuclear deformation of ^{238}U on the fission fragment mass distribution in the reaction of $^{36}S + ^{238}U$
2008 Spring Meeting of the Physical Society of Japan, Osaka, Japan (Mar. 23, 2008).

K. Nishio, H. Ikezoe, S. Mitsuoka, I. Nishinaka, Y. Watanabe, Y. Nagame, T. Ohtsuki, and K. Hirose
Measurement of fission fragment mass distributions in the sub-barrier reaction of $^{36}S + ^{238}U$
2008 Spring Meeting of the Atomic Energy Society of Japan, Osaka, Japan (Mar. 26., 2008).

K. Nishio, H. Ikezoe, S. Hofmann, F.P. Hessberger, D. Ackermann, S. Antalic, V.F. Comas, Z. Gan, S. Heinz, J.A. Heredia, J. Khuyagbaatar, B. Kindler, I. Kojouharov, P. Kuusiniemi, B. Lommel, R. Mann, M. Mazzocco, S. Mitsuoka, Y. Nagame, T. Ohtsuki, A.G. Popeko, S. Saro, H.J. Schött, B. Sulignano, A. Svirikhin, K. Tsukada, K. Tsuruta, and A.V. Yeremin
Orientation effects of deformed ^{238}U target nuclei on the fusion probability for the heavy element synthesis
International Nuclear Physics Conference 2007 (INPC2007), Tokyo, Japan (Jun. 6, 2007).

K. Nishio, H. Ikezoe, S. Hofmann, F.P. Hessberger, D. Ackermann, S. Antalic, V.F. Comas, Z. Gan, S. Heinz, J.A. Heredia, J. Khuyagbaatar, B. Kindler, I. Kojouharov, P. Kuusiniemi, B. Lommel, R. Mann, M. Mazzocco, S. Mitsuoka, Y. Nagame, T. Ohtsuki, A.G. Popeko, S. Saro, H.J. Schött, B. Sulignano, A. Svirikhin, K. Tsukada, K. Tsuruta, and A.V. Yeremin
Orientation effects of deformed ^{238}U target nuclei on the fusion probability for heavy eleemt synthesis
International Workshop on Nuclear Structure (NS07), Kyoto, Japan (Jun. 14, 2007).

K. Nishio, H. Ikezoe, S. Hofmann, F.P. Hessberger, D. Ackermann, S. Antalic, V.F. Comas, Z. Gan, S. Heinz, J.A. Heredia, J. Khuyagbaatar, B. Kindler, I. Kojouharov, P. Kuusiniemi, B. Lommel, R. Mann, M. Mazzocco, S. Mitsuoka, Y. Nagame, T. Ohtsuki, A.G. Popeko, S. Saro, H.J. Schött, B. Sulignano, A. Svirikhin, K. Tsukada, K. Tsuruta, and A.V. Yeremin
Orientation effects of deformed target nuclei on the fusion probability for heavy element synthesis
3rd. International Conf. on the Chemistry and Physics of the Transactindie Elements (TAN07), Davos, Switzerland, Davos (Sep. 24, 2007).

J. Murata

T-violating transverse electron polarization in polarized nuclear beta decay
International Nuclear Physics Conference (INPC 2007), Tokyo, Japan (Jun. 6, 2007).

T. Hashimoto, S. Mitsuoka, K. Nishio, T.K. Sato, A. Osa, S. Ichikawa, M. Matsuda, H. Ikezoe, H. Ishiyama, Y.X. Watanabe, Y. Hirayama, N. Imai, H. Miyatake, S.C. Jeong, M.H. Tanaka, N. Yoshikawa, T. Nomura, S.K. Das, Y. Mizoi, T. Fukuda, S. Bishop, A. Sato, and T. Shimoda

Direct measurement of the astrophysical ^{8}Li(d, t)^{7}Li reaction
Direct Reaction with Exotic Beams 2007, Wako, Japan (May. 30, 2007).

H. Ishiyama, Y.X. Watanabe, Y. Hirayama, N. Imai, H. Miyatake, M.H. Tanaka, N. Yoshikawa, S.C. Jeong, Y. Fuchi, T. Nomura, I. Katayama, H. Kawakami, T. Hashimoto, K. Nishio, S. Mitsuoka, H. Ikezoe, M. Matsuda, S. Ichikawa, T.K. Sato, A. Osa, S.K. Das, Y. Mizoi, T. Fukuda, T. Shimoda K. Otsuki, and T. Kajino

A systematic study of astrophysical nuclear reaction rates via ^{8}Li
International Nuclear Physics Conference 2007 (INPC2007), Tokyo, Japan (Jun. 5, 2007).

T. Hashimoto, H. Ishiyama, Y.X. Watanabe, Y. Hirayama, N. Imai, H. Miyatake, S.C. Jeong, M.H. Tanaka, N. Yoshikawa, T. Nomura, S. Mitsuoka, K. Nishio, T.K. Sato, S. Ichikawa, H. Ikezoe, A. Osa, M. Matsuda, S.K. Das, Y. Mizoi, T. Fukuda, A. Sato, and T. Shimoda

Direct measurement of ^{8}Li + d reactions of astrophysical interest
10th International Symposium on Origin of Matter and Evolution of Galazies, Hokkaido, Japan (Dec. 6, 2007).

H. Ishiyama, Y.X. Watanabe, Y. Hirayama, N. Imai, H. Miyatake, M.H. Tanaka, N. Yoshikawa, S.C. Jeong, Y. Fuchi, T. Nomura, I. Katayama, H. Kawakami, T. Hashimoto, K. Nishio, S. Mitsuoka, H. Ikezoe, M. Matsuda, S. Ichikawa, T.K. Sato, A. Osa, S.K. Das, Y. Mizoi, T. Fukuda, T. Shimoda K. Otsuki, and T. Kajino

Determination of astrophysical nuclear reaction rates on neutron-rich nuclei
3rd Japanese-German EFES(JSPS)-DEG/GSI workshop on Nuclear Structure and Astrophysics, Frauenw im Chiemsee, German (Sep. 30, 2007).

H. Ishiyama, Y.X. Watanabe, H. Miyatake, M.H. Tanaka,Y. Fuchi, Y. Hirayama, N. Imai, S.C. Jeong, I. Katayama, T. Nomura, T. Hashimoto, S. Mitsuoka, K. Nishio, M. Matsuda, A. Osa, T.K. Sato, S. Ichikawa, H. Ikezoe, Y. Mizoi, S.K. Das, T. Fukuda, Y. Yamaguchi, T. Shimoda, K. Otsuki, and T. Kajino

Development of the GEM-MSTPC for cross section measurements with low-energy RNBs
Japanese-French workshop on Next generation of detectors with RI beams, Ganil, France (Feb. 14, 2007).

H. Ishiyama

Determination of astrophysical nuclear reaction rates with radioactive nuclear beams at TRIAC
Year meeting of the Physical Society of Japan, Sapporo, Japan (Sep. 21, 2007).

T. Hashimoto, H. Ishiyama, Y.X. Watanabe, Y. Hirayama, N. Imai, H. Miyatake, S.C. Jeong, M.H. Tanaka, N. Yoshikawa, T. Nomura, S. Mitsuoka, K. Nishio, T.K. Sato, S. Ichikawa, H. Ikezoe, A. Osa, M. Matsuda,

S.K. Das, Y. Mizoi, T. Fukuda, A. Sato, and T. Shimoda

Direct measurements of the ^{8}Li(d, p), (d, t) and (d, α) reactions
Year meeting of the Physical Society of Japan, Sapporo, Japan (Sep. 21, 2007).

Y. Mizoi, T. Fukuda, S.K. Das, H. Ishiyama, Y.X. Watanabe, M-H. Tanaka, H. Miyatake, and T. Hashimoto

Development of the GEM-MSTPC for low-energy nuclear reactions
Year meeting of the Physical Society of Japan, Sapporo, Japan (Sep. 22, 2007).

K. Yamaguchi, H. Ishiyama, M-H. Tanaka, Y.X. Watanabe, H. Miyatake, Y. Hirayama, N. Imai, Y, Fuchi, S.C. Jeong, T. Nomura, Y. Mizoi, T. Fukuda, S.K. Das, and T. Hashimoto

Development of the GEM-MSTPC for low-energy nuclear reactions II
Year meeting of the Physical Society of Japan, Osaka Japan (Mar. 24, 2008).

8. 4 Nuclear Chemistry

Journal / Proceedings

Y. Nagame, I. Nishinaka, Y.L. Zhao, and H. Nakahara
Symmetric and asymmetric scission properties in the fission of pre-actinides through heavy actinides
Rum. Rep. Phys., 59 (2007) 362-376.

Y. Kasamatsu, A. Toyoshima, H. Toume, K. Tsukada, H. Haba, and Y. Nagame
Anion-exchange behavior of Nb, Ta, and Pa as homologues of Db in HF/HNO_3 solutions
J. Nucl. Radiochem. Sci., 8 (2007) 69-72.

H. Haba, T. Akiyama, D. Kaji, H. Kikunaga, T. Kuribayashi, K. Morimoto, K. Morita, K. Ooe, N. Sato, A. Shinohara, T. Takabe, Y. Tashiro, A. Toyoshima, A. Yoneda, and T. Yoshimura
Startup of superheavy element chemistry at RIKEN
Eur. Phys. J., D45 (2007) 81-86.

Y. Ishii, A. Toyoshima, K. Tsukada, M. Asai, H. Toume, I. Nishinaka, Y. Nagame, S. Miyashita, T. Mori, H. Suganuma, H. Haba, M. Sakamaki, S. Goto, H. Kudo, K. Akiyama, Y. Oura, H. Nakahara, Y. Tashiro, A. Shinohara, M. Schädel, W. Brüchle, V. Pershina, and J.V. Kratz
Fluoride complexation of element 104, rutherfordium (Rf), investigated by cation-exchange chromatography
Chem. Lett., 37 (2008) 288-289.

A. Toyoshima, H. Haba, K. Tsukada, M. Asai, K. Akiyama, S. Goto, W. Sato, Y. Ishii, I. Nishinaka, T. K. Sato, Y. Nagame, Y. Tani, H. Hasegawa, K. Matsuo, D. Saika, Y. Kitamoto, A. Shinohara, M. Ito, J. Saito, H. Kudo, A. Yokoyama, M. Sakama, K. Sueki, Y. Oura, H. Nakahara, M. Schädel, W. Brüchle, and J. V. Kratz
Hexafluoro complex of rutherfordium in mixed HF/HNO_3 solutions
Radiochim. Acta 96 (2008) 125-134.

Y. Nagame and H. Haba
Production and chemistry of transactinide elements
in *Radiochemistry and Nuclear Chemistry*, Ed. Sandor Nagy, in *Encyclopedia of Life Support Systems (EOLSS),* Developed under the Auspices of the UNESCO, Eolss Publishers, Oxford, UK, 2007 [http://www.eolss.net].

Meetings

Y. Nagame
Aqueous chemistry of the transactinide element, rutherfordium (Rf)

234th American Chemical Society (ACS) National Meeting, Boston, USA (Aug. 21, 2007).

Y. Nagame
Status of superheavy element chemistry
The RIKEN workshop on superheavy elements, Wako, Japan (Aug. 27, 2007).

Y. Kasamatsu
Development of a rapid ion-exchange separation apparatus AIDA-II
The RIKEN workshop on superheavy elements, Wako, Japan (Aug. 27, 2007).

A. Toyoshima
Electrochemistry of superheavy elements
The RIKEN workshop on superheavy elements, Wako, Japan (Aug. 27, 2007).

Y. Nagame
Automated rapid radiochemical separations of the heaviest elements
The 12th International Conference on Modern Trends in Activation Analysis (MTAA12), Tokyo, Japan (Sept. 18, 2007).

Y. Ishii, S. Miyashita, T. Mori, H. Suganuma, H. Toume, Y. Kasamatsu, A. Toyoshima, M. Asai, I. Nishinaka, K. Tsukada, and Y. Nagame
Adsorption behavior of element 104 rutherfordium on cation-exchange resin in HF/HNO_3 solution
The 51st Symposium on Radiochemistry, Shizuoka, Japan (Sept. 24, 2007).

Y. Kasamatsu, H. Toume, A. Toyoshima, K. Tsukada, M. Asai, Y. Ishii, I. Nishinaka, T.K. Sato, N. Shinohara, Y. Nagame, H. Haba, H. Kikunaga, K. Akiyama, S. Goto, T. Ishikawa, H. Kudo, W. Sato, K. Ooe, T. Kuribayashi, A. Shinohara, N. Kinoshita, M. Arai, A. Yokoyama, M. Sakama, Z. Qin, and Ch.E. Düllmann
Chemical behavior of element-105, Db, in mixed HF/HNO_3 solutions
The 51st Symposium on Radiochemistry, Shizuoka (Sept. 24, 2007).

Y. Nagame, A. Toyoshima, Y. Ishii, K. Tsukada, M. Asai, H. Toume, Y. Kasamatsu, I. Nishinaka, T. K. Sato, H. Haba, H. Kikunaga, K. Akiyama, Y. Oura, H. Nakahara, W. Sato, A. Shinohara, S. Goto, H. Kudo, A. Yokoyama, M. Sakama, K. Sueki, M. Schädel, W. Brüchle, and J.V. Kratz
Fluoride complex formation of element 104, rutherfordium
3rd International Conference on the Chemistry and Physics of the Transactinide Elements, Davos, Switzerland (Sept. 26, 2007).

Y. Kasamatsu, A. Toyoshima, M. Asai, K. Tsukada, H. Haba, Y. Ishii, H. Toume, I. Nishinaka, K. Akiyama, H. Kikunaga, S. Goto, T. Ishikawa, H. Kudo, W. Sato, K. Ooe, T. Kuribayashi, A. Shinohara, N. Kinoshita, M. Arai, A. Yokoyama, M. Sakama, T.K. Sato, Z. Qin, Ch.E. Düllmann, and Y. Nagame

Anion-exchange behavior of element 105, Db, in HF/HNO_3 media
3rd International Conference on the Chemistry and Physics of the Transactinide Elements, Davos, Switzerland (Sept. 26, 2007).

A. Toyoshima, Y. Kasamatsu, K. Tsukada, A. Kitatsuji, H. Haba, Y. Ishii, H. Toume, M. Asai, K. Akiyama, K. Ooe, W. Sato, A. Shinohara, and Y. Nagame
Electrochemical oxidation of nobelium
3rd International Conference on the Chemistry and Physics of the Transactinide Elements, Davos, Switzerland (Sept. 26, 2007).

K.Tsukada, Y. Kasamatsu, M. Asai, A. Toyoshima, Y. Ishii, H. Toume, and Y. Nagame
New apparatus AIDA-II for aqueous chemistry of the heaviest elements
3rd International Conference on the Chemistry and Physics of the Transactinide Elements, Davos, Switzerland (Sept. 27, 2007).

A. Toyoshima
Chemical properties of Rf
The Specialist's Meeting on the Nuclear Science of Heavy Elements, KURRI, Kumatori, Japan (Dec. 11, 2007).

A. Toyoshima
Electrochemistry of superheavy elements
The Specialist's Meeting on the Nuclear Science of Heavy Elements, KURRI, Kumatori, Japan (Dec. 11, 2007).

M. Asai
Single atom chemistry
The Specialists' Meeting on the Nuclear Science of Heavy Elements, KURRI, Kumatori, Japan (Dec. 11, 2007).

Y. Kasamatsu, A. Toyoshima, M. Asai, K. Tsukada, H. Haba, Y. Ishii, H. Toume, I. Nishinaka, K. Akiyama, H. Kikunaga, S. Goto, T. Ishikawa, H. Kudo, W. Sato, K. Ooe, T. Kuribayashi, A. Shinohara, N. Kinoshita, M. Arai, A. Yokoyama, M. Sakama, T.K. Sato, and Y. Nagame
Adsorption of element-105 (Db) on anion-exchange resin in HF/HNO_3 solutions
The 88th Spring Meeting of the Chemical Society of Japan, Tokyo, Japan (Mar. 28, 2007).

8. 5 Nuclear Theory

Journal / Proceedings

T. Maruyama, S. Chiba, H.-J. Schulze, and T. Tatsumi
Hadron-quark mixed phase in hyperon stars
Phys. Rev., D76 (2007) 123015-1-12.

T. Maruyama, S. Chiba, H.-J. Schulze, and T. Tatsumi
Quark deconfinement transition in hyperonic matter
Phys. Lett., B659 (2008) 192-196.

T. Maruyama, S. Chiba, H.-J. Schulze, and T. Tatsumi
Hyperon-quark mixed phase in dense matter
Proceedings of Int. Symp. Exotic States of Nuclear Matter, Catania, Italy (Jun. 11-15, 2007), World Scientific (2008) 290-297.

Y. Utsuno, T. Otsuka, T. Mizusaki, and M. Honma
Structure of unstable nuclei in the sd-pf shell region by shell model with proper tensor force
Eur. Phys. J. Special Topics, 150 (2007) 187-188.

S. Chiba, H. Koura, T. Hayakawa, T. Maruyama, T. Kawano, and T. Kajino
Direct and semi-direct capture in low-energy (n,γ) reactions of neutron-rich tin isotopes and its implications for r-process nucleosynthesis
Phys. Rev., C77 (2008) 015809-1-7.

S. Oryu, S. Nishinonara, and S. Chiba
The rigorous few-body Coulomb treatments and its application to the proton-proton phase-shift calcualtion
Quantum Probability and White Noise Analysis Volume XXI, Quantum Bio-Informatics, From Quantum Information to Bio-Informatics, Eds. L. Accardi, W. Freudenberg, and M. Ohya, World Scientific (2008) 229-246.

S. Nishinohara, S. Chiba, and S. Oryu
The Coulomb scattering in momentum space for few-body systems
Nucl. Phys., A790 (2007) 277-281.

L. Bonneau, T. Kawano, T. Watanabe, and S. Chiba,
Nucleon direct-semidirect radiative capture with Skyrme-Hartree-Fock-BCS bound state
Phys. Rev., C75 (2007) 054618-1-10.

S. Kunieda, S. Chiba, K. Shibata, A. Ichihara, and E.Sh. Sukhovitskii

Coupled-channels optical model analyses of nucleon-induced reactions for medium and heavy nuclei in the energy region from 1 keV to 200 MeV
J. Nucl. Sci. Technol., 44 (2007) 838-852.

K. Morita, K. Morimoto, D. Kaji, T. Akiyama, S. Goto, H. Haba, E. Ideguchi, K. Katori, H. Koura, H. Kudo, T. Ohnishi, A. Ozawa, T. Suda, K. Sueki, F. Tokanai, T. Yamaguchi, A. Yoneda, and A. Yoshida
Experiment on synthesis of an isotope $^{277}112$ by $^{208}Pb+^{70}Zn$ reaction
Journal of the Physical Society of Japan, 76 (2007) 043201.

K. Morita, K. Morimoto, D. Kaji, T. Akiyama, S. Goto, H. Haba, E. Ideguchi, K. Katori, H. Koura, H. Kikunaga, H. Kudo, T. Ohnishi, A. Ozawa, N. Sato, T. Suda, K. Sueki, F. Tokanai, T. Yamaguchi, A. Yoneda, and A. Yoshida
Observation of second decay chain from $^{278}113$
Journal of the Physical Society of Japan, 76 (2007) 045001.

A. Gade, P. Adrich, D. Bazin, M.D. Bowen, B.A. Brown, C.M. Campbell, J.M. Cook, S. Ettenauer, T. Glasmacher, K.W. Kemper, S. McDaniel, A. Obertelli, T. Otsuka, A. Ratkiewicz, K. Siwek, J.R. Terry, J.A. Tostevin, Y. Utsuno, and D. Weisshaar
Spectroscopy of ^{36}Mg : Interplay of normal and intruder configurations at the neutron-rich boundary of the "island of inversion"
Phys. Rev. Lett., 99 (2007) 072502-1-4.

P. Doornenbal, P. Reiter, H. Grawe, T. Otsuka, A. Al-Khatib, A. Banu, T. Beck, F. Becker, P. Bednarczyk, G. Benzoni, A. Bracco, A. Burger, L. Caceres, F. Camera, S. Chmel, F.C.L. Crespi, H. Geissel, J. Gerl, M. Gorska, J. Grebosz, H. Hubel, M. Kavatsyuk, O. Kavatsyuk, M. Kmiecik, I. Kojouharov, N. Kurz, R. Lozeva, A. Maj, S. Mandal, W. Meczynski, B. Million, Zs. Podolyak, A. Richard, N. Saito, T. Saito, H. Schaffner, M. Seidlitz, T. Striepling, Y. Utsuno, J. Walker, N. Warr, H. Weick, O. Wieland, M. Winkler, and H.J. Wollersheim
The T = 2 mirrors ^{36}Ca and ^{36}S : A test for isospin symmetry of shell gaps at the driplines
Phys. Lett., B647 (2007) 237-242.

V. Tripathi, S.L. Tabor, P.F. Mantica, Y. Utsuno, P. Bender, J. Cook, C.R. Hoffman, S. Lee, T. Otsuka, J. Pereira, M. Perry, K. Pepper, J.S. Pinter, J. Stoker, A. Volya, and D. Weisshaar
Competition between normal and intruder states inside the "island of inversion"
Phys. Rev., C76 (2007) 021301(R)-1-5.

J.R. Terry, B.A. Brown, C.M. Campbell, J.M. Cook, A.D. Davies, D.-C. Dinca, A. Gade, T. Glasmacher, P.G. Hansen, B.M. Sherrill, H. Zwahlen, D. Bazin, K. Yoneda, J.A. Tostevin, T. Otsuka, Y. Utsuno, and B. Pritychenko
Single-neutron knockout from intermediate energy beams of $^{30\ 32}Mg$: Mapping the transition into the "island of inversion"

Phys. Rev., C77 (2008) 014316-1-12.

P. Himpe, G. Neyens, D.L. Balabanski, G. Belier, J.M. Daugas, F.de Oliveira Santos, M.De Rydt, K.T. Flanagan, I. Matea, P. Morel, Yu.E. Penionzhkevich, L. Perrot, N.A. Smirnova, C. Stodel, J.C. Thomas, N. Vermeulen, D.T. Yordanov, Y. Utsuno, and T. Otsuka,
g factor of the exotic N = 21 isotope ^{34}Al : probing the N = 20 and N = 28 shell gaps at the border of the "island of inversion"
Phys. Lett., B658 (2008) 203-208.

Meetings

Y. Utsuno, T. Otsuka, T. Mizusaki, and M. Honma
Shell evolution and exotic structure in the sd-pf shell by the tensor force
ECT Workshop "Advanced Many-Body Methods for Nuclear Physics, Trento, Italy (Jul. 5, 2007).

Y. Utsuno, T. Otsuka, T. Mizusaki, M. Honma, and B.A. Brown,
Role of shell evolution in the structure of exotic nuclei in the sd-pf shell
Workshop at the INT Fall-07 Program on Correlations in Nuclei : From Di-nucleons to Clusters, Seattle, USA (Nov. 26, 2007).

Y. Utsuno, T. Otsuka, M. Honma, T. Mizusaki, N. Shimizu, and B.A. Brown
Large-scale shell model calculation for exotic nuclei—collaboration between Japan and US
The 2nd LACM-EFES-JUSTIPEN Workshop, Oak Ridge, USA (Jan. 23, 2008).

Y. Utsuno, T. Otsuka, M. Honma, T. Mizusaki, and B.A. Brown
Exploring the single-particle structure in the exotic sd-pf shell region with a new effective interaction
Workshop on Future Prospects for Spectroscopy and Direct Reactions 2008, East Lansing, USA (Feb. 27, 2008).

S. Hashimoto, M. Kohno, K. Ogata, and M. Kawai
Analysis of (K^-, K^+) inclusive spectrum with semiclassical distorted wave model
The International Workshop on Nuclear Physics at J-PARC, Tokai, Japan (Jun. 2, 2007).

S. Hashimoto, M. Kohno, K. Ogata, and M. Kawai
Analysis of (K^-, K^+) reaction on heavy targets with semiclassical distorted wave model
The 62nd annual meeting of the physical society of Japan, Sapporo, Japan (Sep. 21, 2007)

T. Maruyama, S. Chiba, and T. Tatsumi
Bulk properties of kaonic nuclei in the mean-field calculation
International Nuclear Physics Conference (INPC2007), Tokyo (Jun. 5, 2007).

T. Maruyama, S. Chiba, H.-J. Schulze, and T. Tatsumi
Hyperon-quark mixed phase in compact stars
International Nuclear Physics Conference (INPC2007), Tokyo (Jun. 6, 2007).

T. Maruyama, S. Chiba, H.-J. Schulze, and T. Tatsumi
Hyperon-quark mixed phase in dense matter
Int. Symp. on Exotic States in Nuclear Matter, Catania, Italy (Jun. 15, 2007).

T. Maruyama, S. Chiba, and T. Tatsumi
Non-uniform structure of matter and equation of state
Nuclear Dynamics in Heavy-ion Reactions and Neutron Stars, Beijinig, China (Jul. 11, 2007).

T. Muto, T. Maruyama, and T. Tatsumi
Structure of multi-antikaonic nuclei in the relativistic mean-field model
Chiral Symmetry in Hadron and Nuclear Physics, Osaka, Japan (Nov. 14, 2007).

T. Maruyama, S. Chiba, H.-J. Schulze, and T. Tatsumi
Hyperon-quark mixed phase in compact stars
Quark Matter 2008, Jaipur, India (Feb. 5, 2008).

M.S. Smith, E.J. Lingerfelt, C.D. Nesaraja, W.R. Hix, L.F. Roberts, H. Koura, G.M. Fuller, and D. Tytler
Nuclear data for astrophysics : Resources, challenges, strategies, and software solutions
The 2007 International Conference on Nuclear Data for Science and Technology (ND2007), Nice, France (Apr. 26, 2007).

H. Koura, T. Tachibana, and S. Chiba
Systematical study of nuclear decay modes and a limit of existence of nuclei
International Nuclear Physics Conference (INPC2007), Tokyo, Japan, (Jun. 6, 2007).

H. Koura
Decay modes of superheavy nuclei - shell structure and border of existence -
Cosponsored workshop by RIBF mini workshop and Grand-in-Aid “Search for New Element and Chemistry of Superheavy Elements” of MEXT of Japan, ”Problem to synthesis for superheavy elements,” Wako, Japan (Jul. 24, 2007).

K. Oyamatsu, K. Iida, and H. Koura
Masses of unstable nuclei and the equation of state of asymmetric nuclear matter II
The Physical Society of Japan 62nd Annual Meeting, Sapporo, Japan (Sep. 22, 2007).

H. Koura, T. Tachibana, and S. Chiba
Nuclear decay modes of superheavy nuclei and limit of existence of nuclei

International Conference on the Chemistry and Physics of the Transactinide Elements (TAN07), Davos, Switzerland (Sep. 24, 2007).

H. Koura
Nuclear mass formula and its applications - Decay modes of superheavy nuclei and limit of existence of nuclei -
Crossing Workshop of Nucleus-Hadron Physics, Tsukuba, Japan (Nov. 20, 2007).

H. Koura
Decay modes of superheavy nuclei and region of existence of nuclei
4th Meeting on Nuclear Physics of Slow and Stop Radio Isotope (SSRI4), Sendai, Japan (Dec. 20, 2007).

H. Koura
R-process element abundance considering nuclear fission in the region of superheavy, neutron-rich nuclei
3rd Japanese-German EFES(JSPS)-DFG/GSI workshop on Nuclear Structure and Astrophysics, Chiemsee, Germany (Sep. 30, 2007).

H. Koura, T. Tachibana, and S. Chiba
Systematical study of nuclear fission in the region of superheavy and neutron-rich nuclei
Fourth International Conf. on Fission and Properties of Neutron-Rich Nuclei, Florida, U.S.A. (Nov. 14, 2007).

S. Tatsuda, T. Asano, K. Yamamoto, M. Ohta, T. Wada, S. Chiba, H. Koura, T. Maruyama, T. Tachibana, T. Kajino, K. Sumiyoshi, and K. Ohtsuki
Fission modes of neutron-rich nuclei in the r-process nucleosynthesis
The 10th International Symposium on Origin of Matter and Evolution of Galaxies (OMEG07), Sapporo, Japan (Dec. 4, 2007).

M.S. Smith, F. Kondev, H. Koura, E. Lingerfelt, K. Buckner, and C. Nesaraja
Nuclear masses : theoretical models, experimental evaluations, & web disseminations
The 2nd LACM-EFES-JUSTIPEN Workshop, Oak Ridge, U.S.A. (Jan. 25, 2008).

K. Oyamatsu, K. Iida, and H. Koura
Masses of unstable nuclei and the equation of state of Aaymmetric nuclear matter III
The Physical Society of Japan 63rd Annual Meeting, Higashi-Osaka, Japan (Mar. 24, 2008).

T. Maruyama, T. Maruyama, S. Chiba, and T. Tatsumi
RMF treatment of nuclear matter at finite temperature
The Physical Society of Japan 63rd Annual Meeting, Higashi-Osaka, Japan (Mar. 24, 2008).

T. Muto, T. Maruyama, and T. Tatsumi

Multi-kaon bound state of nuclei
The Physical Society of Japan 63rd Annual Meeting, Higashi-Osaka, Japan (Mar. 24, 2008).

H. Matsuyama, T. Maruyama, and K. Yabana
Simulation of nuclear collisions by quark molecular dynamics
The Physical Society of Japan 63rd Annual Meeting, Higashi-Osaka, Japan (Mar. 26, 2008).

S. Chiba, S. Tatsuda, T. Wada, K. Sumiyoshi, K. Otsuki, T. Kajino, H. Koura, T. Maruyama, T. Tachibana, and M. Ohta
The r-process element abundance taking account of a realistic fission fragment mass distribution
International Nuclear Physics Conference (INPC2007), Tokyo, Japan (Jun. 5, 2007).

S. Chiba, S. Nishinohara, and S. Oryu
Exact Coulomb treatment for nuclear reactions in momentum space
International Nuclear Physics Conference (INPC2007), Tokyo, Japan (Jun. 6, 2007).

T. Yoshida, T. Suzuki, S. Chiba, T. Kajino, A. Takamura, K. Kimura, H. Yokomakura, D.H. Hartmann, and T. Otsuka
Neutrino favor mixing in supernova nucleosynthesis
International Nuclear Physics Conference (INPC2007), Tokyo, Japan (Jun. 5, 2007).

S. Tatsuda, T. Wada, M. Ohta, K. Sumiyoshi, K. Otsuki, T. Kajino, H. Koura, S. Chiba, and T. Tachibana
Systematic study for the shell effect in the fission fragment mass distribution ruptured form neutron rich nuclei
International Nuclear Physics Conference (INPC2007), Tokyo, Japan (Jun. 5, 2007).

T. Suzuki, S. Chiba, T. Kajino, T. Yoshida, and T. Otsuka
Neutrino-nucleus reactions based on the recent advances in shell-model calculations
International Nuclear Physics Conference (INPC2007), Tokyo, Japan (Jun. 6, 2007).

S. Chiba, H. Koura, T. Maruyama, S. Kunieda, and E. Soukhovitksii
Systematics and uncertainties of Hamiltonian parameters of soft-rotator model for actinides and its implications for nuclear-data calculations
Int. Conf. on Nuclear Data for Science and Technology (ND2007), Nice, France (Apr. 25, 2007).

M. Ohta, S. Tatsuda, K. Yamamoto, T. Wada, K. Sumiyoshi, K. Otsuki, T. Kajino, H. Koura, and S. Chiba
Systematic study for the mass distribution of fission fragments in the neutron rich region
Int. Conf. on Nuclear Data for Science and Technology (ND2007), Nice, France (Apr. 25, 2007).

S. Kunieda, S. Chiba, K. Shibata, A. Ichihara, and E. Soukhovitsii
Systematical nucleon-induced optical model analysis for medium and heavy nuclei with coupled-channel

framework
Int. Conf. on Nuclear Data for Science and Technology (ND2007), Nice, France (Apr. 24, 2007).

J.-Y. Lee, I. Hahn, E. Soukhovitskii, and S. Chiba
Analysis of nuclear level structure and nucleon interaction data
Int. Conf. on Nuclear Data for Science and Technology (ND2007), Nice, France (Apr. 24, 2007). .

R. Capote, E. Soukhovitskii, J.M. Quesada, and S. Chiba
Lane consistency of the dispersive coupled channel optical model potential
Int. Conf. on Nuclear Data for Science and Technology (ND2007), Nice, France (Apr. 23, 2007).

S. Chiba, H. Koura, T. Maruyama, M. Ohta, S. Tatsuda, T. Wada, T. Tachibana, T. Kajino, K. Sumiyoshi, and K. Ohtsuki
Impact of fission fragment mass distribution on the r-process abundance pattern
Annual meeting of Physical Society of Japan, Sapporo, Japan (Sep. 24, 2007).

T. Maruyama, T. Tatsumi, H.-J. Schulze, and S. Chiba,
Hyperon-quark mixed phase in compact stars
Annual meeting of Physical Society of Japan, Sapporo, Japan (Sep. 24, 2007).

T. Muto, T. Maruyama and T. Tatsumi.
Multi-kaon bound state of nuclei
Annual meeting of Physical Society of Japan, Sapporo, Japan (Sep. 21, 2007).

M. Ohta, S. Tatsuda, T. Wada, S. Chiba, H. Koura, T. Maruyama, T. Kajino, and K. Ohtsuki
Systematic calculation of fission fragment mass distribution by a semi-empirical model
Fall meeting of Atomic Energy Society of Japan, Kitakyushu, Japan (Sep. 27-29, 2007).

S. Chiba, H. Koura, T. Maruyama, M. Ohta, S. Tatsuda, T. Wada, T. Tachibana, K. Sumiyoshi, K. Ohtsuki, and T. Kajino
The r-process element abundance with a realistic fission fragment mass distribution
The 10th Int. Symp. on Origin of Matter and Evolution of Galaxies (OMEG07), Sapporo, Japan
(Dec. 5, 2007)

8. 6 Atomic Physics and Solid State Physics

Meetings

S. Kawatsura, K. Takahiro, M. Sataka, M. Imai, H. Sugai, H. Shibata, and K. Komaki

High Rydberg states produced in high energy collisions of N^{q+} (q=1-3) + He
The 25th International Conference on Photonic, Electronic and Atomic Collisions (XXV ICPEAC), Freiburg, Germany (Jul. 25, 2007).

S. Kawatsura, K. Takahiro, M. Sataka, M. Imai, K. Ozaki, H. Sugai, H. Shibata, and K. Komaki

Ejected electron spectra from high Rydberg states of Ne^{q+} ions passing through C foils
International Symposium on Charged Particle and Photon Interactions with Matter (ASR-2007), Tokai, Japan (Nov. 7, 2007).

8. 7 Radiation Effects in Materials

Journal / Proceedings

T. Sonoda, M. Kinoshita, N. Ishikawa, M. Sataka, Y. Chimi, N. Okubo, and A. Iwase
Clarification of the properties and accumulation effects of ion tracks in CeO_2
Nucl. Instrum. Methods Phys. Res., B 266 (2008) 2882-2886.

K. Yasuda, T. Yamamoto, and S. Matsumura
The atomic structure of disordered ion tracks in magnesium aluminate spinel
Journal of Materials 59 (2007) 27-30.

K. Yasuda, T. Yamamoto, S. Seki, K. Shiiyama, and S. Matsumura
Production and stability of radiation-induced defects in $MgAl_2O_4$ under electronic excitation
Nucl. Instrum. Methods Phys. Res., B 266 (2008) 2834-2841.

N. Matsunami, M. Sataka, S. Okayasu, and M. Tazawa
Electronic sputtering of nitrides by high-energy ions
Nucl. Instrum. Methods Phys. Res., B256 (2007) 333-336.

F. Hori, M. Fukuzumi, A. Kawasuso, Y. Zushi, Y. Chimi, N. Ishiawa, and A. Iwase
Characterization of swift heavy ion induced defects in FeRh alloy by using positron beam technique
Phys. stat. sol. (c) 4 (2007) 3530-3533.

M. Sasase, K. Shimura, K. Yamaguchi, H. Yamamoto, S. Shamoto, and K. Hojou
Sputter etching effect of the substrate on the microstructure of β-$FeSi_2$ thin film prepared by ion beam sputter deposition method
Nucl. Instrum. Methods Phys. Res., B257 (2007) 186-189.

Meetings

T. Sonoda, M. Kinoshita, N. Ishikawa, M. Sataka, Y. Chimi, S. Okubo, A. Iwase, and K. Yasunaga
Clarification of the properties and accumulation effects of ion tracks in CeO_2
14th International Conference on Radiation Effects in Insulators (REI-2007), Caen, France (Aug. 30, 2007).

T. Sonoda, N. Ishikawa, M. Sataka, S. Okubo, K. Yasunaga, K. Yasuda, K. Shiiyama, S. Matsumura, A. Iwase, and M. Kinoshita,
New cross-over project study (6)　High density electronic excitation effects in Xe-ions-implanted fluorite ceramics as simulations of high burnup nuclear fuels

2007 Fall Meeting of the Atomic Energy Society of Japan, Kitakyushu, Japan (Sep. 28, 2007).

T. Sonoda, K. Yasunaga, N. Ishikawa, M. Sataka, Y. Chimi, S. Okubo, A. Iwase, and M. Kinoshita,
Clarification of ion tracks in CeO_2 under irradiation with high energy ions of typical fission products
NXO International Workshop, Tokyo, Japan (Nov. 14, 2007).

N. Ishikawa, Y. Chimi, O. Michikami, Y. Ohta, K. Ohhara, M. Lang, and R. Neumann
Study of structural change in CeO_2 irradiated with high-energy ions by means of X-ray diffraction measurement
14th International Conference on Radiation Effects in Insulators (REI-2007), Caen, France (Aug. 28, 2007).

N. Ishikawa, K. Ohhara, M. Sataka, S. Sakai, O. Michikami, and Y. Ohta
X-ray and raman studies of CeO_2 irradiated with high-energy heavy ions
NXO International Workshop, Tokyo, Japan (Nov.14, 2007).

K. Ohhara, N. Ishikawa, S. Sakai, Y. Matsumoto, O. Michikami, and Y. Ohta
X-ray and raman studies of CeO_2 irradiated with 200MeV Au
8th Workshop on Ion-beam Analysis of Surface and Interface, Sendai, Japan (Dec. 7, 2007).

K. Ohhara, N. Ishikawa, S. Sakai, Y. Matsumoto, O. Michikami, and Y. Ohta
Irradiation damage in CeO_2 irradiated with high-energy ions
Spring Meeting of the Physical Society of Japan, Osaka, Japan (Mar. 23, 2008).

N. Matsunami, M. Sataka, S. Okayasu, and M. Tazawa
Electronic sputtering of nitrides
2007 Fall Meeting, Japan Physical Society, Sapporo, Japan (Sep. 22, 2007).

A. Iwase
Ion irradiation induced ferromagnetism in FeRh alloys
The Doyama Symposium on Advanced Materials, Tokyo, Japan (Sep. 6, 2007)

M. Sasase, K. Shimura, K. Yamaguchi, H. Yamamoto, S. Shamoto, and K. Hojou
Sputter etching effect of the substrate on the microstructure of β-$FeSi_2$ thin film prepared by ion beam sputter deposition method
17th International Vacuum Congress (IVC-17), Stockholm, Sweden (Jul. 3, 2007).

This is a blank page.

CHAPTER 9

Personnel and Committee

This is a blank page.

9.1 Personnel

Department of Research Reactor and Tandem Accelerator

Kiyonobu	Yamashita	Director
Suehiro	Takeuchi	Deputy Director
Yuichi	Terakado	Manager of Administration Section

Department of Research Reactor and Tandem Accelerator

Tandem Accelerator Section *(* General Manager)*

Scientific Staff

Masao	Sataka*	
Akihiko	Osa	
Makoto	Matsuda	

Technical Staff

Yoshihiro	Tsukihashi	
Susumu	Hanashima	
Shin-ichi	Abe	
Nobuhiro	Ishizaki	
Takamitsu	Nakanoya	
Hiroshi	Kabumoto	
Masahiko	Nakamura	
Ken-ichi	Kutsukake	
Yoshinori	Otokawa	
Takuhiro	Asozu	

Entrusted Operators

Takahiro	Yoshida	
Takahiro	Usami	(Apr. – Jul.)
Takayuki	Ishiguro	
Kazushi	Yamaguchi	
Hikaru	Nisugi	
Nobuo	Seki	
Teruo	Onodera	

Entrusted Assistant

Kenjiro	Obara	

Department of Radiation Protection

Facility Radiation Control Section I

Kenji	Yamane	
Takashi	Nakazawa	
Katsuji	Yasu	

Hayato	Hiraga	
Daisuke	Higashi	

Advanced Science Research Center

Yoshihiko	Hatano	Director
Hiroshi	Ikezoe	Deputy Director

Advanced Science Research Center

Research Group for Physics of Heavy Nuclei

(Group Leader)*

Hiroari	Miyatake*	
Tetsuro	Ishii	
Shin-ichi	Ichikawa	
Satoshi	Chiba	
Toshiki	Maruyama	
Shin-ichi	Mitsuoka	
Katsuhisa	Nishio	
Hiroyuki	Koura	
Yutaka	Utsuno	
Tetsuya	Sato	
Takashi	Hashimoto	(Post Doc.)
Hiroyuki	Makii	(Post Doc.)
Daisuke	Nagae	(Post Doc.)
Shintaro	Hashimoto	(Student)
Hiroki	Sato	(Student)

Advanced Science Research Center

Research Group for Nuclear chemistry of Superheavy Elements

(Group Leader)*

Yuichiro	Nagame*	
Kazuaki	Tsukada	
Ichiro	Nishinaka	
Masato	Asai	
Atsushi	Toyoshim	(Post Doc.)
Yoshitaka	Kasamatsu	(Post Doc.)
Yasuo	Ishii	(Student)
Hayato	Toume	(Student)

Advanced Science Research Center

Research Group for Material Design under Extreme Conditions

Satoru	Okayasu	
Hiroyuki	Sugai	
Norito	Ishikawa	
Teruo	Kato	

Nuclear Science and Engineering Directorate

Innovative Nuclear Science Research Group

(Group Leader)*

Masumi	Oshima*	
Hideo	Harada	Sub Leader
Hideki	Iimura	
Mitsuo	Koizumi	
Kazuyoshi	Furutaka	
Yuichi	Hatsukawa	
Fumito	Kitatani	
Shoji	Nakamura	
Yosuke	Toh	
Atsushi	Kimura	
Tadahiro	Kin	(Post Doc.)

Nuclear Science and Engineering Directorate

Nuclear Data Center

(Group Leader)*

Jun-ichi	Katakura*	
Keiichi	Shibata	
Tokio	Fukahori	
Akira	Ichikawa	
Osamu	Iwamoto	
Nobuyuki	Iwamoto	
Satoshi	Kunieda	
Naohiko	Otsuka	(Apr. – Dec.)

Nuclear Science and Engineering Directorate

Research Group for Irradiation Field Materials

*(* Group Leader)*

Shiro	Jitsukawa*	
Nariaki	Okubo	
Daijyu	Yamaki	

Quantum Beam Science Directorate

Laser Accelerator Group

Takehito Hayakawa

Toshiyuki Shizuma

High Energy Accelerator Research Organization (KEK)

Institute of Particle and Nuclear Studies – Radioactive Nuclear Beams Project Group

(Group Leader)*

Physics Division IV

Hiroari Miyatake*

Sun-Chan Jeong

Masahiko Tanaka

Hironobu Ishiyama

Yutaka Watanabe

Nobuaki Imai

Yoshikazu Hirayama

Yoshihide Fuchi

Michihiro Oyaizu

Ichiro Katayama

Hirokane Kawakami

Physics Division I

Shoji Suzuki

High Energy Accelerator Research Organization (KEK)

Accelerator Laboratory

Accelerator Division I

Shigeaki Arai

Masashi Okada

9. 2 Research Planning and Assessment Committee

Chairperson	Shigeru	Kubono	(Professor, The University of Tokyo)
Vice Chairperson	Ken-ichiro	Komaki	(Professor, The University of Tokyo)
Member	Kouichi	Hagino	(Associate Professor, Tohoku University)
	Tadashi	Kambara	(Senior Scientist, RIKEN*)
	Kenji	Kimura	(Professor, Kyoto University)
	Noriaki	Matsunami	(Associate Professor, Nagoya University)
	Motoharu	Mizumoto	(Special-appointment Professor, Tokyo Institute of Technology)
	Tetsuo	Noro	(Professor, Kyushu University)
	Tsutomu	Ohtsuki	(Associate Professor, Tohoku University)
	Tadashi	Shimoda	(Professor, Osaka University)
	Yuichi	Hatsukawa	(Quantum Beam Science Directorate, JAEA**)
	Hiroshi	Ikezoe	(Deputy Director, Advanced Science Research Center, JAEA)
	Shiro	Jitsukawa	(Nuclear Science and Engineering Directorate, JAEA)
	Kazumasa	Narumi	(Advanced Science Research Center, JAEA)
	Suehiro	Takeuchi	(Deputy Director, Dep. Research Reactor and Accelerator, JAEA)
Organizer	Akihiko	Osa	(Tandem Accelerator Section, JAEA)
	Masao	Sataka	(Tandem Accelerator Section, JAEA)

* The Institute for Physical and Chemical Research

** Japan Atomic Energy Agency

This is a blank page.

CHAPTER 10

Cooperative Researches and Common Use Program in JAEA

This is a blank page.

10. 1 Cooperative Researches List

Title	Contact Person & Organization
1. Process of structural change in light-water reactor fuel with irradiation damage by fission products	Takeshi SONODA Central Research Institute of Electric Power Industry
2. Process of irradiation damage in nuclear reactor materials with Fe base alloys	Akihiro IWASE Osaka Prefecture University
3. Dynamic behavior of heavy ions in material	Kiyoshi KAWATSURA Kyoto Institute of Technology
4. Study of nuclear deformation by Coulomb excitation and lifetime measurement	Masahiko SUGAWARA Chiba Institute of Technology
5. Study of super-deformed state and high-spin shell structure in A=30 region	Eiji IDEGUCHI University of Tokyo
6. Coulomb excitation on neutron-rich Xe nuclei of fission products	Sun-Chan JEONG High Energy Accelerator Research Organization
7. Nuclear spectroscopy using lasers for refractory element isotope in Re region	Takayoshi HORIGUCHI Hiroshima International University
8. Aqueous chemistry of super-heavy elements Rf and Db	Hisaaki KUDO Niigata University
9. Alpha-gamma spectroscopy for super-heavy nuclei using californium target	Keisuke SUEKI University of Tsukuba
10. Development of electrochemical apparatus for single atom chemistry	Atsushi SHINOHARA Osaka University
11. Study of nuclear fission from excited states of heavy-actinide nuclei	Akihiko YOKOYAMA Kanazawa University
12. Study of nuclear structure in the region of A=180 nuclei by the transfer reaction	Eiji IDEGUCHI University of Tokyo
13. Experimental study of fusion barrier distribution for super-heavy element synthesis	Sun-Chan JEONG High Energy Accelerator Research Organization
14. Study of element synthesis in the universe via short-lived nuclei	Hiroari MIYATAKE High Energy Accelerator Research Organization

10. 1 Cooperative Researches List (contd.)

Title	Contact Person & Organization
15. Search of unknown nuclei in neutron-rich lanthanide	Michihiro SHIBATA Nagoya University
16. In-beam gamma-ray spectroscopy of super-heavy nuclei using californium target	Toshiyuki KOUNO Tokyo Institute of Technology
17. Development of spectrometer for in-beam gamma-ray spectroscopy of super-heavy nuclei	Toshiyuki KOUNO Tokyo Institute of Technology
18. Production of heavy elements by heavy-ion fusion reaction using actinide targets and measurement of the decay properties	Tsutomu OHTSUKI Tohoku University
19. Ion source development for the JAEA on line isotope separator	Sun-Chan JEONG High Energy Accelerator Research Organization
20. β-decay spectroscopy of nuclear spin polarized nuclei in the region of ^{132}Sn	Yoshikazu HIRAYAMA High Energy Accelerator Research Organization
21. Generation of polarized Cs and Ba isotope by using tilted-foil method and measurement of nuclear magnetic moment	Kensaku MATSUTA Osaka University
22. Development for search of time-reversal symmetry violation using polarized nuclei	Jiro MURATA Rikkyo University
23. Measurement of the ^{8}Li (α, n) ^{11}B reaction cross section for astrophysical interest	Tomokazu FUKUDA OsakaElectro-Communication University
24. Measurement of hyperfine field of ^{111}Cd in the high-oriented pyrolytic graphite	Wataru SATO Osaka University
25. Coulomb excitation of unstable nuclei	Nobuaki IMAI High Energy Accelerator Research Organization
26. Diffusion study in super-ionic conducting materials using the short-lived nuclei	Sun-Chan JEONG High Energy Accelerator Research Organization

10. 2 Common Use Program in JAEA

Title	Contact Person & Organization
1. Radiation-induced magnetic transition in FeRh alloys	Akihiro IWASE Osaka Prefecture University
2. Study on electronic structure and processes for highly charged heavy-ions by zero-degree electron spectroscopy	Kiyoshi KAWATSURA Kyoto Institute of Technology
3. Atomic structure and ion distribution in ion tracks in spinel irradiated with swift heavy ions	Kazuhiro YASUDA Kyushu University
4. Study of decay properties of fission products using JAEA-ISOL	Michihiro SHIBATA Nagoya University
5. Effect of neutron transfer in heavy-ion fusion reaction	Yutaka WATANABE High Energy Accelerator Research Organization
6. Production of radioactive-isotope tracers for chemistry of heavy and super heavy elements	Shinichi GOTO Niigata University
7. Systematic study of signature inversion and shape coexistence in high-spin states of A=170-190 nuclei	X.H. Zhou Institute of Modern Physics Chinese Academy of Science
8. Electronic excitation effects on non-metals by high energy heavy ions	Noriaki MATSUNAMI Nagoya University
9. Measurement of hyperfine field in oxide magnetic material using gamma-ray perturbed angular correlation	Wataru SATO Osaka University
10. Synthesis of water-soluble radioisotope-metallofullerenes	Keisuke SUEKI University of Tsukuba

This is a blank page.

国際単位系（SI）

表１．SI 基本単位

基本量	SI 基本単位	
	名称	記号
長さ	メートル	m
質量	キログラム	kg
時間	秒	s
電流	アンペア	A
熱力学温度	ケルビン	K
物質量	モル	mol
光度	カンデラ	cd

表２．基本単位を用いて表されるSI組立単位の例

組立量	SI 基本単位	
	名称	記号
面積	平方メートル	m^2
体積	立法メートル	m^3
速さ，速度	メートル毎秒	m/s
加速度	メートル毎秒毎秒	m/s^2
波数	毎メートル	m-1
密度（質量密度）	キログラム毎立法メートル	kg/m^3
質量体積（比体積）	立法メートル毎キログラム	m^3/kg
電流密度	アンペア毎平方メートル	A/m^2
磁界の強さ	アンペア毎メートル	A/m
（物質量の）濃度	モル毎立方メートル	mol/m^3
輝度	カンデラ毎平方メートル	cd/m^2
屈折率	（数の） 1	1

表５．SI 接頭語

乗数	接頭語	記号	乗数	接頭語	記号
10^{24}	ヨタ	Y	10^{-1}	デシ	d
10^{21}	ゼタ	Z	10^{-2}	センチ	c
10^{18}	エクサ	E	10^{-3}	ミリ	m
10^{15}	ペタ	P	10^{-6}	マイクロ	μ
10^{12}	テラ	T	10^{-9}	ナノ	n
10^{9}	ギガ	G	10^{-12}	ピコ	p
10^{6}	メガ	M	10^{-15}	フェムト	f
10^{3}	キロ	k	10^{-18}	アト	a
10^{2}	ヘクト	h	10^{-21}	ゼプト	z
10^{1}	デカ	da	10^{-24}	ヨクト	y

表３．固有の名称とその独自の記号で表されるSI組立単位

組立量	SI 組立単位			
	名称	記号	他のSI単位による表し方	SI基本単位による表し方
平面角	ラジアン(a)	rad		$m \cdot m^{-1}=1$(b)
立体角	ステラジアン(a)	sr(c)		$m^2 \cdot m^{-2}=1$(b)
周波数	ヘルツ	Hz		s^{-1}
力	ニュートン	N		$m \cdot kg \cdot s^{-2}$
圧力，応力	パスカル	Pa	N/m^2	$m^{-1} \cdot kg \cdot s^{-2}$
エネルギー，仕事，熱量	ジュール	J	N・m	$m^2 \cdot kg \cdot s^{-2}$
工率，放射束	ワット	W	J/s	$m^2 \cdot kg \cdot s^{-3}$
電荷，電気量	クーロン	C		s・A
電位差（電圧），起電力	ボルト	V	W/A	$m^2 \cdot kg \cdot s^{-3} \cdot A^{-1}$
静電容量	ファラド	F	C/V	$m^{-2} \cdot kg^{-1} \cdot s^4 \cdot A^2$
電気抵抗	オーム	Ω	V/A	$m^2 \cdot kg \cdot s^{-3} \cdot A^{-2}$
コンダクタンス	ジーメンス	S	A/V	$m^{-2} \cdot kg^{-1} \cdot s^3 \cdot A^2$
磁束	ウエーバ	Wb	V・s	$m^2 \cdot kg \cdot s^{-2} \cdot A^{-1}$
磁束密度	テスラ	T	Wb/m^2	$kg \cdot s^{-2} \cdot A^{-1}$
インダクタンス	ヘンリー	H	Wb/A	$m^2 \cdot kg \cdot s^{-2} \cdot A^{-2}$
セルシウス温度	セルシウス度(d)	℃		K
光束	ルーメン	lm	cd・sr(c)	$m^2 \cdot m^{-2} \cdot cd=cd$
照度	ルクス	lx	lm/m^2	$m^2 \cdot m^{-4} \cdot cd=m^{-2} \cdot cd$
（放射性核種の）放射能	ベクレル	Bq		s^{-1}
吸収線量，質量エネルギー分与，カーマ	グレイ	Gy	J/kg	$m^2 \cdot s^{-2}$
線量当量，周辺線量当量，方向性線量当量，個人線量当量，組織線量当	シーベルト	Sv	J/kg	$m^2 \cdot s^{-2}$

(a)ラジアン及びステラジアンの使用は、同じ次元であっても異なった性質をもった量を区別するときの組立単位の表し方として利点がある。組立単位を形作るときのいくつかの用例は表４に示されている。
(b)実際には、使用する時には記号rad及びsrが用いられるが、習慣として組立単位としての記号“１”は明示されない。
(c)測光学では、ステラジアンの名称と記号srを単位の表し方の中にそのまま維持している。
(d)この単位は、例としてミリセルシウス度m℃のようにSI接頭語を伴って用いても良い。

表４．単位の中に固有の名称とその独自の記号を含むSI組立単位の例

組立量	SI 組立単位		
	名称	記号	SI 基本単位による表し方
粘度	パスカル秒	Pa・s	$m^{-1} \cdot kg \cdot s^{-1}$
力のモーメント	ニュートンメートル	N・m	$m^2 \cdot kg \cdot s^{-2}$
表面張力	ニュートン毎メートル	N/m	$kg \cdot s^{-2}$
角速度	ラジアン毎秒	rad/s	$m \cdot m^{-1} \cdot s^{-1}=s^{-1}$
角加速度	ラジアン毎平方秒	rad/s^2	$m \cdot m^{-1} \cdot s^{-2}=s^{-2}$
熱流密度，放射照度	ワット毎平方メートル	W/m^2	$kg \cdot s^{-3}$
熱容量，エントロピー	ジュール毎ケルビン	J/K	$m^2 \cdot kg \cdot s^{-2} \cdot K^{-1}$
質量熱容量（比熱容量），質量エントロピー	ジュール毎キログラム毎ケルビン	J/(kg・K)	$m^2 \cdot s^{-2} \cdot K^{-1}$
質量エネルギー（比エネルギー）	ジュール毎キログラム	J/kg	$m^2 \cdot s^{-2} \cdot K^{-1}$
熱伝導率	ワット毎メートル毎ケルビン	W/(m・K)	$m \cdot kg \cdot s^{-3} \cdot K^{-1}$
体積エネルギー	ジュール毎立方メートル	J/m^3	$m^{-1} \cdot kg \cdot s^{-2}$
電界の強さ	ボルト毎メートル	V/m	$m \cdot kg \cdot s^{-3} \cdot A^{-1}$
体積電荷	クーロン毎立方メートル	C/m^3	$m^{-3} \cdot s \cdot A$
電気変位	クーロン毎平方メートル	C/m^2	$m^{-2} \cdot s \cdot A$
誘電率	ファラド毎メートル	F/m	$m^{-3} \cdot kg^{-1} \cdot s^4 \cdot A^2$
透磁率	ヘンリー毎メートル	H/m	$m \cdot kg \cdot s^{-2} \cdot A^{-2}$
モルエネルギー	ジュール毎モル	J/mol	$m^2 \cdot kg \cdot s^{-2} \cdot mol^{-1}$
モルエントロピー，モル熱容量	ジュール毎モル毎ケルビン	J/(mol・K)	$m^2 \cdot kg \cdot s^{-2} \cdot K^{-1} \cdot mol^{-1}$
照射線量（X線及びγ線）	クーロン毎キログラム	C/kg	$kg^{-1} \cdot s \cdot A$
吸収線量率	グレイ毎秒	Gy/s	$m^2 \cdot s^{-3}$
放射強度	ワット毎ステラジアン	W/sr	$m^4 \cdot m^{-2} \cdot kg \cdot s^{-3}=m^2 \cdot kg \cdot s^{-3}$
放射輝度	ワット毎平方メートル毎ステラジアン	$W/(m^2 \cdot sr)$	$m^2 \cdot m^{-2} \cdot kg \cdot s^{-3}=kg \cdot s^{-3}$

表６．国際単位系と併用されるが国際単位系に属さない単位

名称	記号	SI 単位による値
分	min	1 min=60s
時	h	1h =60 min=3600 s
日	d	1 d=24 h=86400 s
度	°	1° =(π/180) rad
分	’	1’ =(1/60)° =(π/10800) rad
秒	”	1” =(1/60)’ =(π/648000) rad
リットル	l、L	1l=1 $dm^3=10^{-3}m^3$
トン	t	1t=10^3 kg
ネーパ	Np	1Np=1
ベル	B	1B=(1/2)ln10(Np)

表７．国際単位系と併用されこれに属さない単位でSI単位で表される数値が実験的に得られるもの

名称	記号	SI 単位であらわされる数値
電子ボルト	eV	1eV=1.60217733(49)×10^{-19}J
統一原子質量単位	u	1u=1.6605402(10)×10^{-27}kg
天文単位	ua	1ua=1.49597870691(30)×10^{11}m

表８．国際単位系に属さないが国際単位系と併用されるその他の単位

名称	記号	SI 単位であらわされる数値
海里		1海里=1852m
ノット		1ノット=1海里毎時=(1852/3600)m/s
アール	a	1a=1 $dam^2=10^2m^2$
ヘクタール	ha	1ha=1 $hm^2=10^4m^2$
バール	bar	1 bar=0.1MPa=100kPa=1000hPa=10^5Pa
オングストローム	Å	1 Å=0.1nm=10^{-10}m
バーン	b	1 b=100$fm^2=10^{-28}m^2$

表９．固有の名称を含むCGS組立単位

名称	記号	SI 単位であらわされる数値
エルグ	erg	1 erg=10^{-7} J
ダイン	dyn	1 dyn=10^{-5}N
ポアズ	P	1 P=1 dyn・s/cm^2=0.1Pa・s
ストークス	St	1 St =1$cm^2/s=10^{-4}m^2/s$
ガウス	G	1 G ≙10^{-4}T
エルステッド	Oe	1 Oe ≙(1000/4π)A/m
マクスウェル	Mx	1 Mx ≙10^{-8}Wb
スチルブ	sb	1 sb =1$cd/cm^2=10^4cd/m^2$
ホト	ph	1 ph=$10^4$1x
ガル	Gal	1 Gal =1$cm/s^2=10^{-2}m/s^2$

表10．国際単位に属さないその他の単位の例

名称	記号	SI 単位であらわされる数値
キュリー	Ci	1 Ci=3.7×10^{10}Bq
レントゲン	R	1 R = 2.58×10^{-4}C/kg
ラド	rad	1 rad=1cGy=10^{-2}Gy
レム	rem	1 rem=1 cSv=10^{-2}Sv
X線単位		1X unit=1.002×10^{-4}nm
ガンマ	γ	1γ=1 nT=10^{-9}T
ジャンスキー	Jy	1 Jy=10^{-26}W・m^{-2}・Hz^{-1}
フェルミ		1 fermi=1 fm=10^{-15}m
メートル系カラット		1 metric carat = 200 mg = 2×10^{-4}kg
トル	Torr	1 Torr = (101 325/760) Pa
標準大気圧	atm	1 atm = 101 325 Pa
カロリー	cal	
ミクロン	μ	1 μ =1μm=10^{-6}m

（第７版，1998年改訂）

この印刷物は再生紙を使用しています